A Method to Evaluate and Predict the Performance of Baseball Bats Using Finite Elements

TIMOTHY J. MUSTONE
B.S.M.E. UNIVERSITY OF MASSACHUSETTS LOWELL (1996)

SUBMITTED IN PARTIAL FULFILLMENT OF THE REQUIREMENTS
FOR THE DEGREE OF MASTER OF SCIENCE
DEPARTMENT OF MECHANICAL ENGINEERING
UNIVERSITY OF MASSACHUSETTS LOWELL

Signature of Author:_____**Date:**_____

Signature of Thesis Supervisor: _____

Signatures of Thesis Committee Members: _____

_____

A Method to Evaluate and Predict the Performance of Baseball Bats Using Finite Elements

TIMOTHY J. MUSTONE
B.S.M.E. UNIVERSITY OF MASSACHUSETTS LOWELL (1996)

SUBMITTED IN PARTIAL FULFILLMENT OF THE REQUIREMENTS
FOR THE DEGREE OF MASTER OF SCIENCE
DEPARTMENT OF MECHANICAL ENGINEERING
UNIVERSITY OF MASSACHUSETTS LOWELL
2003

Thesis Supervisor: Dr. James A. Sherwood
Professor, Department of Mechanical Engineering

ABSTRACT

This thesis investigates the relative performance of traditional solid wood bats to high-performance metal bats using a combination of experimental testing to validate finite element modeling. Experimental work that was conducted first involves measuring the physical characteristics of a bat, such as length, weight, diameter profile, mass moment of inertia (MOI) and the location of the center of gravity (*cg*). Through experimental modal analysis, natural frequencies of the bat are also measured. From these experimental results, calibrated finite element models of wood and metal baseball bats are created. Compression testing of a baseball was performed to support the development of a realistic finite element model of a baseball that was validated using a standard coefficient of restitution (COR) test. These independently validated finite element models were then combined to predict batted-ball performance. These predictions were then compared with experimental data on batted-ball performance that was provided using the Baum Hitting Machine (BHM), a state of the art machine that simulates realistic swing and pitch speeds to generate batted-ball exit velocity data. These models were developed to not only provide a tool to corroborate collected BHM data, but also provide insight into the bat-ball impact, could be used to predict batted-ball exit velocity, and thus aid in the design of future bats.

ACKNOWLEDGMENTS

Major League Baseball and Rawlings Sporting Goods, Inc. for providing the grant to establish the UMass Lowell Baseball Research Center.

The National Collegiate Athletic Association, for using the UMass Lowell Baseball Research Center as an official test center.

Representatives from baseball bat manufacturers: Worth, Rawlings, Hoosier Bat Company, Easton Sports and Hillerich and Bradsby (H&B) for providing insight into baseball bat design and testing methodologies.

Past and present students who have worked in the UMass Lowell Baseball Research Center, for continuing what was started and making improvements along the way.

Dr. Peter Avitabile and Dr. Struan Robertson, for taking the time to be a part of my thesis committee.

To all my friends who have helped me, by continually asking how the thesis is going.

Larry Fallon of Sports Engineering, for introducing baseball bat testing to UMass Lowell and for being a great friend.

Dr. Jim Sherwood, for being not only my thesis advisor, but also a friend and someone whom I've learned a great deal from.

My parents, John and Muriel Mustone, for always pushing me to do my best; my brothers Jamie and Andy and my sister Missy, for all those whiffle ball games in the back yard.

My daughter Quinn, for making me laugh with those baby giggles when I needed a break from typing; and my wife Mea, for your unconditional love and support - I couldn't have done any of it without you.

TABLE OF CONTENTS

ABSTRACT iii
ACKNOWLEDGMENTS iv
TABLE OF CONTENTS v
LIST OF TABLES vii
LIST OF FIGURES viii
1 INTRODUCTION 1
1.1 NCAA Addresses Bat Performance 1
1.2 Scope 5
2 BACKGROUND 6
2.1 Introduction to Engineering Concepts relating to Baseball 6
2.1.1 Coefficient of Restitution 6
2.1.2 Mass Moment of Inertia and Parallel Axis Theorem 9
2.1.3 Center of Percussion and Sweet Spot 11
2.2 Wood vs. Metal 12
2.2.1 The Bat-Ball Collision and Energy Transfer 12
2.3 Performance Statistics of Wood vs Metal 20
2.3.1 Thurston's Cape Cod League Study 20
2.3.2 Sports Engineering Field Performance Study 21
2.4 Crisco's Final Report to the NCAA 22
2.4.1 Relationship between Reaction Time and Injuries due to the Batted Ball 23
2.4.2 Predicting Ball Performance 24
2.4.3 Predicting Bat Performance 28
2.4.4 Effects of Bat Mass and Inertia 33
3 EXPERIMENTAL TESTING 38
3.1 BHM Experimental Data 38
3.1.1 Instrumented Bat Impacts 39
3.1.2 BHM Batted-Ball Velocity Data 41
3.2 Frequency Analysis 50
3.2.1 Experimental Procedure 50
3.2.2 Results 51
3.3 Ball Compression Testing 52
4 MODELING 54
4.1 Analysis Tools Used 54
4.2 Early BHM Models 55
4.2.1 The 290° Swing vs. The 0° Swing 58
4.2.2 Rotation vs. Translation 60
4.3 Modeling Calibration 62
4.3.1 Calibrating the Baseball Model 63
4.3.2 Calibrated Ball Results 64
4.3.3 Calibrating the Baseball Bat Models 67
4.3.4 Calibrated Baseball Bat Results 69
5 LESSONS LEARNED 74
5.1 A Note on Damping 74

5.2 Appropriate Model for COR Test 75
5.3 Modifying contact analysis parameters 77
5.4 Corrected Aluminum Bat Model 80
5.4.1 Wall Thickness and Nodal Reference Plane for Shell Elements 80
5.4.2 MOI Calibration 83
5.5 Updated Model Comparison 83
6 CONCLUSIONS AND recommendations 90
6.1 Conclusions 90
6.2 Recommendations 91
7 APPENDICES 93
7.1 Automatic Time Step Information 93
7.2 Damping Information 101
7.3 Mooney-Rivlin Material Model Information 108
7.4 LS-DYNA COR test input deck 114
7.5 LS-DYNA -3 aluminum bat model input deck 116
7.6 LS-DYNA Implicit input deck for modal analysis 119
8 REFERENCES 120

LIST OF TABLES

Table 2.1 – Comparison of player's statistics (1997 data). 20
Table 2.2 – Statistical summary of field performance data. 22
Table 2.3 – Ball compression test results. 28
Table 2.4 – Results of parametric study. 36
Table 3.1 – Experimental frequency results. 51
Table 4.1 – Summary of material properties used for initial modeling. 57
Table 4.2 – Summary of aluminum bat calibration results. 68
Table 4.3 – Summary of wood bat calibration results. 69
Table 5.1 – Summary of updated aluminum bat calibration results. 83
Table 5.2 – Summary of wood bat calibration results. 83
Table 5.3 – Summary of batted-ball velocity comparison. 85

LIST OF FIGURES

Figure 2.1 - Two bodies in motion, before (top), during (middle) and after (bottom) a collision. 7
Figure 2.2 – Baseball bat MOI terminology. 10
Figure 2.3 – Comparing typical MOI values for wood and metal bats. 11
Figure 2.4 – An example of the bending deformation 13
Figure 2.5 – Bat-ball collision showing local trampoline 14
Figure 2.6 – Example of a hollow metal bat with a composite barrel-reinforcement. 15
Figure 2.7 – Motion of the swinging bat. 16
Figure 2.8 – Variables denoted in swing equations. 17
Figure 2.9 – Plot demonstrating Equation 2.17. 19
Figure 2.10 – Cross-section of a baseball. 27
Figure 2.11 – An example of the ASTM ball compression test and resulting data. 27
Figure 2.12 – Schematic of Brandt test setup. 29
Figure 2.13 – Assorted views of the BHM. 31
Figure 3.1 – Sensor location for BHM instrumented bat impacts. 39
Figure 3.2 – Example of clipped acceleration data for metal bat impacts. 39
Figure 3.3 – Calculated bending stress at the handle for a metal bat impact. 40
Figure 3.4 – BHM schematic, overhead view. 42
Figure 3.5 – Sample BHM data sheet. 43
Figure 3.6 – Example of variability within and between ball lots (valid hits only). 44
Figure 3.7 – Representative BHM data for wood bat performance. 46
Figure 3.8– Representative BHM data for metal bat performance. 47
Figure 3.9 – Comparison of wood and metal bat BHM data. 49
Figure 3.10 – Diagram of experimental modal analysis setup. 51
Figure 3.11 – Average load versus displacement results for three MLB baseballs. 53
Figure 4.1 – Initial bat-ball impact models for the 56
Figure 4.2 – 290° swing model (left) and 0° swing model (right). 58
Figure 4.3 – Results of BHM swing study for 290° and 0° swings. 59
Figure 4.4 – Batted-ball velocity for an aluminum bat rotating and translating to impact. 61
Figure 4.5 – Close-up of maximum batted-ball velocities. 61
Figure 4.6 – New finite element meshes for the aluminum bat (top) 62
Figure 4.7 – Sequence of ball deformation during contact with flat surface. 64
Figure 4.8 – Initial comparison of batted-ball velocities 65
Figure 4.9 –Aluminum bat modeling results using a calibrated ball model. 66
Figure 4.10 – Initial wood bat modeling results using a calibrated ball model. 66
Figure 4.11 – Deformed aluminum bat models showing 1st (top) and 2nd bending modes. 68
Figure 4.12 – Deformed wood bat models showing 1st (top) and 2nd bending modes. 68
Figure 4.13 – Batted-ball velocities for the calibrated 70
Figure 4.14 – Comparison of the barrel deformation during impact. 71
Figure 4.15 – Stress contour plots of wood bat animation. 72
Figure 4.16 – Stress contour plots of aluminum bat animation. 73

Figure 5.1 – Displacement and velocity of original baseball COR model. 76
Figure 5.2 – Improved COR model results for baseball displacement and velocity. 77
Figure 5.3 – Examples of nodal penetration of the ball into the wood block. 78
Figure 5.4 – Increasing the contact stiffness results in reducing the penetration. 79
Figure 5.5 – New plastic cap model, with reinforcing ribs. 81
Figure 5.6 – Sectioned view showing interface with cap. 82
Figure 5.7 – Updated aluminum bat model. 82
Figure 5.8 – Batted-ball velocity for updated models. 84
Figure 5.9 – Time-history plot of the batted-ball displacement. 86
Figure 5.10 – Deformation plots of batted-ball model with the wood bat. 89

1 INTRODUCTION

1.1 NCAA Addresses Bat Performance

In 1974, the National Collegiate Athletic Association (NCAA) permitted the use of aluminum bats in collegiate baseball games under its jurisdiction. The initial purpose for this change from traditional solid wood to aluminum was to reduce operating costs due to broken bats. The original aluminum bats performed similar to wood, with the exception that the aluminum bats did not break. As aluminum alloy performance and competition among the sporting goods manufacturers increased, so did the performance of the aluminum bats resulting in a new generation of high-performance baseball bats being developed. These new bats used the latest advances in technology, including new metal alloys, damping materials and sensors and barrel reinforcements such as air bladders and composite materials.

Baseball bat performance comes down to a simple physics problem: the higher the initial exit velocity of a batted ball, the farther the ball will travel. As more technological advances were added to metal bats, the performance gap versus traditional wood bats widened. This increasing performance has upset the balance between the offense and defense of the game, compromising the integrity of the game itself.

At the 1995 College World Series, a record 48 home runs were hit during the 16-game series, breaking the previous mark of 29. During the 1998 College World Series, 64 home runs were hit setting another record. The score of the 1998 final championship game was 21 to 14, a typical football score, not a baseball score. Clearly one or more factors were causing this increase in offense.

A side effect of the increasing bat performance is the potential danger to pitchers who might be unable to defend themselves against a line drive hit by these new bats. A batted-ball traveling at an elevated velocity could sometimes reach the pitcher faster than it takes for the pitcher to defend himself. Although there has been no definitive study, media outlets most often report injuries to pitchers from Little League, high school and college caused by the use of these high-performance baseball bats, in comparison to reporting injuries caused by wood bats.

Amherst College head baseball coach Bill Thurston conducted a preliminary study in 1997 that compared the hitting statistics of players who participated in NCAA Division I baseball with aluminum bats and then played in the Cape Cod League the following summer.[1] The Cape Cod League is one of a handful of summer leagues that uses traditional wood bats. A total of 88 college players were considered in the statistical study. To be eligible for the study, a player had to have a minimum of 70 at-bats in the Cape Cod League. In summary, Thurston found that the average batting average for all the players decreased by 100 points, the number of home runs per-at-bat decreased by 65% and the number of strikeouts per-at-bat increased by 41%, while the number of walks remained the same. It became evident how much the aluminum bat can influence the offensive aspects of the game.

Major League Baseball (MLB) became involved in the debate because a considerable number of its players are drafted from the college ranks. After playing with an aluminum bat for most of their baseball career, with the exception of playing in a summer league that exclusively uses wood bats, rookie players have a difficult time adjusting to hitting the ball with a wood bat. It takes on average two years for a player to learn how to hit

with a wood bat. Because of the inherent difference between playing with a wood bat and playing with a metal bat, talent scouts from MLB organizations have difficulty evaluating a potential draft-pick's offensive skills. They have to translate the skill that a player has hitting with a metal bat to how that player will do when he uses a wood bat.

To better understand the bat performance issue, consider the timeline of events regarding how the NCAA has addressed bat performance as discussed in the February 1999 edition of the NCAA News.[2] The first step that the NCAA took to curb the new generation of aluminum bats was for the 1989 season. It restricted the weight of a metal bat by setting a limit on how light they could be stating that the numerical difference between the length and weight of a bat could not exceed five units, that is, a 34-in bat could weigh no less than 29 oz. After the 1994 NCAA baseball season, the NCAA Baseball Rules Committee met with the metal-bat manufacturers to discuss performance issues. It was agreed that the performance level would not increase and that the Brandt test, developed by New York University physics professor R. A. Brandt, PhD, would be used to measure the performance. The Brandt test, to be discussed later, is a test designed to measure the batted-ball performance of slow-pitch softball bats. Over the next three seasons, the NCAA suspected that bat performance had increased. However, the manufacturers reported that bat performance had not increased per the Brandt test. In the fall of 1997, the NCAA was made aware of a letter written by Brandt, stating that his test, adopted by the manufacturers as the bat performance testing standard, does not accurately measure bat performance for baseball. As a result, Dr. J. J. Trey Crisco of the National Institute for Sport Science and Safety (NISSS) and Brown University was contracted to investigate several aspects of bat and ball performance, including the

evaluation of current testing methods. The findings of his report, to be discussed later, only added to the controversy.

In July 1998, the NCAA Baseball Rules Committee held a "bat summit" where invited researchers and guests were gathered to discuss bat-ball performance issues. The guests in attendance included NCAA representatives, National Federation of High School (NFHS) Baseball Rules Committee members and several bat manufacturers. A former baseball bat design consultant for Hillerich & Bradsby (H&B, makers of the Louisville TPX brand of metal bats and Louisville Slugger brand of wood bats) alleged that the manufacturers of metal bats had misled and deceived the NCAA about bat performance and testing standards. After assessing the gathered information, the rules committee decided to develop new standards to limit the performance of metal bats, making them perform more like wood bats. In developing the new standards, three requirements were mandated: to minimize risk, to maintain a balance between offense and defense and to preserve the integrity of the game. The three new recommended standards were:

1. Changing the weight to length unit difference from -5 (with the grip) to -3 (without the grip), meaning that a 34-in bat can weigh no less than 31 oz
2. Reducing the barrel diameter from 2 $^{3}/_{4}$ to 2 $^{5}/_{8}$ in
3. Limiting the batted-ball velocity to 94 mph, given a 70-mph pitch speed and a 70-mph swing speed at the point of impact, designated as the 6 in from the barrel-end of the bat

In a press release issued by the NCAA[3], the Baseball Rules Committee felt that these changes were necessary to make the game safer for all players and to improve competitive balance between offensive and defensive aspects of the game. The committee also felt that technological innovations, rather than player's skills, were impacting the outcome of the games, threatening the integrity of college baseball.

1.2 Scope

This thesis will examine several aspects of baseball bat performance, which could also be translated to softball bats, and primarily looks at the relative performance of high-performance metal bats to traditional solid wood bats. Experimental work pertaining to bat performance involves first measuring the physical characteristics of a bat, such as length, weight, diameter profile, moment of inertia (MOI) and the location of the center of gravity (*cg*). Through modal analysis, the natural dynamic characteristics of the bat are measured. From these experimental results, calibrated finite element models of wood and metal baseball bats are created. Compression testing of a baseball was performed to support the development of a realistic finite element model of a baseball. This baseball model was then used to examine the batted-ball performance of wood and metal baseball bats using finite element modeling techniques. Experimental data on batted-ball performance was provided using the Baum Hitting Machine (BHM), a state of the art machine that simulates realistic swing and pitch speeds to generate batted-ball exit velocity data. The finite element models not only provide a tool to corroborate collected BHM data, but also provide insight into the bat-ball impact, could be used to predict batted-ball exit velocity, and thus aid in the design of future bats.

2 BACKGROUND

2.1 Introduction to Engineering Concepts relating to Baseball

Before discussing the performance of baseballs and baseball bats, a few engineering concepts are presented. The coefficient of restitution (COR) is used to quantify the elasticity or "liveliness" of the baseball. The moment of inertia (MOI) of the baseball bat has an important effect on the swing speed that a batter can generate. This swing speed in turn has an effect on the batted-ball velocity. Several other concepts, like the center of gravity or balance point of the baseball bat, the center of percussion and the "sweet spot" also play a role in baseball bat performance. The following is a brief description of each concept.

2.1.1 Coefficient of Restitution

The most accepted means of quantifying ball performance is to measure the COR of the baseball as it strikes a stationary object, usually a thick white ash board rigidly mounted to a wall. The COR is a measure of how elastic or inelastic two bodies are when they come into contact with each other and must be measured experimentally. The following is a brief derivation of the COR, as defined by Riley and Sturges.[4] Consider two bodies, *A* and *B* that are positioned on the same path as shown in Figure 2.1. Bodies *A* and *B* are given initial velocities, v_{Ai} and v_{Bi}, respectively.

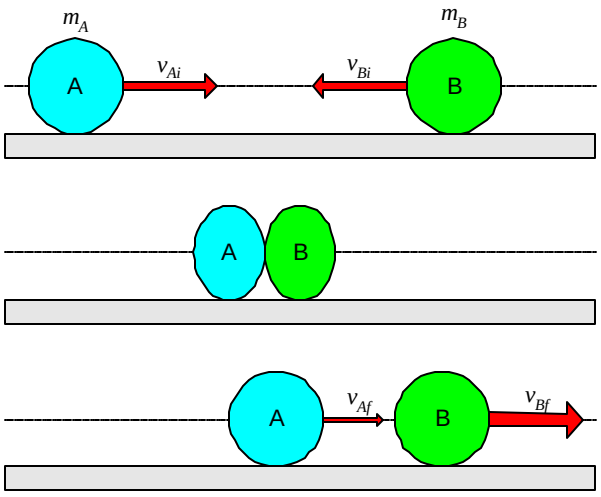

Figure 2.1 - Two bodies in motion, before (top), during (middle) and after (bottom) a collision.

It is assumed that during the brief interval that the two bodies are in contact, the velocity of one or both of the bodies in motion may change and the positions of the bodies do not change significantly. Also, non-impulsive forces and the friction forces between the two bodies may be neglected.

Given the masses of each body, m_A and m_B, the total momentum for the two bodies before (i) and after (f) the collision is conserved:

$$m_A v_{Ai} + m_B v_{Bi} = m_A v_{Af} + m_B v_{Bf} \qquad \textbf{Equation 2.1}$$

Now consider the impulse forces acting on the individual bodies while the bodies are deforming during and after the collision. When the two bodies are in contact, the momentum equation gives

$$m_A v_{Ai} - \int_{t_i}^{t_c} F_d\,dt = m_A v_c \qquad \textit{and} \qquad m_B v_{Bi} - \int_{t_i}^{t_c} F_d\,dt = m_B v_c \qquad \textbf{Equation 2.2}$$

where F_d is the interaction force on the bodies as they deform, t_i is at some initial time, v_c is the common velocity of the two bodies at the end of the deformation phase of the

collision, which occurs at time t_c. As the two bodies become separated again, conservation of linear momentum yields

$$m_A v_c - \int_{t_c}^{t_f} F_r dt = m_A v_{Af} \qquad and \qquad m_B v_c - \int_{t_c}^{t_f} F_r dt = m_B v_{Bf} \qquad \textbf{Equation 2.3}$$

where F_r is the interaction force on the bodies as they are restored to their original state with final velocities v_{Af} and v_{Bf} at some final time, t_f.

The coefficient of restitution e is defined as the ratio of the impulse during the collision and the impulse as the bodies are restored

$$e = \frac{\int_{t_c}^{t_{fc}} F_r dt}{\int_{t_i}^{t_c} F_d dt} = \frac{m_A v_c - m_A v_{Af}}{m_A v_{Ai} - m_A v_c} = \frac{v_c - v_{Ai}}{v_{Ai} - v_c}$$

Equation 2.4

$$e = \frac{\int_{t_c}^{t_{fc}} F_r dt}{\int_{t_i}^{t_c} F_d dt} = \frac{m_B v_c - m_B v_{Bf}}{m_B v_{Bi} - m_B v_c} = \frac{v_c - v_{Bi}}{v_{Bi} - v_c}$$

Solving these two equations for e by eliminating the unknown velocity v_c, yields a simplified form

$$e = -\frac{v_{Bf} - v_{Af}}{v_{Bi} - v_{Ai}} = -\frac{(v_{B/A})_f}{(v_{B/A})_i} \qquad \textbf{Equation 2.5}$$

where the COR is the negative ratio of the relative velocities of two bodies after and before a collision.

The COR is not a value that is regarded as a material property because it not only depends on the material of both impacted bodies, but for nonlinear material systems, it also depends on the velocity at which they collide. It will also vary with respect to

different sizes, shapes and the temperature of the impacting bodies. For values of $e=1$, the collision is considered to be a perfectly elastic impact, that is, there is no energy loss due to the deformation of the bodies at impact. For values of $e=0$, the collision is considered to be a perfectly plastic impact. The relative velocity of the two bodies after impact is zero and the two particles move together at the same speed.

2.1.2 Mass Moment of Inertia and Parallel Axis Theorem

The mass moment of inertia is a measure of a body to resist a rotational acceleration about an axis and is the best measure of how easily a bat can be swung. It is simply denoted as MOI, noting that it refers to the *mass* moment of inertia and not to be confused with an *area* moment of inertia. Studies described later have shown that batted-ball velocity increases with increasing bat swing speed. Therefore, the MOI, because it is an indicator of swing speed, can provide one measure of bat performance.

The definition of the MOI[5] is simply a differential mass, dm, multiplied by the square of the distance to an axis of rotation, r^2, summed over the entire mass m, as defined by Equation 2.6. The resulting units are $MASS \cdot DISTANCE^2$ (usually $oz \cdot in^2$ for baseball bats). The MOI is traditionally calculated about an axis running through the center of gravity, as illustrated in Figure 2.2, but using the parallel-axis theorem, the MOI can be calculated about any arbitrary axis location, for example, the x' axis, as defined in Equation 2.7.

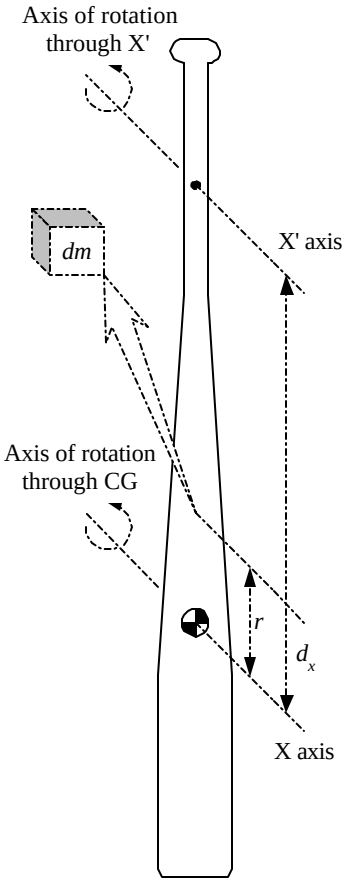

Figure 2.2 – Baseball bat MOI terminology.

MOI Definition

$$I = \int_m r^2 dm \qquad \textbf{Equation 2.6}$$

Parallel-axis Theorem

$$I_{x'} = I_{cg} + d_x^2 m \qquad \textbf{Equation 2.7}$$

The weight, length and location of the center of gravity all play a part in determining the MOI of the bat. The center of gravity is also referred to as the balance point. Bats that are "end-loaded" or "end-heavy" have relatively high MOI values with a *cg* located closer to the barrel end of the bat. These bats typically cannot be swung as fast as lower MOI bats, but they do show a higher batted-ball velocity when compared at the same swing speeds as a result of the higher percentage of mass at the end of the bat. An example of MOI values for aluminum and wood bats as a function of length, is shown in Figure 2.3. This plot not only shows how the MOI increases as the length of the bat

increases, but is also shows the MOI of metal bats are on average lower than wood at equal lengths.

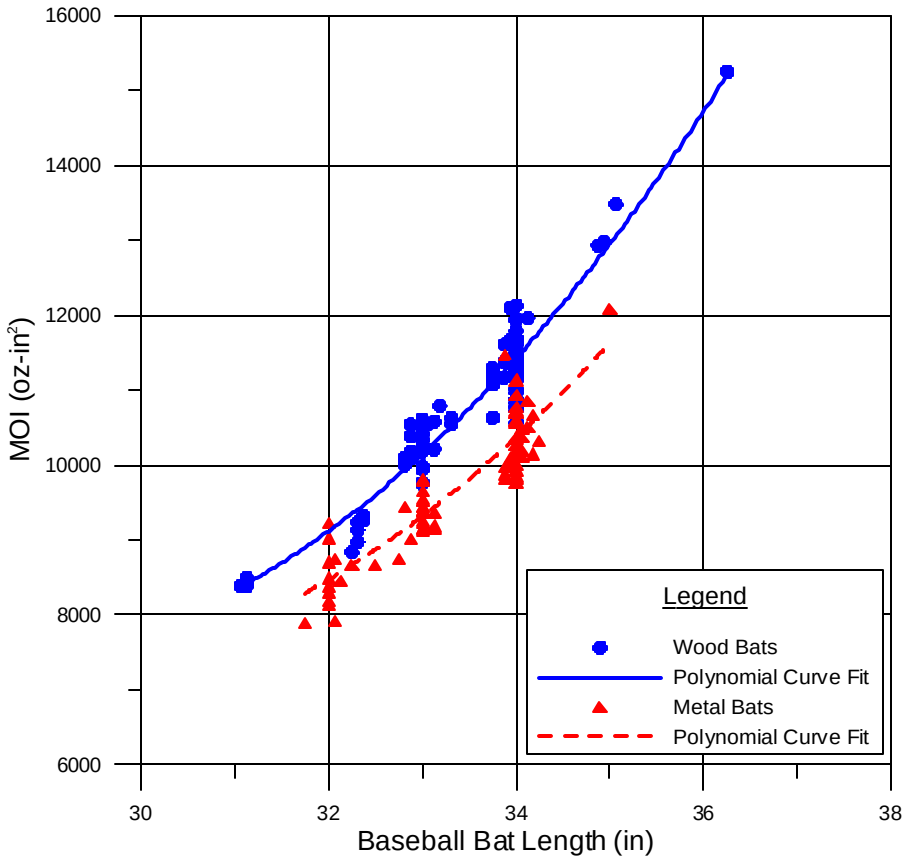

Figure 2.3 – Comparing typical MOI values for wood and metal bats.

2.1.3 Center of Percussion and Sweet Spot

The point on a body moving about a fixed axis at which it may strike an obstacle without communicating a reaction force to the axis is called the center of percussion (COP).[6] Suppose that a baseball bat is rotating during that swing about an axis at the handle where the hands grip the bat and the baseball impacts the bat at the COP. For this case, the batter will not feel any vibration at the handle, and therefore, that batter will

describe the collision as “hitting it on the sweet spot” of the bat. But the “sweet spot” can also be defined as the location on the bat that will yield the maximum batted-ball velocity, and does not necessarily coincide with the COP. There are vibration nodes belonging to the 1st and 2nd bending modes of the bat that are also located in this general area of the barrel (± 1 in) and it is suspected that they too have an affect on the batted-ball velocity. Further experimentation should be done to quantify this effect.

2.2 Wood vs. Metal

The physical differences between wood and metal baseball bats are quite obvious. A wood bat is solid, usually weighs 2 units less than its length and is not very durable. A metal bat on the other hand, is hollow, weighs either 3 or more units less than its length and is more durable than wood. A significant difference between wood and metal bats is the energy-transfer mechanism between the bat and the baseball during the collision. The difference between the energy-transfer mechanisms is a fundamental result of the wood bat being solid and the metal bat being hollow.

2.2.1 The Bat-Ball Collision and Energy Transfer

In looking at the difference in performance between wood and metal bats, the generic bat-ball collision must first be understood. This understanding includes the complex motion of the bat to the ball and the energy transfer between the bat and the ball during and after the collision. In his book **The Physics of Baseball**[7], Adair reviews the different aspects of a bat-ball collision. The complex motion of the bat towards the ball is a combination of rotation and translation of both the batter and the bat. The swing is mostly translation in the beginning stages and then mostly rotation just before hitting the

ball. However, the basic mechanics and motion of a swing will be the same whether the batter is using a wood bat or a metal bat.

The total energy of a bat-ball collision is the sum of the kinetic energy generated by the batter during the swing and the kinetic energy of the baseball pitched towards home plate. When the ball collides with the bat, some energy is stored in the ball as it deforms on the barrel to almost half of its original diameter. Some energy is stored in the bat as it bends or deforms due to the impact with the ball, as shown in Figure 2.4. Some energy is lost when frictional forces of the collision are dissipated through heat. However, the amount of energy stored in the bat and how it is transferred back to the baseball is the major difference between wood and metal baseball bats.

Figure 2.4 – An example of the bending deformation of a baseball bat after it strikes the ball.

As previously noted, a metal bat is hollow. When the ball impacts the bat as shown in Figure 2.5, the barrel elastically deforms and becomes oval in shape, storing energy

from the collision. When the material springs back to its original shape, the stored energy in the bat is returned to the ball, propelling off of the bat at a faster rate than if using a wood bat. Within this global hoop-deformation mode in hollow metal bats is a phenomenon known as the trampoline effect. This trampoline effect is a local deformation in the bat at the point of impact that also stores energy during contact with the ball and then returns it to the ball as the bat returns to its original shape. The trampoline effect also causes the baseball to deform less, which is significant because the baseball is not a good energy storage device. When impacted with the solid wood bats, the baseball deforms more, thus dissipating some of the collision energy.

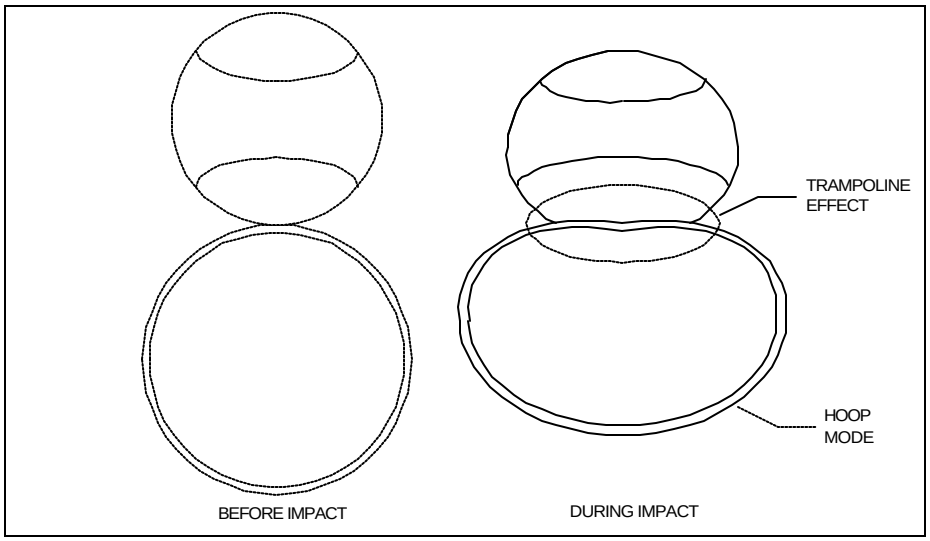

Figure 2.5 – Bat-ball collision showing local trampoline effect and global hoop deformation mode of metal bats.

By using newer metal alloys that have higher yield-strength, the trampoline effect can increase the exit velocity of a baseball. Where the diameter profile along the length of a solid wood bat is more of an artistic design, a metal bat is often engineered to give the

maximum performance possible, i.e. the fastest batted-ball velocity. The location of the center of gravity, the moment of inertia, the sweet spot, the material selection, the diameter profile, barrel reinforcements and the damping characteristics of a metal bat are all considered in designing a metal bat. Figure 2.6 shows an example of a high-performance aluminum-bat barrel with a composite reinforcement.

Figure 2.6 – Example of a hollow metal bat with a composite barrel-reinforcement.

Robert Watts and Terry Bahill in their book **Keep Your Eye on the Ball: The Science and Folklore of Baseball** examine the relationship between the input energy from the swing and the batted-ball velocity.[8] The actual swing of a batter is a complex combination of both translation and rotation, shown in Figure 2.7. While the player is rotating the bat's barrel from their shoulder to the ball, the bat as a whole is translating from behind home plate to just in front of home plate. During this translation, the bat rotates about a point between the player and the bat's knob.

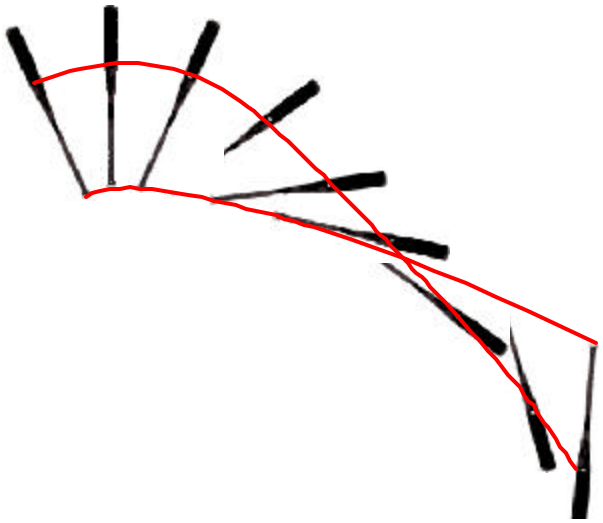

Figure 2.7 – Motion of the swinging bat.

Based on the two types of motion that the bat undergoes, there are two types of kinetic energy developed from the swing as described by

$$KE_{translation} = \frac{1}{2} m_{bat} v_{bat_{cg}}^2 \qquad \textbf{Equation 2.8}$$

$$KE_{rotation} = \frac{1}{2} I_{bat_{cg}} w_{bat_{cg}} \qquad \textbf{Equation 2.9}$$

where $I_{bat\ cg}$ is the moment of inertia of the baseball bat about its center of gravity and $\omega_{bat\ cg}$ is the angular velocity of the bat about its center of gravity. The total energy of the swing is equal to the work W done by the player to put the bat into motion:

$$W = KE_{translation} + KE_{rotation} \qquad \textbf{Equation 2.10}$$

where there is a maximum amount of work that a player can put into the motion of the bat and still maintain control to hit the ball.

Watts and Bahill also show that this rotational kinetic energy can be further broken down into a combination of two rotational motions, which can be used to derive an equation for batted-ball velocity. Ultimately, these equations can be used to locate a

point on the bat that provides maximum energy transfer, in other words, highest batted-ball velocity.

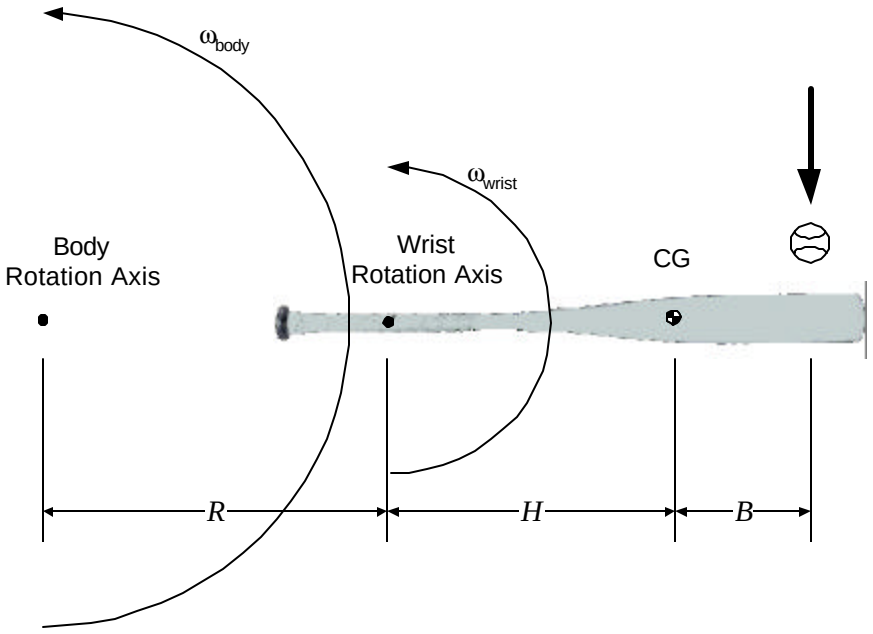

Figure 2.8 – Variables denoted in swing equations.

Suppose that a batter's swing can be drawn as shown in Figure 2.8 where two angular accelerations are applied to the bat: w_{body} due to the rotation of the body and w_{wrist} due to the rotation of the batter's wrists during the swing. The linear velocity of the bat at the *cg* (v_{2b}) and at the point of impact (v_B) before a collision with the ball is

$$v_{2b} = (R + H)w_{body} + Hw_{wrists}$$
$$v_B = (R + H + B)w_{body} + (H + B)w_{wrist} \qquad \textbf{Equation 2.11}$$

Combining these two equations yields

$$v_B = B(w_{body} + w_{wrist}) + v_{2b} \qquad \textbf{Equation 2.12}$$

Making the substitution of $w_2 = w_{body} + w_{wrist}$ simplifies the equation further.

During the bat-ball collision, suppose that the force exerted on the bat from the impact with the ball is $-F_1$, resulting in a torque on the bat about its *cg* is equal to $-BF_1$. Equating this torque over time *t* to the change in angular momentum yields for the bat

$$-BF_1 t = I_0(w_{2a} - w_{2b}) \qquad \textbf{Equation 2.13}$$

Similarly for the ball

$$BF_1 t = Bm_1(v_{1a} - v_{1b}) \qquad \textbf{Equation 2.14}$$

Assume that the rotational kinetic energy of the ball is negligible when compared to the translational kinetic energy. Conserving angular momentum between the bat and the ball during the collision produces

$$I_0(w_{2a} - w_{2b}) + Bm_1(v_{1a} - v_{1b}) = 0 \qquad \textbf{Equation 2.15}$$

Recall that Equation 2.1 and Equation 2.5 also apply to the energy stored during a bat-ball collision. It should be noted that Equation 2.5 is modified here to represent the fact that the impact is not at the *cg* location of the bat, such that the COR is defined as

$$e = -\frac{v_{1a} - v_{2a} - Bw_{2a}}{v_{1b} - v_{2b} - Bw_{2b}} \qquad \textbf{Equation 2.16}$$

Equations 2.1, 2.15 and 2.16 can now be solved simultaneously to find the batted-ball velocity v_{1a}.

$$v_{1a} = \frac{-v_{1b}\left(e - \frac{m_1}{m_2} - \frac{m_1 B^2}{I_0}\right) + (1+e)(v_{2b} + Bw_{2b})}{1 + \frac{m_1}{m_2} + \frac{m_1 B^2}{I_0}} \qquad \textbf{Equation 2.17}$$

By substituting into Equation 2.17 representative values for wood and metal bats, a plot of the batted-ball velocity as a function of the location of the impact point on the bat from the barrel end can be created. The peaks of Figure 2.9 show where along the length of the bat the maximum energy transfer occurs. This location of maximum energy

transfer is commonly referred to as the sweet spot on the bat. Notice that not only is the peak batted-ball velocity higher for the metal bat versus the wood bat, but it is spread out over a greater length of the barrel. As the point of impact gets closer to the handle, the batted-ball velocity drops off more for the wood bat than for the metal bat. This example shows why an inside pitch travels farther when hit with a metal bat than with a wood bat – higher batted-ball velocity.

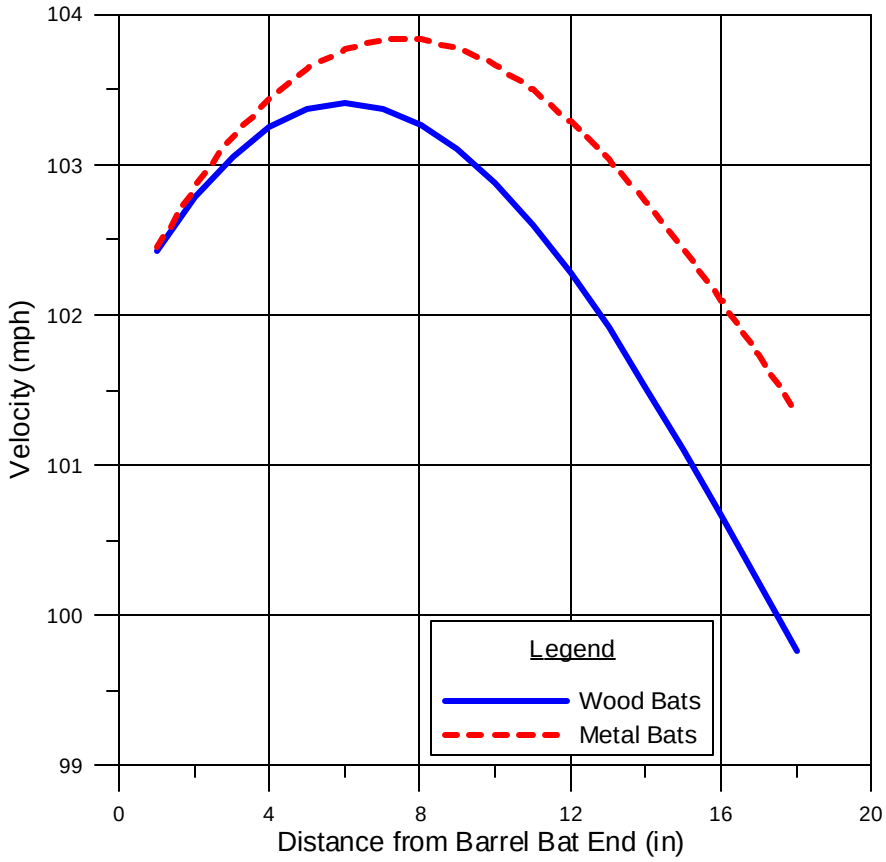

Figure 2.9 – Plot demonstrating Equation 2.17.

2.3 Performance Statistics of Wood vs Metal

There is much anecdotal evidence of how a metal bat outperforms the traditional wood bat. Two studies are selected here to demonstrate some empirical evidence.

2.3.1 Thurston's Cape Cod League Study

In Thurston's study, he examined several offensive statistics: batting average, slugging percentage, home runs per at bat, base on balls per at bat, strikeouts per at bat, runs scored per at bat and runs batted in (RBI) based on percent runs driven in per at bat. Table 2.1 summarizes his results, which were averaged for all players.

Table 2.1 – Comparison of player's statistics (1997 data).

Statistic	When the player used an aluminum bat…	When the player used a wood bat…	Percent Change
Batting Average	0.339	0.231	-0.108 (-31.8%)
Slugging Percentage	0.555	0.325	-0.230 (-41.4%)
Home Runs	1 per 25 at bats	1 per 74 at bats	- 65%
Base on Balls	1 per 8.33 at bats	1 per 8.33 at bats	No Change
Strikeouts	1 per 5.88 at bats	1 per 4.17 at bats	+ 41%
Runs Scored	1 per 4 at bats	1 per 8.33 at bats	- 52%
RBI	1 per 4.55 at bats	1 per 9.09 at bats	- 50%

After reviewing this collection of data, the impact of an aluminum bat versus a wood bat on the game is evident. A player hits for a higher average, hits more home runs per at bat, strikes out less per at bat and drives in more runs per at bat with an aluminum bat than he does with a wood bat. Also, more runs are scored per at bat with aluminum than with wood. When looking at the individual statistics, 70 players had a batting average over 0.300 when using an aluminum bat. When using a wood bat, only 5 players had a batting average over 0.300. The largest difference between the wood and aluminum bat

can be seen in the 65% decrease in home runs per at bat. Fifty-eight players had at least one home run every 40 at bats when they used an aluminum bat, while only 16 players had the same success when they used a wood bat. The increase of strikeouts per at bat from 0.17 with aluminum bats to 0.24 with wood bats could be a measure of swing speed, in that a player can swing an aluminum bat faster than he can swing a wood bat. Also, the lower MOI of an aluminum bat gives the batter better control to move the bat up and down in the strike zone as he swings. The slower swing speed with a wood bat may not allow a hitter to catch up to a fastball and make contact. In addition, to make up for the slower swing speed with wood, the batter has to commit his swing earlier than he would with an aluminum bat. If a batter can wait until the last possible moment before starting his swing, he has the better chance of making contact with the ball. The earlier a batter commits to swinging at a pitched ball, the less chance he has at making contact because he basically is guessing at where the ball will be. The runs scored and runs batted in per at bat were cut in half when the players used wood bats. The ball is put in play more with a metal bat than with a wood bat, resulting in a greater chance of scoring a run.

2.3.2 Sports Engineering Field Performance Study

With assistance from UMass Lowell's Baseball Research Center (UMLBRC), Larry Fallon of Sports Engineering conducted several field performance studies that compared the distance a ball travels when hit with professional quality wood bats versus aluminum bats. The two C405 aluminum bats used in the study were from two different manufacturers and were both -5 bats. In these studies, approximately 40 Rookie and Single-A class players from two Major League Baseball organizations used wood and aluminum bats while taking their regular batting practice drills. The baseball field was

measured and flags were positioned radially from home plate every 10 ft starting at 250 ft and ending outside the outfield fence at 450 ft. The distance a ball traveled in the air to where it first landed was recorded to an accuracy of 5 ft.

A statistical summary of the raw data shown in Table 2.2 concludes that the C405 aluminum bats hit the ball farther. Over 1,000 hits were completed with wood bats and over 650 hits with aluminum bats. Only one ball was hit with a wood bat farther than 390 ft, while a total of 18 balls were hit 390 ft or more with the aluminum bat – the furthest at 440 ft.

Table 2.2 – Statistical summary of field performance data.

	Wood Bat	**C405 Aluminum Bat**
Percentage of hits over 250 ft	33.5 %	37.3 %
Percentage of hits over 300 ft	12.8 %	21.8 %
Percentage of hits over 350 ft	3.0 %	8.3 %
Average distance over 250 ft	294.4 ft	315.4 ft
Average distance over 300 ft	332.3 ft	347.6 ft
Average distance over 350 ft	368.7 ft	386.3 ft

As shown in these two studies, field performance data for metal and wood bats point to an increase in performance of metal bats over wood.

2.4 Crisco's Final Report to the NCAA

In October 1996, J. J. Trey Crisco of the National Institute for Sports Science and Safety (NISSS) was commissioned by the NCAA to re-evaluate the preliminary limits on bat and ball performance and to critique other issues related to performance.[9] Crisco was tasked to examine five aspects of the bat and ball performance:

1. To determine the injury patterns from the batted ball
2. To evaluate what response time is necessary to avoid impact from a batted ball

3. To evaluate existing test methods for predicting ball performance
4. To evaluate existing test methods for predicting bat performance
5. To determine the effects of bat mass and inertia on swing velocity

Crisco's year-long study encompassed much of the recent work done on investigating the performance of baseball bats by collecting many "papers in progress" and enlisting other facilities to conduct supporting research. Because of the extent of his study, its conclusions are used here as a guide.

2.4.1 Relationship between Reaction Time and Injuries due to the Batted Ball

Based on data from the NCAA Injury Surveillance System, Crisco concluded that baseball had one of the lowest overall injury rates in any collegiate sport. The acceptable risk of receiving an injury due to a batted ball had yet to be determined and the exact level of acceptability should be established using values determined from scientific studies. Also, the existing standards of bat and ball performance as it relates to injuries were based on practical experience with little scientific basis.

With respect to quantifying the relationship between reaction time and injuries due to batted balls, Cassidy and Burton[10] examined research literature on the reaction time of baseball players and the amount of time it takes for a player to move an arm to a defensive position. They concluded that the average college or professional player is able to begin their response to the ball 125 ms after the ball is impacted and that it takes approximately 200 ms to complete the arm movement for a defensive position. Based on these two findings, a player is calculated to have approximately 325 ms to react to a batted ball and move his arm to catch or block the ball. This value has become quite controversial.

A pitcher is typically 55 ft from home plate when he finishes delivering the ball to the catcher. Suppose that a ball is then hit directly back at the pitcher. Based on the 325 ms reaction time, if a batter hits a line drive up the middle, then the pitcher would not have enough time to react to the ball if it was traveling at 115 mph or faster. This calculation neglects any drag on the ball due to air resistance, so the actual velocity could be slightly less than 115 mph. Regardless, this ball exit velocity was much higher than any wood bat, yet pitchers are still hit by line drives off wood bats. Scientists at the NCAA's July 1998 bat summit agreed that approximately 400 ms, not 325 ms was necessary for a pitcher to defend himself against a line drive.[11] That would reduce the "safe" ball exit velocity to 93.75 mph. Crisco noted that although injuries from balls hit with wood bats have also occurred, the severity of the injury seems to increase with increasing ball velocity. In other words, a pitcher hit with a ball coming off an aluminum bat would suffer a more serious injury than if the bat were made of wood because the ball would be traveling at a higher velocity with more kinetic energy to release in the collision.

2.4.2 Predicting Ball Performance

Because the performance of a baseball bat is usually quantified by the exit speed of the batted ball, the performance of the baseball should also be quantified. Suppose two different lots of baseballs from a single manufacturer were used for testing. One lot has a high COR value ("juiced" or lively balls) and the other has a much lower COR value ("dead" balls). If the "juiced" balls were used to test a wood bat, and the "dead" balls were used to test a metal bat, the relative performance of the wood and metal bats could be equal. On the other hand, if the "juiced" balls were used to test the metal bat instead, then the relative performance of the metal bat could be artificially inflated. This simple

example shows that you cannot address the performance of a baseball bat without also considering the performance of the baseball.

2.4.2.1 COR Testing

As of 1999, the specification regarding collegiate-level ball performance is that the baseball must have a COR between 0.525 and 0.555. Currently, the specification is that the COR must be less than or equal to 0.555 for a ball impacting a stationary wall at an initial velocity of 85 ft/sec (58 mph). The physical specifications on baseballs used in NCAA games are: a ball shall weigh no less than 5 oz and no more than 5.25 oz; the circumference of the baseball shall be no less than 9 in and no more than 9.5 in. The final stipulation is that the ball shall be formed by yarn wrapped around a small core of rubber, cork or a combination of the two, and it shall be covered by two pieces of white horsehide or cowhide tightly stitched together.

The current test method for measuring the COR is ASTM 1887, Standard Test Method for Measuring the Coefficient of Restitution (COR) of Baseballs and Softballs.[12] It uses a ball-throwing device, for example a pitching machine, to propel a ball towards a fixed, flat wall. The velocity of the ball just before impact is 58 mph and the strike plate is made from either 2-inch thick steel or 4-inch thick northern white ash. The velocity of the ball before and after impact is measured using a set of electronic speed gates set 12 inches apart, and the COR is then calculated as the incoming speed divided by the rebound speed.

Crisco noted that the major limitation of the ASTM COR test is the unrealistic inbound velocity of 58 mph. Realistic pitch velocities for a college game range from 75 to 85 mph and bat swing speeds are in the 70 mph range (i.e., the linear velocity of the

bat at the point of impact is 70 mph). The total collision speed would be the sum of the two, equal to 150 mph, well above the experimental speed of 58 mph. There is some debate as to whether this COR test can accurately predict ball performance because the test uses a flat surface, not a cylindrical surface simulating a baseball bat barrel. Given that there are many factors which influence the COR of a baseball, Crisco concluded that the current specification is insufficient for predicting ball performance at realistic velocities.

2.4.2.2 Ball Compression Testing

A baseball is a complex object consisting of nonlinear materials such as leather, yarn, rubber and cork. A cross-section of a baseball is shown in Figure 2.10. Because the ball is nonlinear, it is difficult to quantify baseball field performance other than using a COR test at elevated game speeds. One attempt to supplement the COR testing is to quantify the nonlinear stiffness of baseballs using a compression test, an example of which is shown in Figure 2.11.

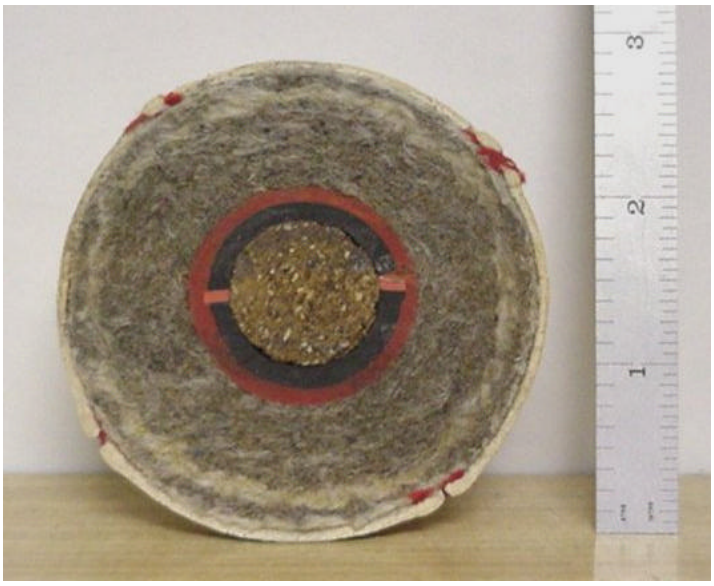

Figure 2.10 – Cross-section of a baseball.

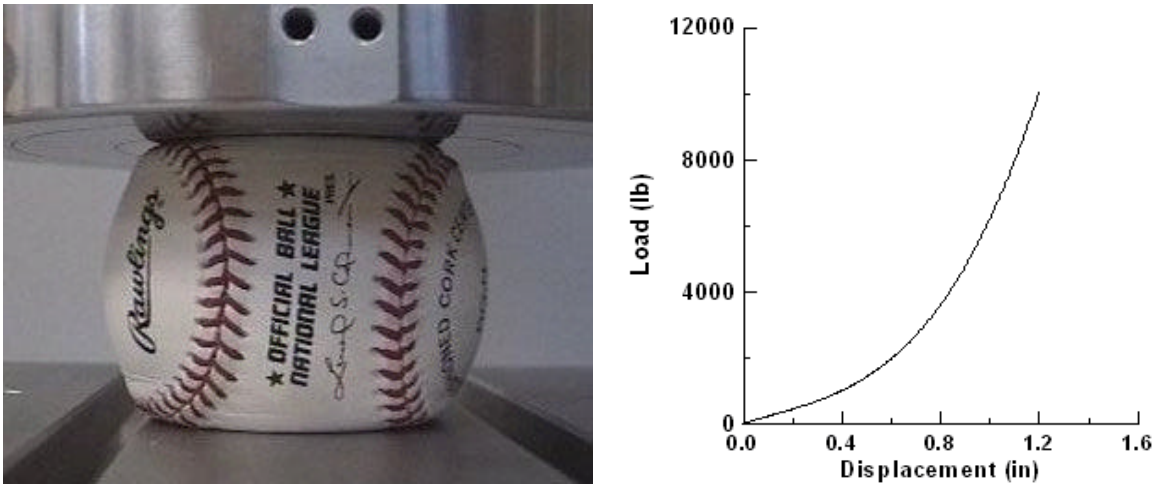

Figure 2.11 – An example of the ASTM ball compression test and resulting data.

ASTM 1888, Standard Test Method for Compression-Displacement of Baseballs and Softballs[13] uses a static compression test to measure the load reached when the ball is compressed 0.25 in between two flat plates. It is a relatively easy test to perform, and it gives a quantitative measure of ball hardness. Unfortunately, it is difficult to extrapolate the ball compression from a static event (0.25 inches of displacement over 12 to 15

seconds) and apply it to a highly dynamic event of a bat-ball collision where the ball is compressed and returns to its original shape in less than 100 milliseconds. Test results from two different ball manufacturers are shown in Table 2.3. The difference between the maximum loads reached between the two sets of 6 baseballs was 68.1 lb. This variation has been observed in experimental batted-ball velocity measurements, where one ball has a higher average exit velocity than another ball when hit with the same bat. However, the potential correlation between a *static* ball compression test and the *dynamic* batted-ball velocity is not fully documented and is not covered in this thesis.

Table 2.3 – Ball compression test results.

Ball Manufacturer & Model	**Rawlings R1NCAA**	**Wilson A1001SST**
Average Weight (oz)	5.108	5.101
Average Load (lb)	353.4	421.5

2.4.3 Predicting Bat Performance

There are two testing methodologies considered for predicting baseball bat performance. The first is ASTM 1991, Standard Test Method for Measuring Baseball Bat Performance Factor[14] as developed by New York University physicist Dr. Richard Brandt, Ph.D. It uses a value called the Bat Performance Factor, or BPF, which is a ratio of the COR of a bat-ball collision and the COR of the same ball impacting a flat, rigid wall. The second methodology uses the Baum Hitting Machine (BHM), developed by Baum Research and Development. This machine uses large servomotors to swing a bat and a ball toward each other at specified velocities and then measures the exit velocity of the batted-ball after impact.

2.4.3.1 Brandt Test and the BPF

The Brandt test uses an air cannon to impact a cantilevered bat on a freely rotating turntable with a baseball, as shown in Figure 2.12. By measuring the inbound velocity of the baseball before impact and then measuring the rebound velocity of the bat after impact, the bat-ball COR is calculated using Equation 2.18:

$$COR_{bat-ball} = \left(1 + \frac{I}{wR^2}\right)\left(\frac{DRt}{drT}\right) - 1 \qquad \textbf{Equation 2.18}$$

where:

D = distance between bat-speed sensors (in)
d = distance between ball-speed sensors (in)
I = moment of inertia ($oz\text{-}in^2$)
R = location of the center of percussion (in)
r = radius of bat speed sensors (in)
T = time for bat to travel through bat speed sensors (s)
t = time for ball to travel through ball speed sensors (s)
w = weight of ball used in test (oz)

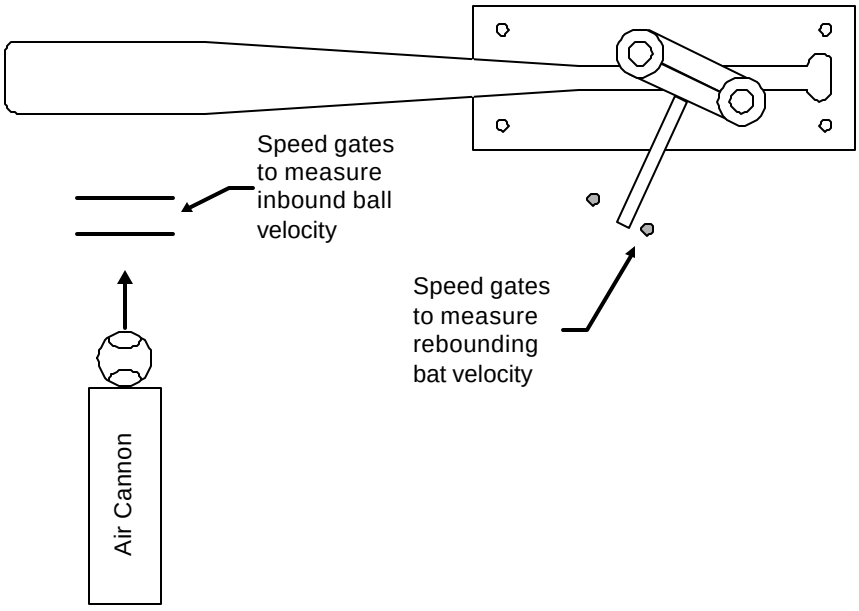

Figure 2.12 – Schematic of Brandt test setup.

The BPF is then calculated as the $COR_{bat\text{-}ball}$ divided by the ball COR as found using ASTM 1887. The batted-ball speed can then be related to BPF by:

$$V_{batted\,ball} = \frac{V(1+e)+v(e-k)}{(1+k)} \qquad \textbf{Equation 2.19}$$

$$k = \left(\frac{w}{W}\right) + \left(\frac{w(R-a)^2}{\left(1-Wa^2\right)}\right) \qquad \textbf{Equation 2.20}$$

where:

V = bat speed (*mph*, measured at point of impact at COP of bat)
v = pitch speed *(mph)*
w = ball weight (*oz*)
W = bat weight (*oz*)
I = moment of inertia ($oz\text{-}in^2$)
e = bat-ball COR (equal to $BPF \cdot COR_{ball}$)
a = distance from pivot to bat center of mass or balance point (*in*)
R = location of COP (*in*)
k = bat-ball inertia ratio (grouping term)

Crisco notes that although the Brandt method has gained wide acceptance, it does not test bat performance at realistic game velocities. Measurements are made at 60 mph and mathematically extrapolated to the desired elevated velocity. Typical values range from 1.0 for wood bats to 1.14 for metal bats. On the other hand, the BHM can test at any combination of velocities, up to a combined 200 mph, and directly measure the COR at these velocities.

2.4.3.2 Baum Hitting Machine

Larry Fallon of Sports Engineering, Dr. James Sherwood of the University of Massachusetts, Lowell and consultant Dr. Robert Collier, were commissioned by MLB to perform a complete and thoroughly independent evaluation of the BHM.[15] This UMass Lowell group also proposed a standard protocol using the BHM to evaluate the

performance of baseball bats. They concluded that the BHM is a state-of-the-art machine capable of accurately measuring ball exit velocity. The BHM, shown in Figure 2.13 has the capability of swinging a bat at speeds up to 100 mph at the contact point and pitching a ball at up to 100 mph.

Figure 2.13 – Assorted views of the BHM.

The operator controls the BHM's movements by setting the coordinates of the bat-ball impact and individual speeds of the bat and ball and records the impact data from the control area, as shown in Figure 2.13(a). The bat-ball impact setup is observed as shown in Figure 2.13(b). A baseball bat is mounted in the bat holding fixture that sits atop one of the motors, while the ball is held in place in the ball "tuning fork" fixture attached to the other motor shown in Figure 2.13(c). Sets of light cells and speed gates measure the

exit velocity of the ball as it moves away from the impact. The ball is eventually stopped by the collection net shown in Figure 2.13(d).

2.4.3.3 Boundary Condition Effects at the Handle

With respect to the two different methodologies, they both test use a rigid or semi-rigid clamping fixture to hold the baseball bat in place as impacts with the baseball. As a result, Crisco concluded that both methods are limited in that they do not consider the biomechanical factors of the batter. However, in research conducted by Van Zandt[16], it was shown through normal mode analysis using computer modeling that hitting performance is independent of boundary conditions prescribed on the handle of the bat and thus allowing the bat to be studied as a "free-body" model. This normal mode analysis showed that the displacement in the bat caused by an impact with a ball, does not propagate to the handle before the ball leaves contact with the bat. Therefore, the boundary conditions at the handle do not play any role in the ball's trajectory or exit velocity. This point is also reinforced with finite element modeling of the bat-ball collision to be discussed later in this thesis. Crisco pointed out that during testing, the bats are rotated about a fixed point on the handle. In contrast to these test methods, an actual batter's swing is a complex combination of rotation and translation, with mostly rotation somewhere between the player and the knob of the bat just before and after impact. Detailed finite element modeling simulating the boundary conditions of the BHM, including a study of the effects of a rotating bat versus a translating bat, was conducted to understand and support the mechanics of the machine. This modeling will be discussed later in this thesis.

2.4.4 Effects of Bat Mass and Inertia

The length-to-weight unit difference is a bat property that is restricted by NCAA rules. It should be noted that the length-to-weight unit difference could be no more than 5 (measured with the grip) at the time of Crisco's report in November 1997; it was changed to no more than 3 (measured without the grip) effective January 1999. Two studies reviewed here show that the moment of inertia (MOI) has a more dominant effect on swing velocity than weight. These studies calculated the MOI about a point on the batter's body located 20 in from the knob end of the bat. They showed that swing speed increased as bat MOI decreased and that over the small range of swing velocities they examined, the relationship between swing speed and MOI was assumed to be linear.

2.4.4.1 Effect of Bat Mass and Inertia on Swing Speed

Fleisig, et al.[17] at the American Sports Medicine Institute (ASMI) investigated the effect of bat mass and inertia on swing velocity by using a high-speed motion-analysis system to measure the swing speed of a baseball bat. They examined the swing speeds of 17 collegiate players using regular aluminum bats and aluminum bats modified by placing a large or small weight at the barrel or the handle. The players then used the bats in a controlled environment, batting balls pitched from a baseball pitching machine. The pitch speed was approximately 58 mph and the machine was located 42 ft from home plate. A statistical analysis of the measured linear velocity of the sweet spot and angular velocity of the bat was then performed.

The ASMI group found that bat swing speeds increased as the bat MOI decreased. This finding was based on the linear velocity data because an ANOVA analysis revealed significant differences among the linear velocities but not for the angular velocities.

Based on the regression, the bat speed (linear velocity of the sweet spot in *mph*) can be predicted by:

$$V = 69.6 - 48.7 \cdot I \qquad \textbf{Equation 2.21}$$

where I is the MOI about the bat handle in units of $lb_f{}^{x}ft^{x}s^{2}$.

2.4.4.2 A Method to Measure Swing Speed

Koenig, et al.[18] at Mississippi State University (MSU) used 20 college-level players and measured their swing speeds using sensors mounted in the ground at home plate. The baseball bats used in this study were a mix of regular high-performance aluminum bats and modified bats with a weight located on the inside of the bat barrel or handle. The lengths of all the bats were 34 in, thus the unit difference between the weight and length of each bat was achieved by altering the weight of the bat. Baseballs were pitched from a baseball pitching-machine at 64 mph located 48 ft from home plate. Baseballs were also hit off a tee. Bat-speed data was collected and fitted to least-square linear curves based on relationships between MOI versus bat speed and the length-to-weight unit difference versus bat speed.

Comparing the bat speeds for pitched versus tee-ball swings, the data for the pitched ball show that there was a slight decrease in bat speed as the MOI increases, while there was no change in bat speed for balls hit off the tee. The MSU group relates these linear curve fits to the MOI using the physical parameters involved in swinging the bat. To idealize the actual swinging of a baseball bat, they assume that the bat's motion is starting from rest and is in pure rotation about a fixed axis. They conclude that the changes in bat speed (in *mph*) as a linear function of the changes in MOI from bat to bat can be expressed by:

$$\Delta V = r \cdot \sqrt{\frac{2qT}{I_{ref}}} \cdot \left(1 - \frac{\Delta I_{bat}}{2I_{ref}}\right) \qquad \textbf{Equation 2.22}$$

where $r \cdot \sqrt{2q}$ relates the angular and radial position of the sensors; $\sqrt{\frac{2qT}{I_{ref}}}$ is a measure of the angular velocity that a batter can give to a reference bat with an MOI of I_{ref} by applying a torque T; and $\left(1 - \frac{\Delta I_{bat}}{2I_{ref}}\right)$ is the amount of change in the angular velocity due to changes in MOI. In layman's terms, the MSU group notes that a 10% increase in the MOI will result in a 4-mph decrease in bat speed over the outside of home plate for swings at pitched balls. It is noted that all bat-speed measurements are made from the outside edge of home plate, not at any specific point on the baseball bat. Additional sensors could be located at different positions at home plate in order to measure different points on the bats.

2.4.4.3 The Ideal Bat Weight

Watts and Bahill[19] discuss what the ideal bat weight should be in order to get the maximum batted-ball velocity. The conservation of momentum and COR equations for the bat and ball in pure translation are given as

$$m_{Ball} v_{Ball_i} + m_{Bat} v_{Bat_i} = m_{Ball} v_{Ball_f} + m_{Bat} v_{Bat_f} \qquad \textbf{Equation 2.23}$$

$$e = -\frac{v_{Bat_f} - v_{Ball_f}}{v_{Bat_i} - v_{Ball_i}} \qquad \textbf{Equation 2.24}$$

These equations can then be solved simultaneously to yield an equation for the velocity of the ball after the collision:

$$v_{Ball_f} = \frac{(m_{Ball} - em_{Bat})v_{Ball_i} + (m_{Bat} + em_{Bat})v_{Bat_i}}{m_{Ball} + m_{Bat}} \qquad \textbf{Equation 2.25}$$

For example, consider a 34-inch 31-ounce bat swung such that its linear velocity at the point of impact was 70 mph. A baseball weighing 5.125 *oz* is traveling at a constant 70 mph in the opposite direction. The COR of the ball is 0.55. The resulting exit velocity of the ball would be 116.2-mph. Increasing and then decreasing each parameter in Equation 2.11 by 10% from the example values can determine the parameters that most affect the batted-ball velocity. The results of this parametric study are shown in Table 2.4 and on the surface show that the COR and the bat swing-speed most affect the batted-ball velocity. Hidden within this parametric study is the relationship between the MOI and swing speed.

Table 2.4 – Results of parametric study.

Parameter Change	Batted-ball Velocity (mph)	Percent Change
Using original values	116.2	0%
Ball weight -10%	118.9	2.3%
Ball weight +10%	113.6	-2.2%
Bat weight -10%	113.3	-2.6%
Bat weight +10%	118.6	2.1%
COR -10%	109.6	***-5.6%***
COR +10%	122.8	***6.0%***
Pitch speed -10%	113.9	-1.9%
Pitch speed+10%	118.5	2.0%
Bat swing speed -10%	106.9	***-7.8%***
Bat swing speed +10%	125.5	***8.7%***

Because rules govern what the COR value of the baseball should be, the players have no control over that parameter. On the other hand, a hitter does have control over the swing speed of the bat. Obviously a lighter bat can be swung faster, but as shown in the

study of Equation 2.25, a decrease in bat weight results in a loss of momentum before the collision and a decrease in ball exit velocity. Also, there are rules prescribing a minimum weight for bats. Therefore, the objective is to make a bat easier to swing, yet maintain the same weight. Altering the location of the *cg* of the bat, which in turn alters the MOI value of the bat, is the simplest solution.

3 EXPERIMENTAL TESTING

Finite element modeling is commonly used in the design process. In order to avoid the old adage of "garbage in equals garbage out" and to reach a certain level of confidence that the modeling is valid, experimental testing is performed.

To validate the finite element models of the bat and ball used in this thesis, experimental testing was conducted using three methods. The first method looks at the mechanics of the BHM itself and collects actual batted-ball velocity data for wood and non-wood bats using the BHM. The second method of validation involves a physical calibration of the baseball bat so the finite element model not only matches the length and weight of the bat, but also the baseball bat's *cg* location and natural frequencies. The last step was to calibrate the baseball model separately using the ASTM COR test method. Because the emphasis is on predicting relative bat performance, detailed experimentation on the baseball was not conducted and is beyond the scope of this thesis.

The following sections describe the experimental data that was collected and how it was used to validate the finite element models of the baseball bat and ball.

3.1 BHM Experimental Data

As previously described, the BHM is a state-of-the-art machine that is used to simulate realistic swing and pitch speeds in order to measure the batted-ball velocity. Initial use of the BHM by Sports Engineering and UMLBRC included a thorough investigation of the testing procedures and equipment used before it could be qualified as an NCAA-approved testing method. One test designed to examine the BHM was to use an instrumented bat while collecting batted-ball velocity data.

3.1.1 Instrumented Bat Impacts

In an attempt to compare bat-ball impacts from the BHM to field impacts, one metal and one wood baseball bat were instrumented with accelerometers and strain gages to record the impact accelerations and bending stresses on the bat. An accelerometer / strain-gage pair was mounted on the barrel opposite the point of impact and at the handle approximately 3 inches from the pivot point as shown in Figure 3.1. Unexpectedly high acceleration levels were recorded that resulted in clipping errors, saturating the accelerometers, as shown in Figure 3.2.

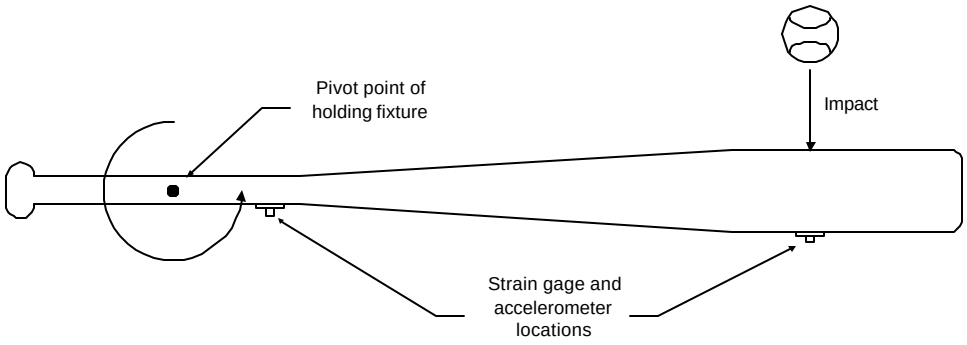

Figure 3.1 – Sensor location for BHM instrumented bat impacts.

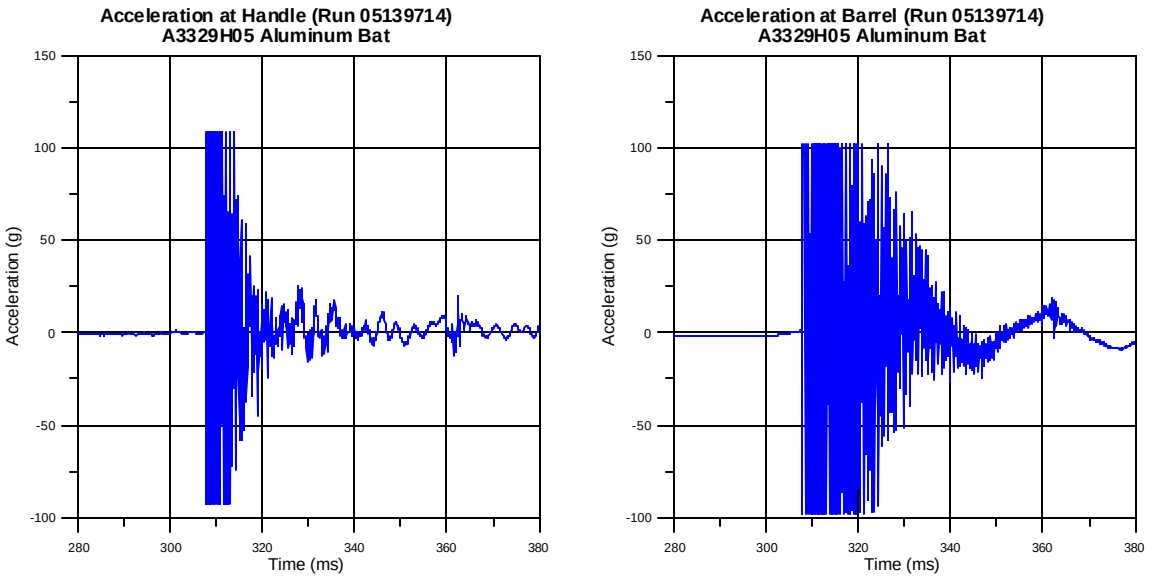

Figure 3.2 – Example of clipped acceleration data for metal bat impacts.

The strain gage data was used to investigate the BHM torque motor used to swing the baseball bat through the point of impact and its affects, if any, on batted-ball velocity. If a servomotor is met with resistance, the servo-loop will increase the motor power in order to reach the prescribed rotational velocity. If the servomotor power is increased while the bat is in contact with the baseball during impact, it could potentially add energy to the ball as it leaves the bat, artificially increasing the ball exit velocity. Examination of the strain gage data at the handle of the baseball bat in Figure 3.3 shows that the bat does coast to the impact with the ball, and that the angular velocity of the bat is no longer under the influence of the servomotor. This coasting is also significant from a modeling point of view in that a simple initial velocity can be applied to the bat instead of a more complex velocity profile as a function of the servo-loop response of the bat-ball impact.

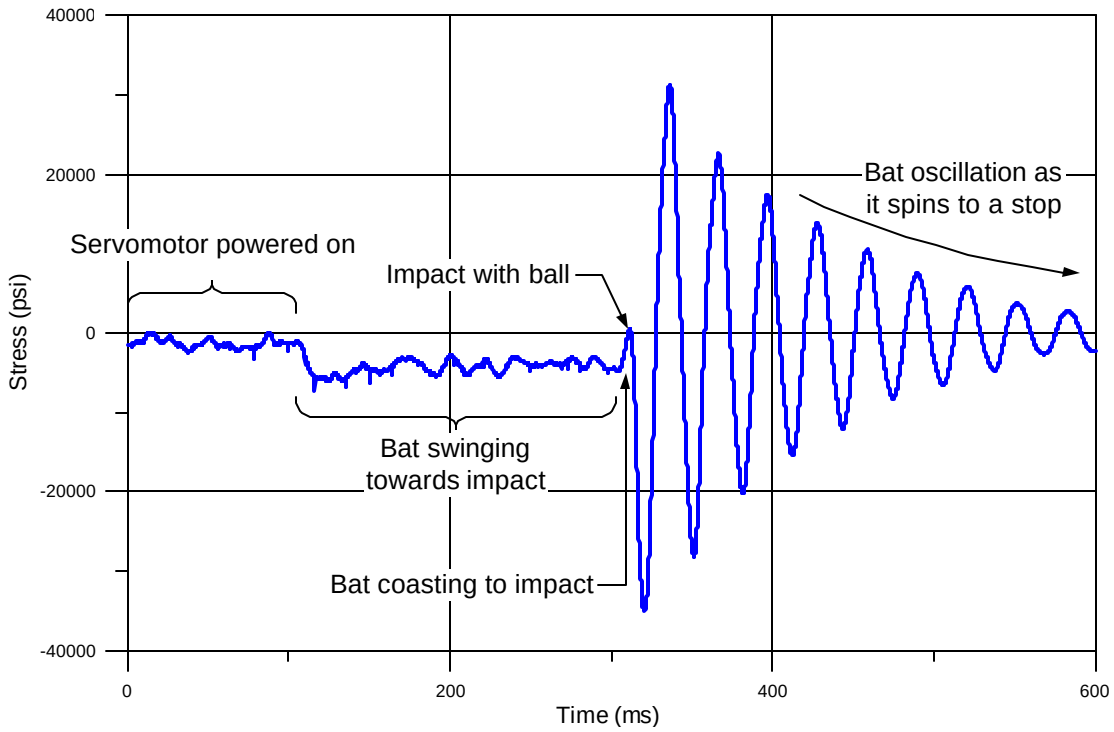

Figure 3.3 – Calculated bending stress at the handle for a metal bat impact.

Further examination of Figure 3.3 reveals the different stages of the bat's motion during BHM testing. In the first 100 ms, the bat is essentially at rest, but is vibrating as a result of the powered servomotor. At approximately *t=110 ms*, the servomotors are fired, causing the bat to bend back due to the applied angular velocity. Approximately 5 ms before the bat and ball collide, the servomotor for the bat is shut down, allowing it to coast into the collision, shown at approximately *t=300 ms* in Figure 3.3. As a result of the impact, the bat handle is subjected to large oscillating bending stresses that decrease in amplitude as the bat spins to a stop.

3.1.2 BHM Batted-Ball Velocity Data

The BHM is used to provide batted-ball velocity data in a laboratory setting using realistic pitch and swing speeds. A schematic of the BHM is shown in Figure 3.4. Once the bat and ball have been properly mounted and the test documentation is configured in the control panel screen, shown in Figure 3.5, the servomotors are triggered causing the bat and ball to rotate towards each other. Due to the impact with the bat, the ball is propelled through a set of light cells. The inbound velocities of the bat and ball, as well as the ball exit speed measured at 9 and 13 inches away from the point of impact are calculated by the data acquisition system and displayed in the control panel. A second independent set of speed gates measures the ball exit speed at 72 inches from the point of impact. To locate the maximum batted-ball velocity point on the bat, impacts are collected at 5 positions along the length of the barrel, starting at 6 inches from the barrel end of the bat, then at 7.0, 5.0, 6.5 and 5.5. Unless data at all impact positions is desired, testing of the bat can be considered finished when the maximum batted-ball velocity point has been found.

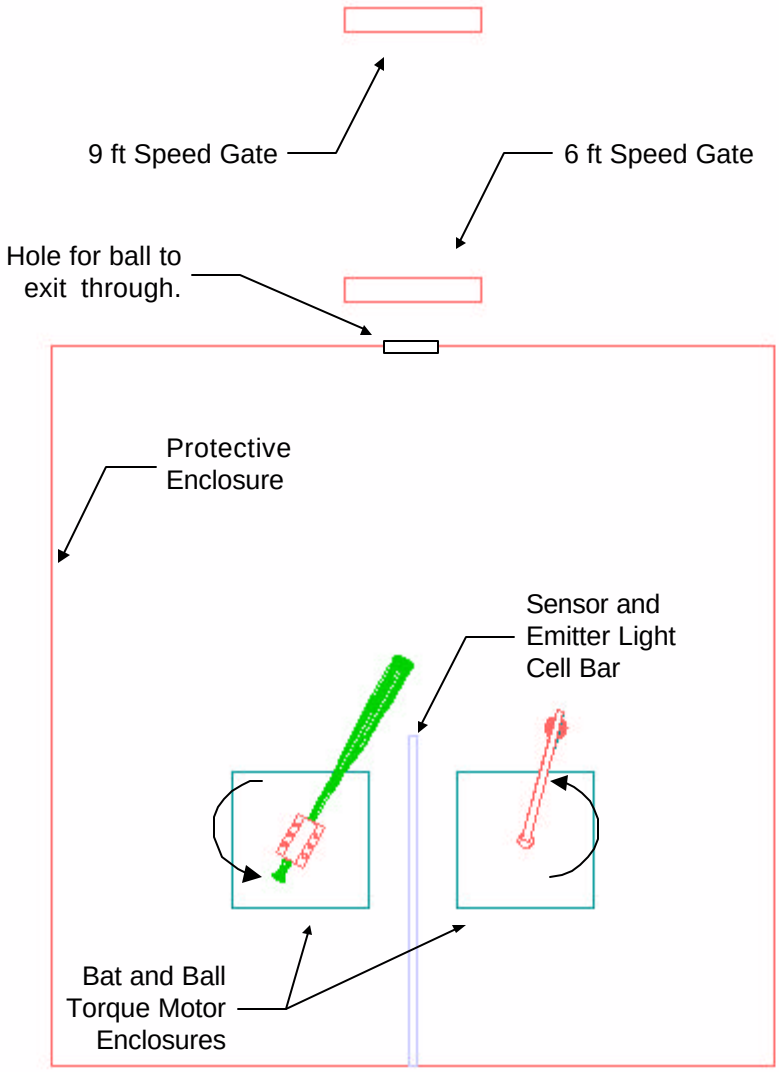

Figure 3.4 – BHM schematic, overhead view.

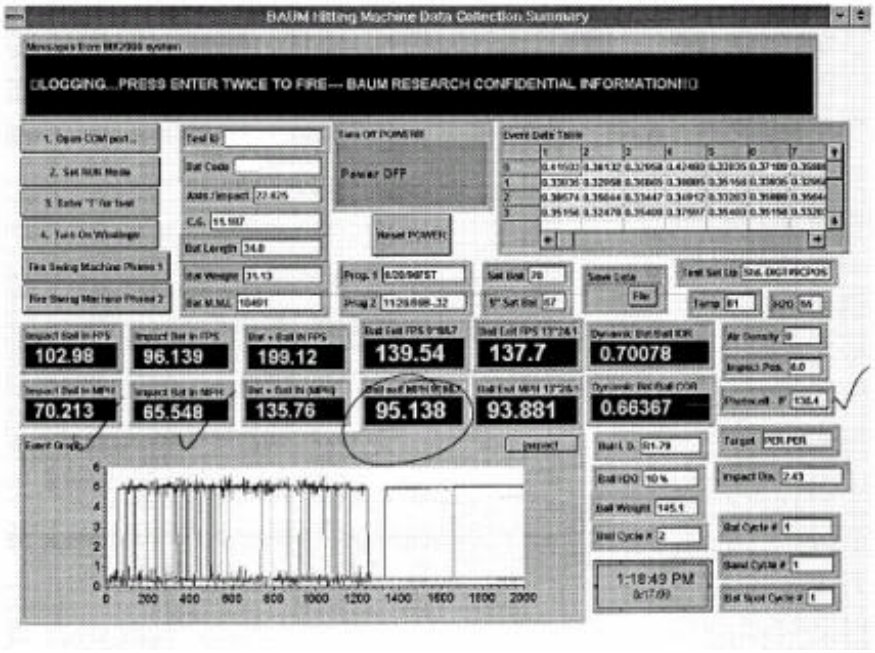

Figure 3.5 – Sample BHM data sheet.

3.1.2.1 Baum Bat and Ball Data

Due to its wood-like performance and increased durability over wood bats, the Baum Bat is a composite bat that is used in the BHM as calibration tool in an attempt to control and quantify the variability from one baseball to another. Baseballs must go through a certification process before they are used to measure bat performance.

Tested in lots of approximately 120, the baseballs are first numbered and weighed to ensure that they meet weight requirements set forth by the respective governing body. The on-weight balls are then tested in the BHM using the Baum Bat to collect batted-ball velocity data. All BHM testing described herein was recorded using bat swing speeds of 70 mph at the 6-inch impact location and pitch speeds of 70 mph. The average exit speed for the entire lot is calculated. Limits of ±1.5 mph are imposed on the data, with any balls lying outside this range removed from testing. The plot in Figure 3.6 illustrates the

variability in two lots of baseballs with ±1.5 mph limits imposed on ball exit velocity. The baseballs in each lot are from the same manufacturer and hit with the same baseball bat. In this case, there is a negligible difference in the average exit velocity of the two lots: 92.11 mph for Lot "A" versus 92.38 mph for Lot "B", but it may not be negligible when comparing a Lot "C". The ball certification is discussed here only to show that some variability in the baseball is recognized and attempts are made to address the abnormalities.

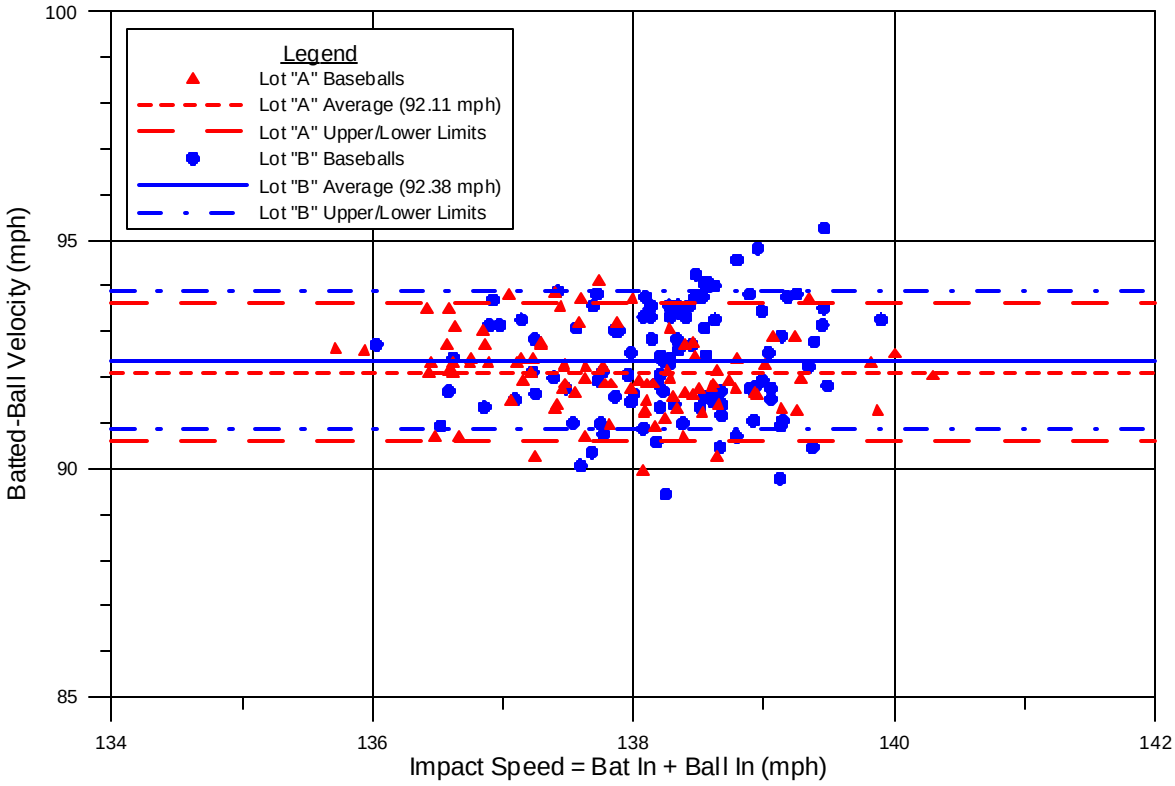

Figure 3.6 – Example of variability within and between ball lots (valid hits only).

3.1.2.2 Wood Bat Data

Wood bat testing with the BHM is limited to three impact locations at 5.5, 6 and 6.5 inches away from the barrel end of the bat. Beyond these three impact locations, the

durability of the wood bat is questionable. Once impacts move away from the sweet spot or center of percussion locations on the barrel, higher bending stresses are transmitted to the handle of the bat and when this impulse reaches the bat-clamping fixture on the BHM, it often causes the bat to break. The end result is that a large number of wood bats are needed for testing.

As previously discussed, the MOI, *cg* location, length, weight, swing speed and pitch speed all play a role in the batted-ball exit velocity. Therefore it is important to select the proper control parameters during testing in order to maintain an "apples-to-apples" method of comparison, as opposed to comparing "apples-to-oranges". In the following presentation of BHM data, the swing speed and pitch speed are held constant for each impact. The resulting data is then categorized by the length and weight of bats, such that only data within each length and weight combination is comparable. Other variables, such as MOI, *cg* location, the bat material (wood, metal or composite) and baseball test lot have to be taken into account when examining the data.

The wood bat data presented in Figure 3.7 are for two test lots of wood bats. The bats are all nominally 34 inches long and weigh 31 oz. The nine wood bats in Lot #1 have a *cg* location at approximately 11.125 inches from the barrel end of the bat. The *cg* location for the six wood bats in Lot #2 averages 11.3 inches. Even though deviations in the *cg* location for bats within each lot may cause the data to appear to have a linear behavior, experience shows that the batted-ball velocity data for each bat behaves in a polynomial fashion. Therefore, the lot is fitted with a polynomial trend line.

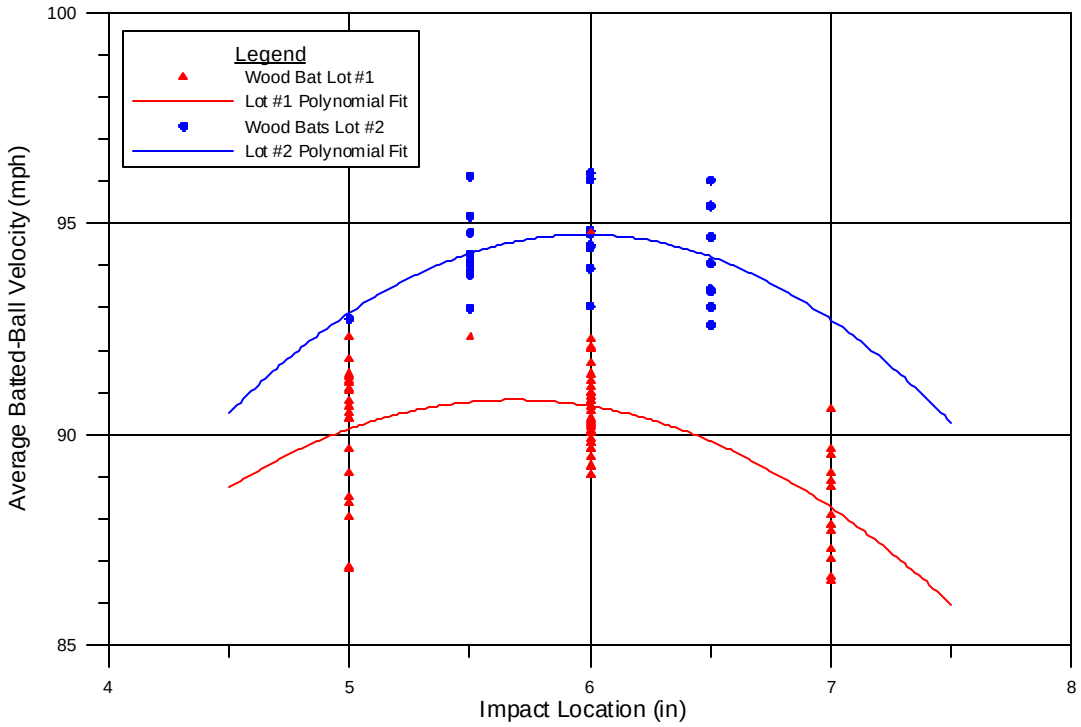

Figure 3.7 – Representative BHM data for wood bat performance.

In addition to the *cg* locations, other factors such as the quality of the wood stock, the moisture content and number of grains across the barrel can contribute to the spread of the data from bat to bat. The difference in peak batted-ball exit velocities between the two populations is approximately 3.5 mph and has been identified as the difference between baseballs from two different manufacturers used in testing these wood bats. The manufacturer of baseballs used in testing Lot #2 would be considered to make a "dead" ball when compared to the manufacturer of baseballs used for Lot #1. Given that the 3.5-mph difference between the two test lots is not a trivial amount, Figure 3.7 demonstrates how the baseball affects the performance of the baseball bat and that an "apples-to-apples" comparison of data must always be made.

3.1.2.3 Metal Bat Data

Two different sample populations were selected to examine the metal bat performance using the BHM, shown in Figure 3.8. The first set of five bats had an average *cg* location at 12.5 inches and MOI values ranging from 2915 to 3222 oz-in^2. The second set of six bats had an average *cg* location of 13.75 in and MOI values ranging from 3170 to 4085 oz-in^2. These MOI values were measured with respect to an axis of rotation at the 6-in location from the knob. All 11 bats were 34 inches in length and nominally weighed 31 oz.

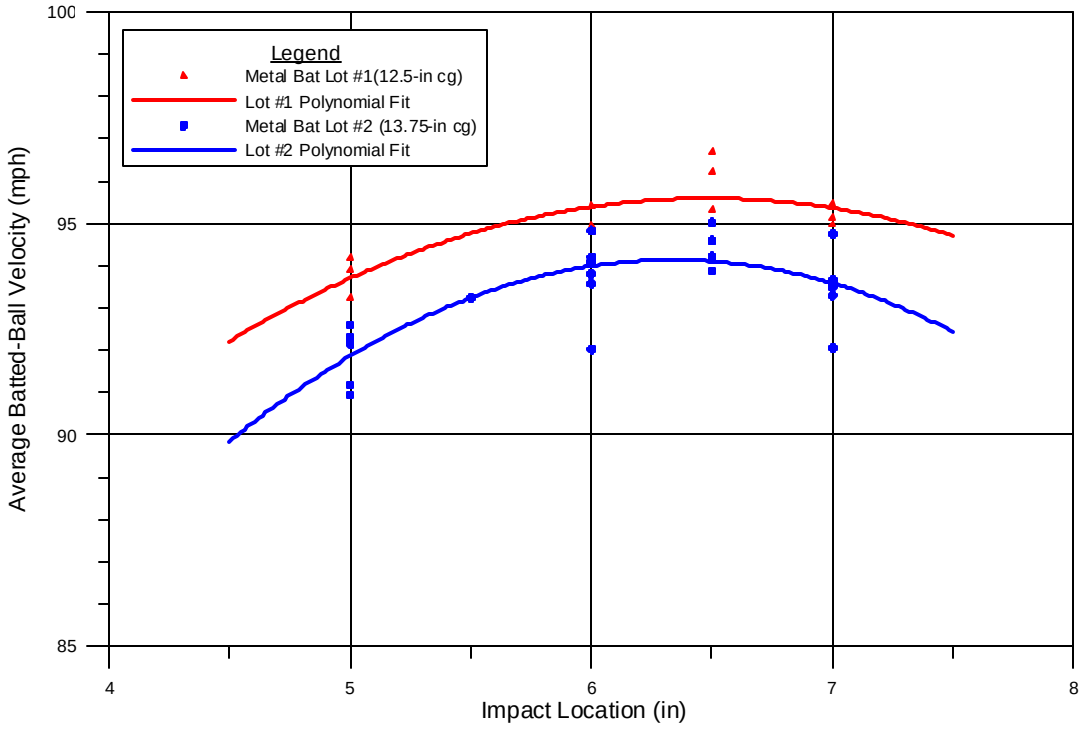

Figure 3.8– Representative BHM data for metal bat performance.

It should be noted that there is a 1.8-mph difference in the ball certification exit velocities between the two sample lots. If this 1.8-mph difference were added to the Lot

#2, the batted-ball velocities for the two sample populations would overlap. But now take into account the 1.25-in difference in *cg* location, and the 17.5% difference in MOI values; surely the batted-ball velocities cannot be equal. If data were taken with actual players instead of a machine, the batted-ball velocities would not be equal because it has been shown that MOI affects swing speed. However, the servomotors in the BHM are not sensitive to different MOI values. If the servomotor is programmed to swing the bat at 70 mph, then it will swing it at 70 mph, regardless of what the MOI value is for the bat under test.

Recall that the "apples-to-apples" method of comparison should be used to examine bat performance data. Because all tests were conducted using the same swing speeds and pitch speeds, and all the bats are nominally the same length and weight, comparing the average ball-certification exit velocity might help establish an "apples-to-apples" comparison. Even though they used different ball lots, Wood Bat Lot #1 and Metal Bat Lot #1 both had essentially the same average ball-certification exit velocities – 94.1 for the wood bats and 94.2 mph for the metal bats. A comparison of the data from these two lots is shown in Figure 3.9. This plot is similar to the Watts and Bahill derivation and plot of Figure 2.9 in that the peak batted-ball velocity for the metal bats is a little higher than wood, spread out over more of the barrel length than wood, and shows no signs of dropping off significantly as the impacts get closer to the handle.

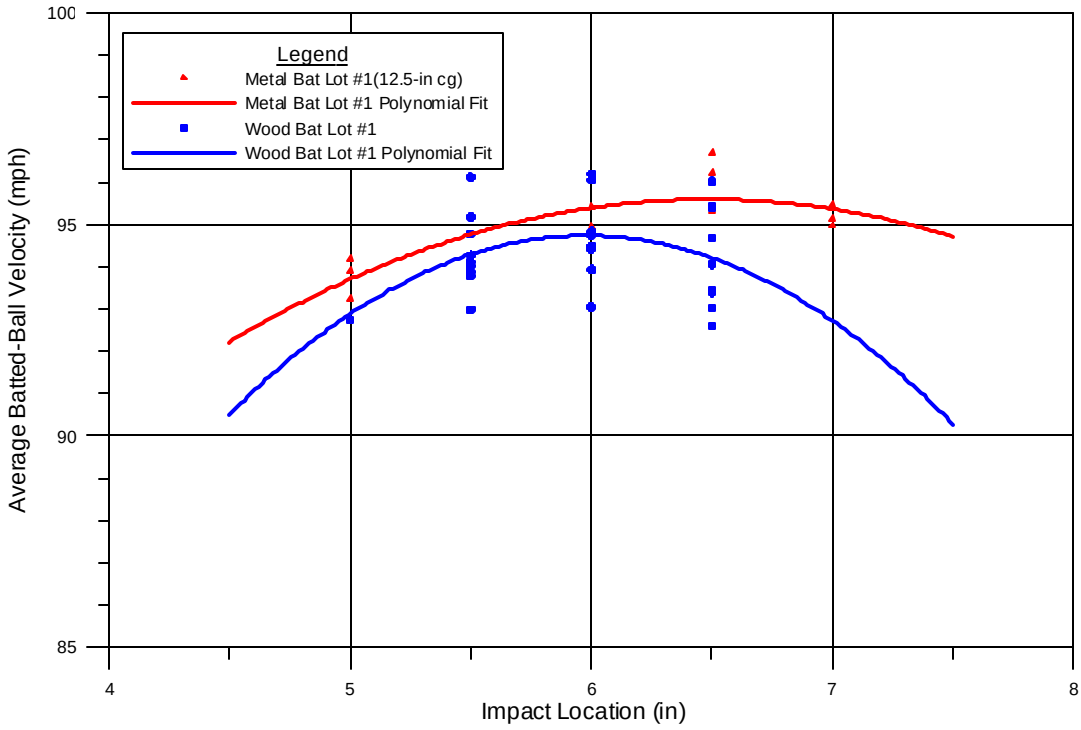

Figure 3.9 – Comparison of wood and metal bat BHM data.

Comparing the batted-ball velocity profiles (the polynomial trend lines) for the wood versus the metal bats used in this demonstration, the peak batted-ball velocity for wood bats is approximately 94.5 mph, where the peak for metal bats is approximately 95.5 mph. As a metric, let the sweet-spot length be defined as the total length of the barrel where the batted-ball velocity is within 1 mph of the maximum. For wood bats, this length, by inspection, is approximately 1 in. On the other hand for the metal bat profile, this length is over 2 in. The point being the metal bat has a higher batted-ball velocity over a longer length of the barrel.

3.2 Frequency Analysis

The primary method used to validate the baseball bat finite element models was to compare measured natural frequencies from an experimental modal analysis setup to results calculated from the finite element model. Physical attributes including length, diameter profile and in the case of metal bats wall thickness were used to create the model. Because of wall thickness approximations, the material's density was then adjusted to calibrate the weight and the center of gravity. Once the physical calibration of the finite element model was accomplished, the frequencies of the first and second bending modes were calculated and compared to experimental data.

3.2.1 Experimental Procedure

To measure the baseball bat's natural frequencies, a simple generic setup was used where the bat was suspended from the ceiling and supported at each end. An impact hammer was used to provide an excitation impulse, the response of which was measured at an accelerometer mounted on the barrel end of the bat. A dynamic signal analyzer recorded the input force amplitude and the acceleration response and then was used to provide an FFT of the results, quickly calculating and displaying the natural frequencies of the baseball bat.

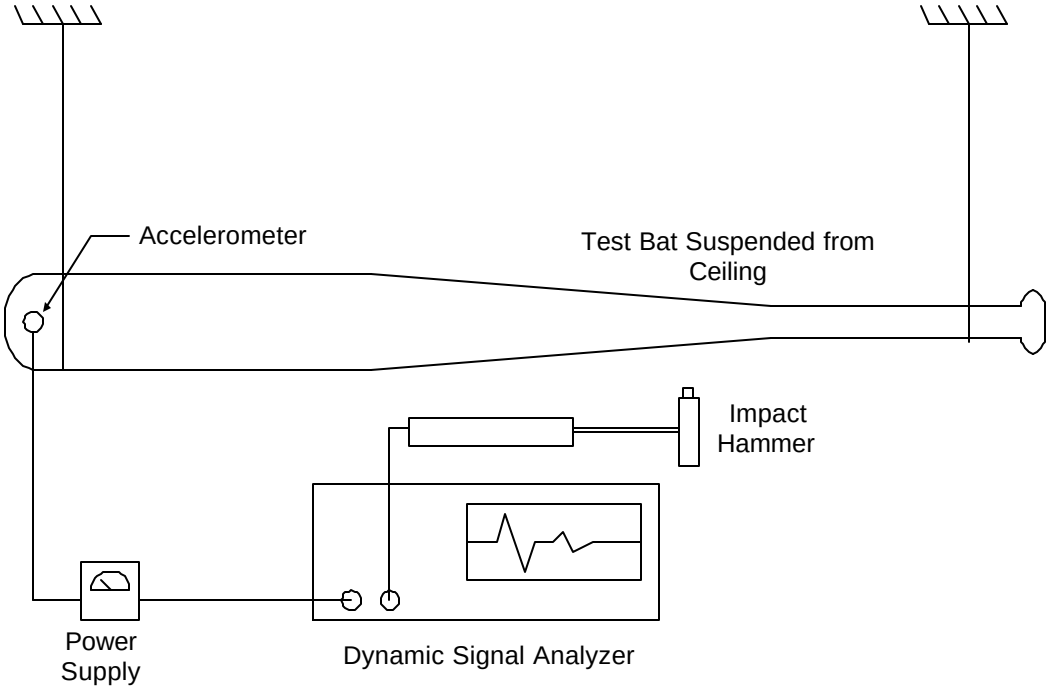

Figure 3.10 – Diagram of experimental modal analysis setup.

3.2.2 Results

The results listed in Table 3.1 show that the metal bat has higher first and second natural frequencies than the solid wood bat. These results will be examined later when used as a calibration metric for the finite element models.

Table 3.1 – Experimental frequency results.

Property	Wood Bat #3	Metal Bat #1
Weight (oz)	31.90	29.49
Length (in)	34	34
CG Location (in)	11.25	12.63
First Mode (Hz)	143	182
Second Mode (Hz)	481	656

3.3 Ball Compression Testing

In order to model a baseball, experimental data that can capture the nonlinear performance of the baseball must be collected. As previously discussed, ASTM 1888 is the standard test method to measure the compression-displacement of a baseball or softball. This method specifies that the user compress the baseball at a rate of 1 in/min and measure the resulting load at a maximum displacement of 0.25 inches. The load is then released, the ball is rotated 90° and the test is repeated. Although the load versus deflection history of the test can be captured, only the average compressive load at 0.25 in of displacement over two test runs is reported, making it a single data-point test that is used as a quantitative baseline comparison for baseballs.

A modified version of the ASTM test was used to collect data for the finite element baseball material model. Using an Instron 1332 testing machine, compression test data was collected on a PC-based data acquisition system. Three elevated crosshead speeds (3, 6 and 30 in/sec) were used, testing one official Major League baseball at each rate. The test was not stopped at 0.25 inches of displacement, but instead stopped at 10,000 lb of load. The difference in the data collected for the three different crosshead speeds was negligible. The average of the data from the three tests is shown in Figure 3.11.

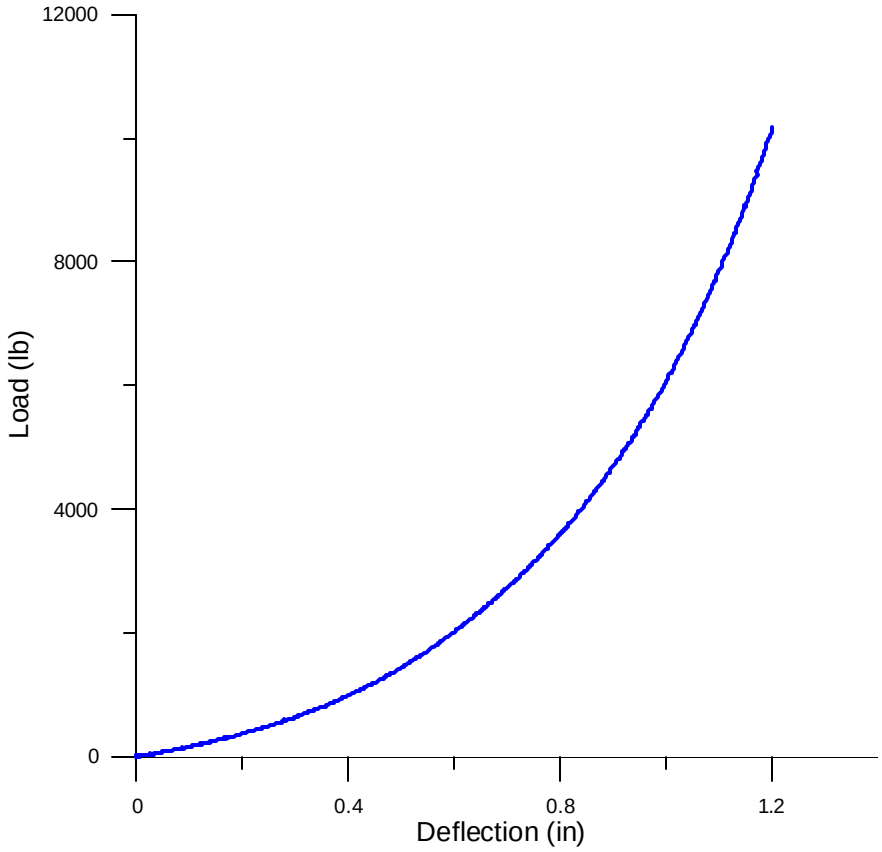

Figure 3.11 – Average load versus displacement results for three MLB baseballs.

4 MODELING

During the initial independent evaluation of the BHM, finite element modeling was used to examine different aspects of the bat-ball collision with respect to the mechanics of the BHM. Simple models were first created to examine the basic physics of the BHM. Then as more experience was gained with BHM testing and with using the various finite element analysis tools, more detail was incorporated into the finite element models. This included validating the baseball and baseball bat models with the experimental data previously described.

The following is an overview of the initial modeling. It is presented here to show the general process that went into developing validated models of the baseball bats and the baseball. An example of a corrected and updated aluminum bat model is presented in the following chapter where results are presented in greater detail along with lessons learned along the way.

4.1 Analysis Tools Used

The baseball bat and ball models were created using HyperMesh, (Altair, Inc.), a high performance finite element pre- and post-processing software package. Once the bat and ball models were created, input files were then generated and transferred for analysis using LS-DYNA (Livermore Software Technology Corp.), an explicit analysis package primarily used to model nonlinear dynamic problems. It has an extensive material model library and is able to model deformable contact. The time step size chosen for this type of non-linear dynamic analysis usually has an effect on the solution, and is automatically calculated by LS-DYNA roughly based on the speed of sound through the material for a given element size. Further details on the time step calculation can be found in the

Appendix. LS-DYNA also contains an implicit solver routine that was used for modal analysis. MSC/Nastran was also used for modal analysis on early baseball bat models.

Simple post-processing, for example looking at mode shapes, was done in HyperMesh. Plotting of time history data was done using LS-TAURUS. More complicated post-processing such as contour plots and animations were created and viewed in eta/FEMB, eta/PostGL and LS-POST, all part of the LS-DYNA software package distributed by LSTC.

Analysis jobs were run on several PC-based machines ranging from single-CPU Pentium II 150 MHz with 128 Mb of RAM to a dual-CPU Pentium II 233 MHz with 256 Mb of RAM to a dual-CPU Pentium II 550 MHz with 1 Gb of RAM. These specifications are presented here because some modeling assumptions were made as a result of computer resource limitations. An analysis job run on the single-CPU Pentium II 150 MHz machine might take 2 days, where that same analysis job run on the dual-CPU Pentium II 550 MHz machine would take 2 hours.

4.2 Early BHM Models

The first models created of the bat-ball impacts were very simple consisting of approximately 3,500 elements and 18,000 degrees of freedom (dof's). The finite element models for the baseball and wood bat were created using 8-noded solid brick elements while the hollow aluminum bat used 4-noded shell elements with a constant thickness of 0.095 in that was based on manufacturer's suggestions. The combined bat and ball models used for the impact analysis are shown in Figure 4.1. The mesh generated for each bat model was created from an outside-diameter profile of the bat along its length, with both bats measuring 34 in. A -5 aluminum bat (34 in, 29 oz) was used with a barrel

diameter measuring 2¾ in. The plastic cap was not included in the first aluminum bat models, but was added soon after as described in a later section.

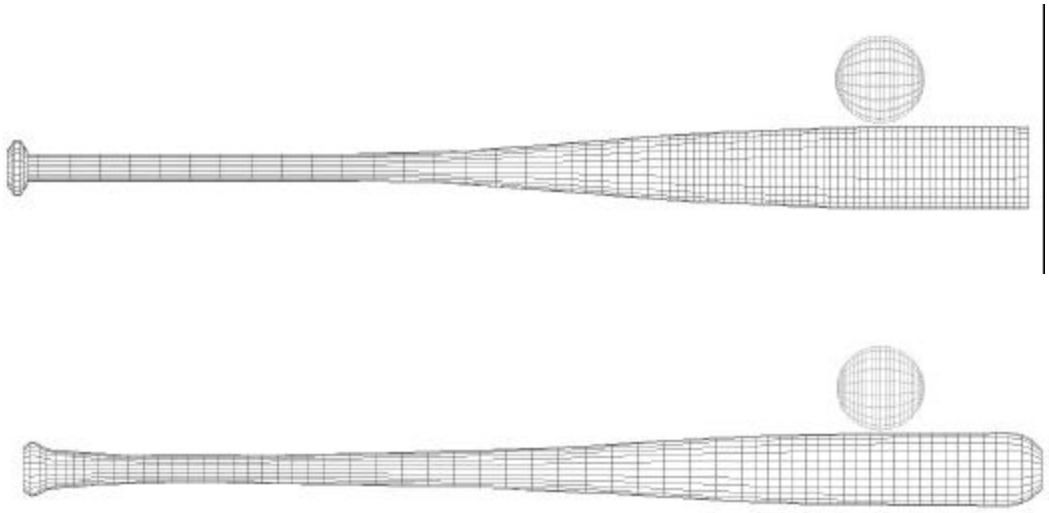

Figure 4.1 – Initial bat-ball impact models for the aluminum bat (top) and wood bat (bottom).

Isotropic material models were used for both the aluminum and wood bats as well as for the baseball, as shown in Table 4.1. The elastic modulus for the baseball was found by trial-and-error, calibrating the deformation results seen in the animation versus high-speed video of the ball compressing onto the barrel of the bat. However, as shown in the experimental data from the ball-compression testing, the load versus deflection curve is nonlinear. The elastic material model is used here for the baseball in order to achieve some modeling results. Using the measured diameter profile to construct the physical size of the bats, they were then calibrated for weight by adjusting the density value for the material.

Surface-to-surface contact was prescribed between the bat and ball. It should be noted that friction effects between the bat and ball were not modeled. The ball was given

an initial velocity of 70 mph and aligned with the bat to impact the bat on its centerline 6 in from the barrel end. The ball was not given a rotational velocity to simulate the spin of the ball, for example, as seen in a fastball. Instead, the ball impacting the bat simulated a pure knuckle-ball pitch. The bat rotational velocity was at first assigned to all the nodes in a 6-in long section of the handle of the bat, centered about the 6-in point on the handle that served as the axis of rotation. This was done to simulate the fixturing of the BHM. The magnitude was such that the linear velocity towards the ball would be 70 mph at the point of impact. This boundary condition was not effective however, because the ball would already come into contact with the barrel of the bat before the rotational velocity prescribed at the handle translated along the bat to the barrel. The rotational velocity prescribed at the handle was then resolved into an initial linear velocity prescribed along the length of the bat as a function of the distance from the 6-in pivot.

Table 4.1 – Summary of material properties used for initial modeling.

Property	**Baseball**	**Wood Bat**	**Aluminum Bat**
Elastic Modulus (psi)	1200	1.77×10^6	10.0×10^6
Poisson's Ratio	0.45	0.30	0.33
Density (lb/in)	0.024	0.026	0.100

The aluminum bat model was used during the initial BHM validation modeling because it had shorter CPU run-times than the wood bat. These basic initial models were sufficient to provide a relative metric for comparison, allowing for fundamental investigations into the physics of the BHM.

4.2.1 The 290° Swing vs. The 0° Swing

Early questions about the validity of the BHM involved the possibility of a whipping effect that the bat could be subjected to as the BHM servomotor spun the bat towards the ball. This whipping effect, if it existed with the BHM, may not be indicative of a human batter swinging a bat. To investigate this effect, two models were run, one that started the bat rotation similar to the actual hitting machine, rotated approximately 290° from the point of impact with the ball, and one that started the bat rotation immediately before impact in a "just-touching" condition with the ball at 0°. The starting point of these models is illustrated in Figure 4.2. It should be noted that these models simulated an 80-mph pitch and an 80-mph swing. For the 290° swing model, the initial velocity prescribed for the ball was "turned on" when the bat completed the 290° swing at was at the 0° location.

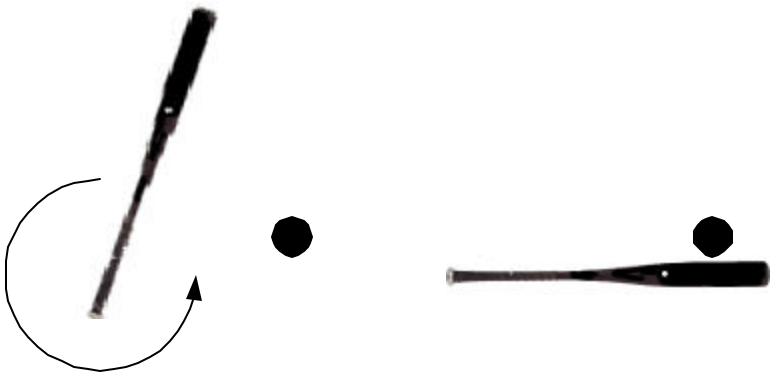

Figure 4.2 – 290° swing model (left) and 0° swing model (right).

The results of the modeling showed that there was a 5% difference in the exit velocities of the ball, as seen in Figure 4.3. For the 290°-swing model, the batted-ball

velocity was 161.2 mph and for the 0° swing, the batted ball velocity was 153.1 mph. These batted-ball velocities are unrealistic due to the elastic baseball. Nevertheless, the models served their purpose of providing a relative measure of the batted-ball velocity. The end result of this modeling study showed that the minor whipping of the bat did add to the exit velocity of the ball, but not significantly. However, it was decided that the 5% difference in batted-ball velocities could be tolerated in exchange for much quicker CPU run-times. Therefore, all future models of the BHM started the bat rotation just before impact.

It became quite clear that a simple elastic material model would not be acceptable to use for the baseball. Modeling efforts were then concentrated on developing a calibrated baseball model described in a later section.

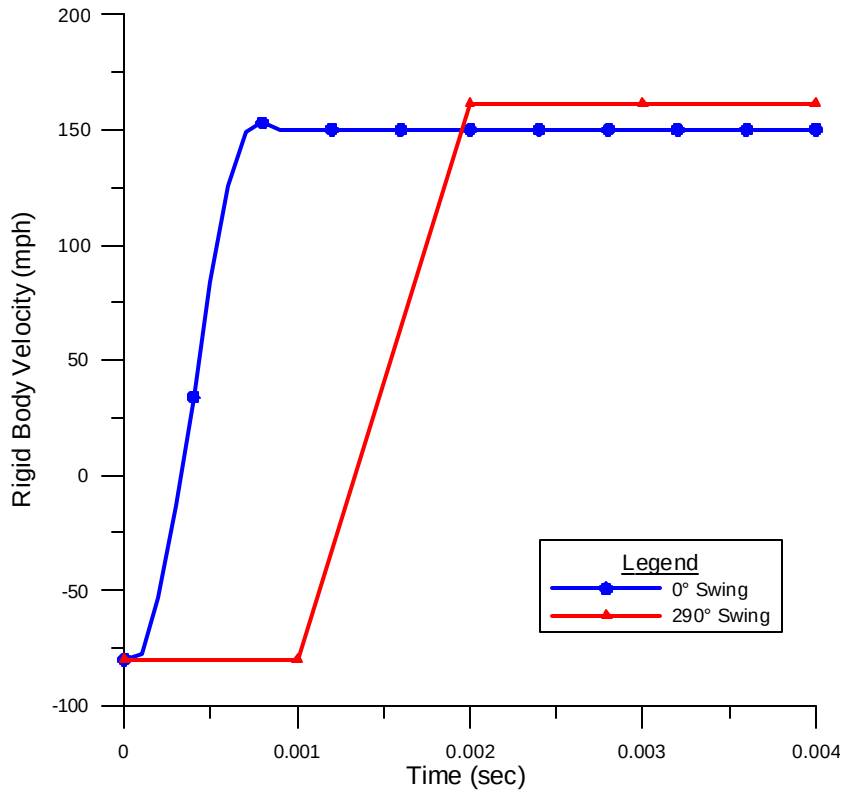

Figure 4.3 – Results of BHM swing study for 290° and 0° swings.

4.2.2 Rotation vs. Translation

After initial calibrated baseball models were developed, a second investigation using the baseball bat models involved the actual motion of the bat towards the ball before impact. The BHM spins the bat in a purely rotational fashion, while the actual swing is a combination of translation and rotation. Knowing the batted-ball velocities coming off a purely rotating bat versus a purely translating bat bound what the batted-ball velocity would be from the complex motion of the batter's swing.

The same bat models were used, except a simple plastic cap made using shell elements of constant thickness (0.25 in) was added to the aluminum bat model.

Whether the bat is given an initial angular velocity pivoting about the 6-in point on the handle causing the bat to rotate towards the ball or an initial linear velocity over the entire length of the bat causing it to translate towards the ball did not significantly affect the exit velocity of the ball. A plot of the two velocity conditions is shown in Figure 4.4 with a closer look at the maximum velocities shown in Figure 4.5. The baseball exit velocity for the rotating bat was 108.9 mph, while the translating-bat exit velocity was 109.2 mph. This negligible difference removes the concern of the machine's ability to simulate realistic batting conditions.

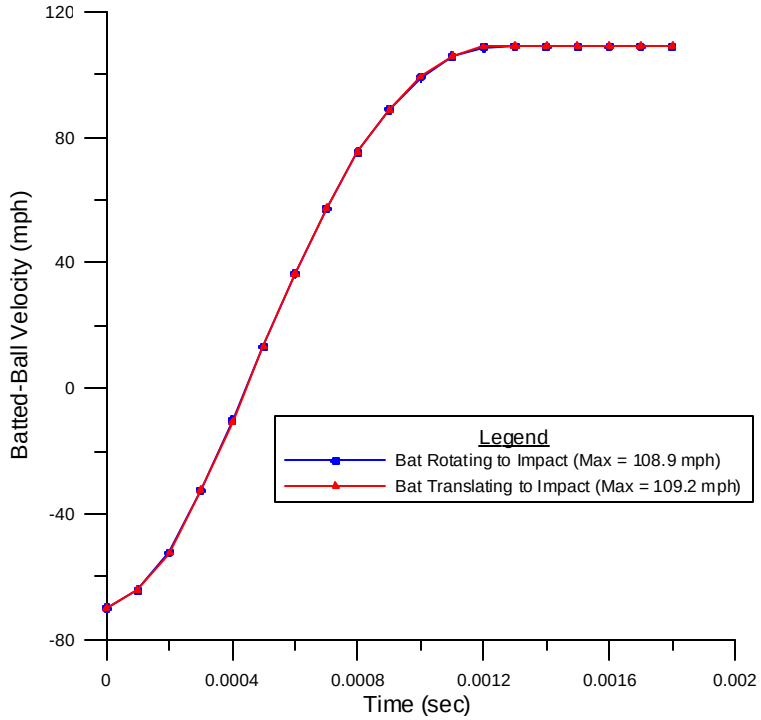

Figure 4.4 – Batted-ball velocity for an aluminum bat rotating and translating to impact.

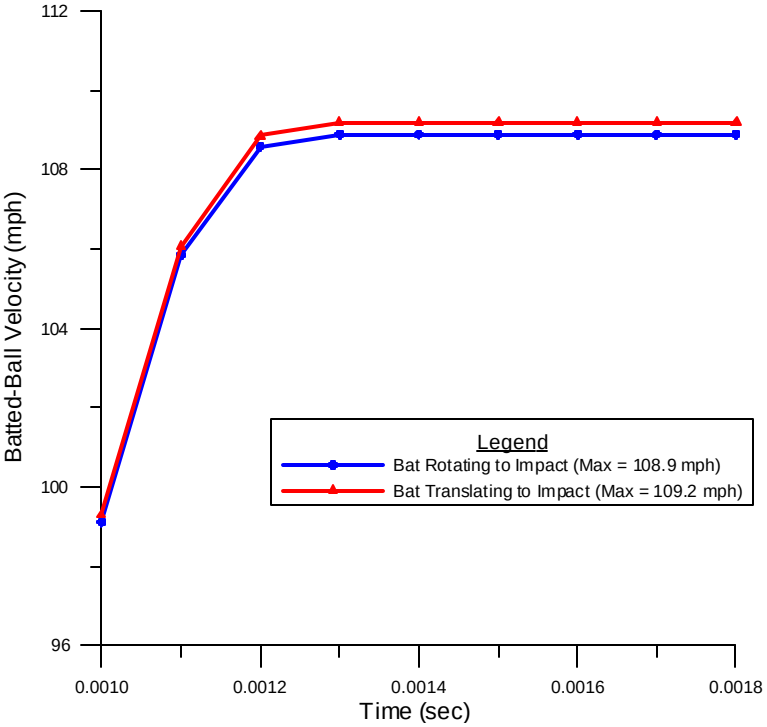

Figure 4.5 – Close-up of maximum batted-ball velocities.

4.3 Modeling Calibration

As more knowledge was gained through both experimental testing using the BHM and general finite element modeling, it became apparent that the initial bat and ball models would have to be better calibrated. By using a Mooney-Rivlin material model, a more realistic representation of the nonlinear stiffness of the baseball could be made by incorporating compression-test data. The baseball model was further calibrated by modeling the ball as tested per the ASTM COR test.

General improvements in the modeling of the bat and ball were made, which included the basic construction of the mesh to improve the mesh geometry, refinement of the mesh around the impact point, adding the plastic cap to the aluminum bat model and improvements in the material models used for the baseball bats. New bat finite element models are shown in Figure 4.6. An orthotropic elastic material model was implemented for the wood bats to model the directional properties of the wood, and an isotropic model with plasticity and kinematic hardening was implemented for the aluminum bat model. The natural frequencies of each baseball bat model was then calculated and compared to the frequencies found using modal analysis techniques. Adjustments were then made to calibrate the model to closely match the weight, *cg* location and 1^{st} and 2^{nd} natural frequencies that were experimentally determined.

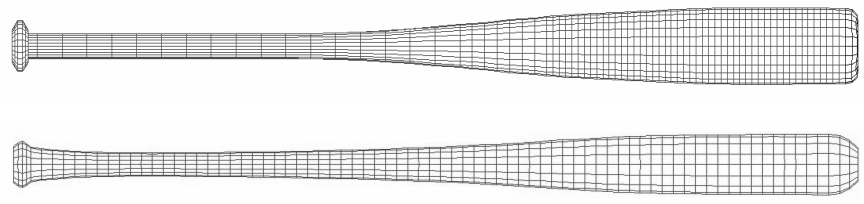

Figure 4.6 – New finite element meshes for the aluminum bat (top) and wood bat (bottom). Note the difference in the diameter profile.

4.3.1 Calibrating the Baseball Model

Calibrating the baseball model was a two-step process. The first step involved incorporating the non-linear stiffness characteristic captured from compression tests previously described, and the second was to use the ASTM COR test (1887) as a guide to validate the COR of the finite element model.

The Mooney-Rivlin material model (Type 27) in the LS-DYNA finite element code was chosen for the baseball model for two basic reasons, neither of which had anything to do with the theory of hyperelastic materials. A detailed explanation of this material model can be found in the Appendix. First, past experience has shown that it is an excellent material model for nonlinear rubber-like materials. Although a baseball certainly does not qualify as a rubber-like material, it does share nonlinear stiffness characteristics. The second reason for its use was that it provides the option of prescribing a load curve for the material model. The Mooney-Rivlin material card provides an option for the deformation behavior to be load versus deflection data with given specimen dimensions, or a stress versus strain curve setting the specimen dimensions to 1.0. Because this ball model is developed as a preliminary approximation, the data was not converted to a stress versus strain curve. The raw load versus deflection data was used, approximating the baseball as a cube with a side length of 2.4 inches, which will fit inside of the spherical boundaries of an official Major League baseball.

The ball model, consisting of 1296 solid elements, was then impacted against a stationary wood block (as shown in Figure 4.7) to calibrate it to known COR values, in this case 0.555. To achieve this COR value, mass damping was added to the model through an iterative process until the rebound velocity would yield a COR of 0.555. By

adding mass damping, rigid body motions would be reduced. High-speed video of a baseball-bat impact was also used as a visual guide to judge the amount of damping needed. Automatic surface-to-surface contact was prescribed. An orthotropic elastic material model (LS-DYNA Type 2) was used for the wood block, using material properties for white ash.

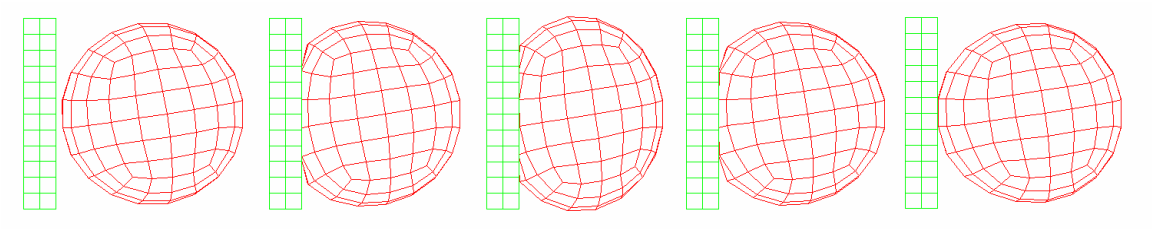

t=0.0 ms t=0.3 ms t=0.6 ms t= 0.9 ms t=1.2 ms

Figure 4.7 – Sequence of ball deformation during contact with flat surface.

4.3.2 Calibrated Ball Results

Batted-ball velocity comparisons between wood and aluminum bats showed the same relative differences as seen in the BHM data, but the magnitudes of the velocities were higher than the BHM data. This comparison is shown in Figure 4.8. At the time of this comparison, the experimental range for batted-ball velocities off aluminum bats (34 in, 29 oz) was approximately 97 mph to 102 mph. The experimental range for batted-ball velocities off wood bats (34 in, 31 oz) was approximately 90 mph to 94 mph. Using the calibrated ball model with damping, the batted ball velocity off the wood bat was 99.1 mph. The batted ball velocity off the aluminum bat was 108.9 mph

Post-processing of these models also included generating time-history animations of the impact event. Screen captures from contour plot animations of the bending stresses for the aluminum bat and the wood bat are shown in Figure 4.9 and Figure 4.10,

respectively. The contour scale is not shown because there was no data for comparison to check and validate the magnitude of the stresses calculated in the model.

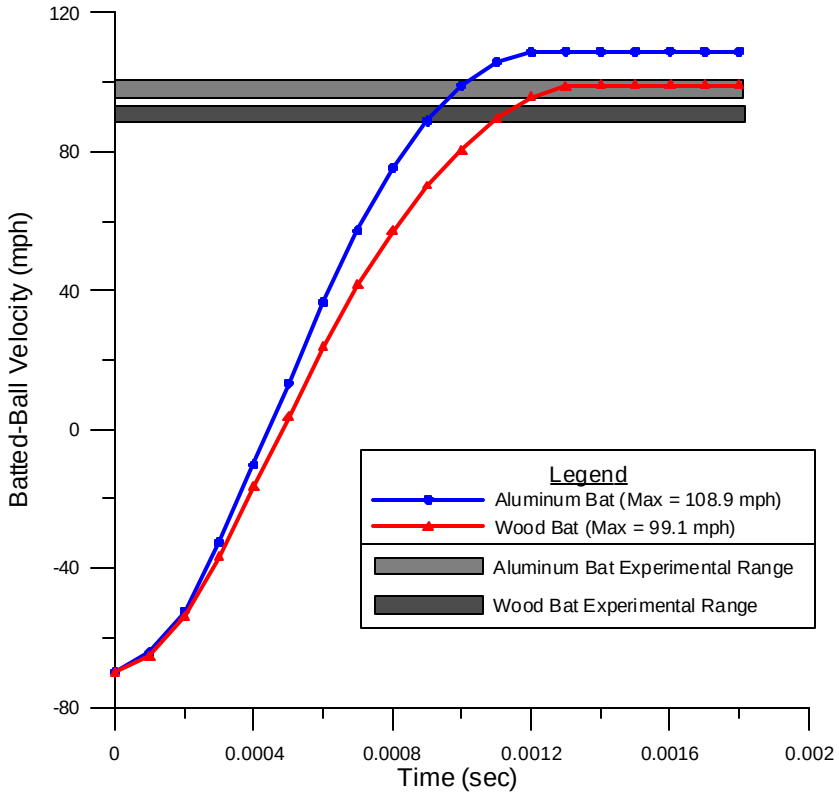

Figure 4.8 – Initial comparison of batted-ball velocities using the damped ball off wood and aluminum bats.

Although only the baseball was calibrated, the relative difference in batted-ball performance between the wood and aluminum bats could be seen. Using the average each experimental range, the difference in performance is approximately 7.5%, where the models predict an 8.9% difference in performance. Although the magnitude of the differences is not particularly close, the general trend is shown with these early models. Different bat-ball impact phenomena are also present in these early results. For the aluminum bat impact shown in Figure 4.9, the hoop deformation mode and trampoline

effect is demonstrated. While for the wood bat shown in Figure 4.8, the local bending deformation of the barrel can be seen as the impulse travels down the length of the bat.

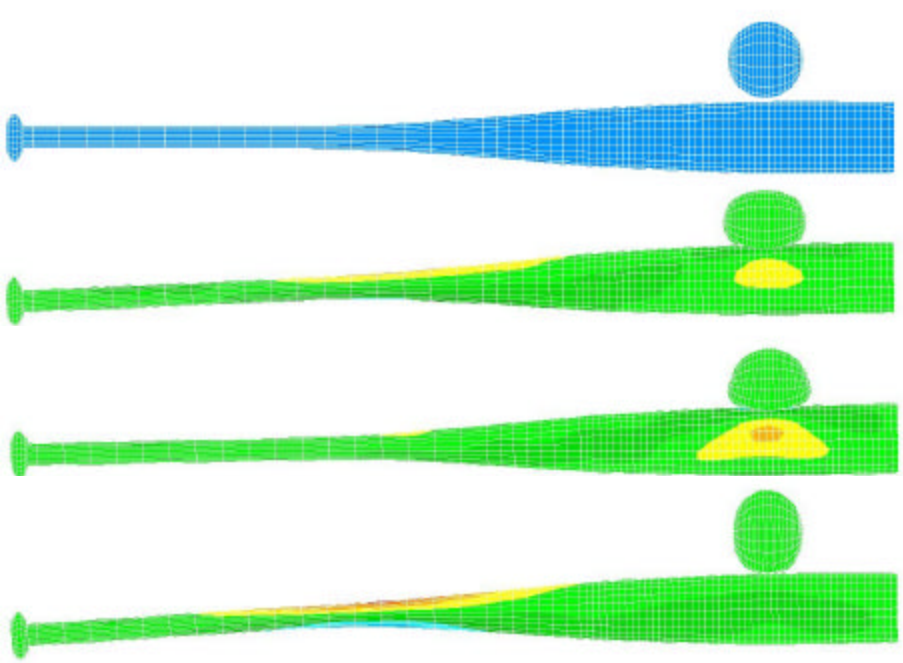

Figure 4.9 –Aluminum bat modeling results using a calibrated ball model.

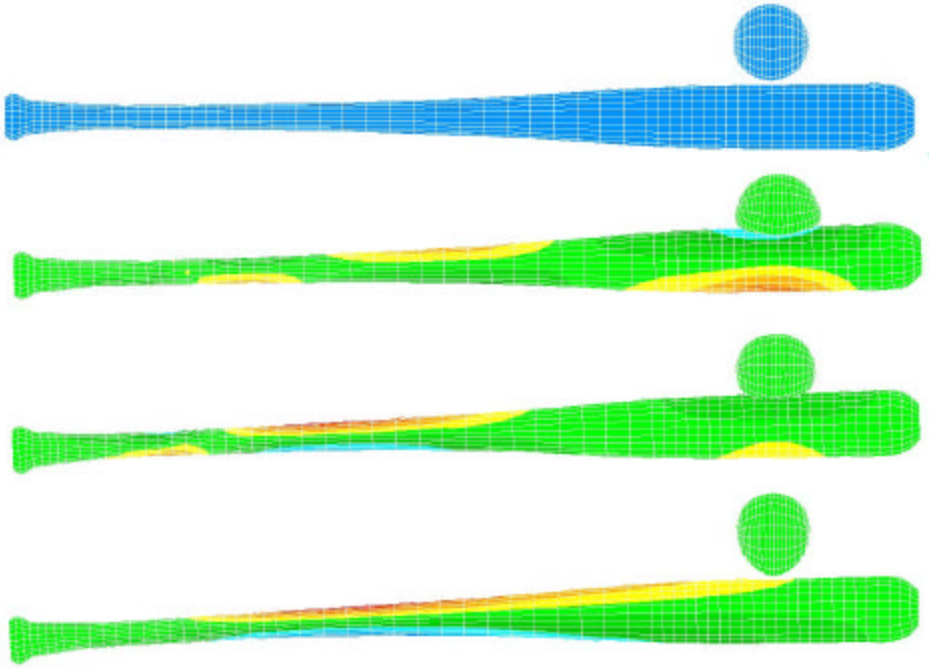

Figure 4.10 – Initial wood bat modeling results using a calibrated ball model.

4.3.3 Calibrating the Baseball Bat Models

With the baseball model calibrated to experimental COR data, the baseball bats also need to be calibrated by some independent means. Early models simply duplicated the physical dimensions of the baseball bats and adjusted the density to duplicate the weight of the bat. Because the modal response of the bat will yield characteristic measurements of natural frequencies through stiffness and mass distribution that could affect batted-ball speed, the bats were calibrated using experimental and analytical modal analyses.

The mesh for the hollow aluminum bat consisted of 2054 shell elements with a uniform thickness of 0.100 in. It should be noted that after a selection of metal baseball bats were cross-sectioned, the average wall thickness was closer to 0.100 in, rather than the values of 0.095 in that was previously used. The C405 alloy was modeled using an elastic-plastic material model with kinematic hardening (LS-DYNA Type 3), recommended for use with shell elements. The mesh for the solid wood bat consisted of 3840 8-noded brick elements. An orthotropic elastic material model (LS-DYNA Type 2) was used to model the directional properties of the wood.

The first and second natural frequencies of the bats were measured experimentally using an impact hammer and a dynamic signal analyzer as previously described. MSC/NASTRAN and later LS-DYNA Implicit were used to calculate the 1st and 2nd bending modes for each of the bats. The refinement of the mesh and the distribution of the mass in the finite element models were tuned so that the calculated natural frequencies correlated closely with the experimentally determined values. Figure 4.11 shows the 1st and 2nd bending modes for the aluminum bat, while Figure 4.12 shows the

results for the wood bat. Table 4.2 and Table 4.3 summarize the calibration data for the aluminum and wood bats, respectively.

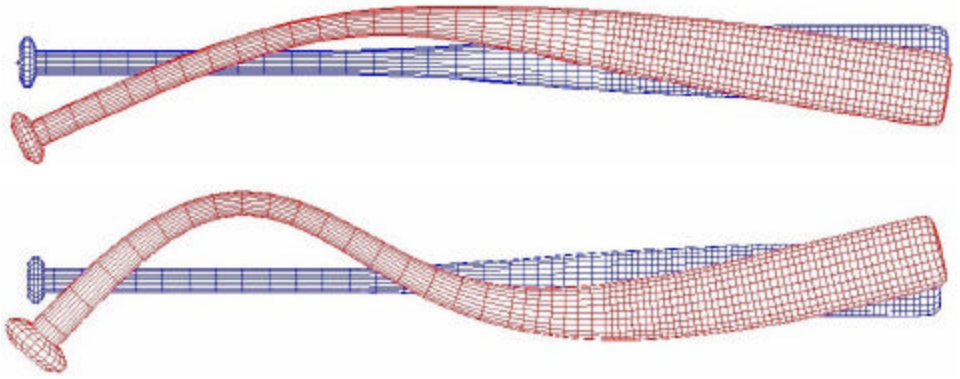

Figure 4.11 – Deformed aluminum bat models showing 1st (top) and 2nd bending modes.

Table 4.2 – Summary of aluminum bat calibration results.

Property	Experimental	Finite Element Model
Length (in)	34	34
Weight (oz)	29.49	29.44
CG Location (in, from barrel end)	12.63	12.62
1st Mode Natural Frequency (Hz)	182	196
2nd Mode Natural Frequency (Hz)	656	682

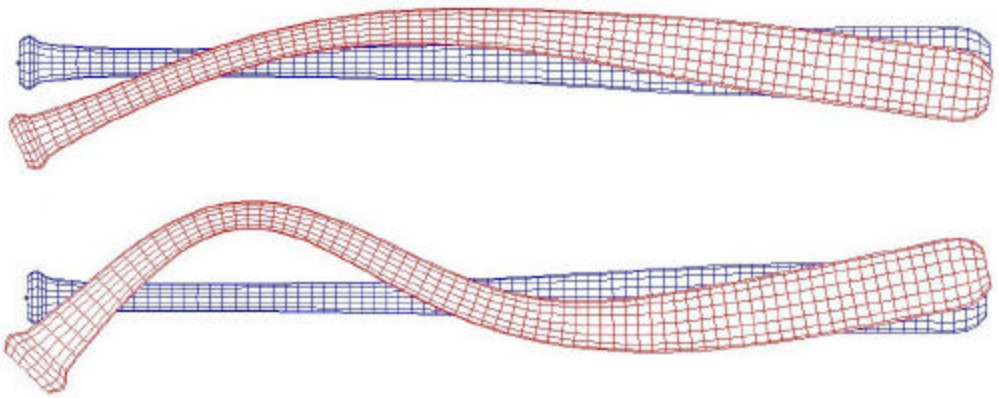

Figure 4.12 – Deformed wood bat models showing 1st (top) and 2nd bending modes.

Table 4.3 – Summary of wood bat calibration results.

Property	Experimental	Finite Element Model
Length (in)	34	34
Weight (oz)	31.40	31.89
CG Location (in, from barrel end)	11.25	11.22
1st Mode Natural Frequency (Hz)	143	145
2nd Mode Natural Frequency (Hz)	481	490

Results of the bat calibration procedure show excellent correlation for the first and second natural frequencies between the experimental data and finite element model of the wood bat. Excellent correlation was also obtained for the weight and *cg* location of the experimental data and the finite element model for the aluminum bat. However, the finite element model predicted a first natural frequency that was approximately 8% higher and a second natural frequency that was approximately 4% higher than the experimental data that was collected. This difference is attributed to a carbon and fiberglass reinforcement applied to the inside diameter of the barrel of the baseball bat, which was not modeled in the finite element model. MOI comparisons were not made at this time, but were conducted at a later date, as described in the Lessons Learned section.

4.3.4 Calibrated Baseball Bat Results

Comparisons can now be made of a calibrated baseball model impacting a calibrated bat model, comparing results for a wood versus an aluminum baseball bat. Each bat was subjected to the same 70-70 impacts as previous models and at the same location of the impact, 6 in from the barrel end of the bat. Mass damping was added to the model in an iterative process to agree with BHM data.

The results of the two models showed that the exit velocity of the ball was 91.5 mph off the wood bat and 101.8 mph off the aluminum bat – a 10 % difference in the exit velocities. A plot of the batted-ball velocities of the two models is shown in Figure 4.13. A detailed view of the barrel deformation is shown in Figure 4.14. The axial bending-stress contour plots for the wood and aluminum bat impact animations are shown with descriptions in Figure 4.15 and Figure 4.16, respectively.

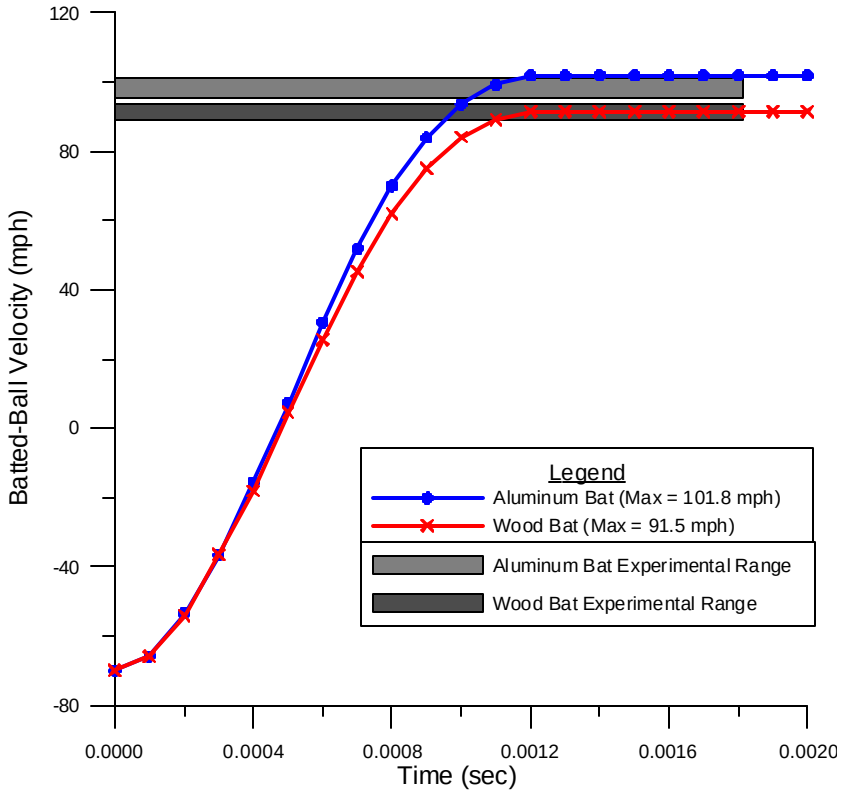

Figure 4.13 – Batted-ball velocities for the calibrated aluminum and the wood bat models.

Aluminum Bat Model

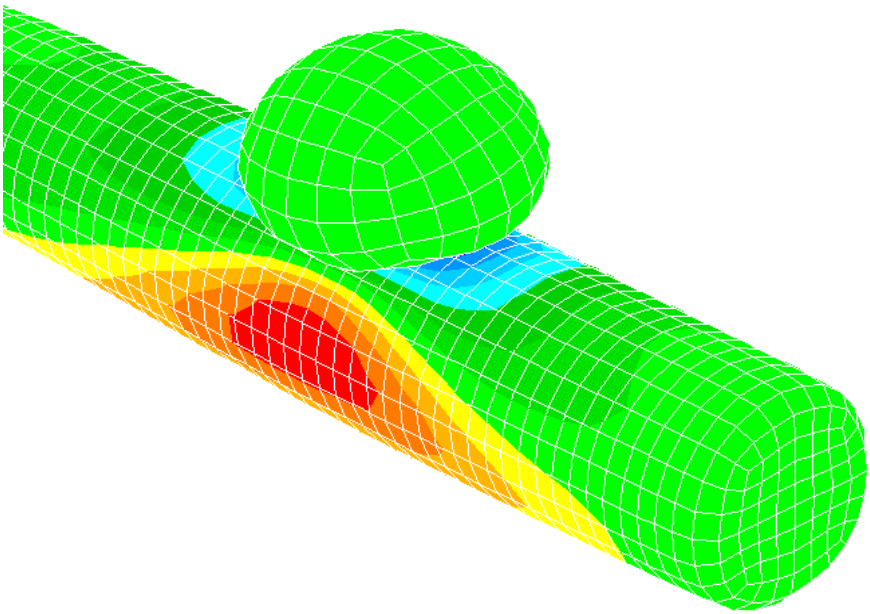

Wood Bat Model

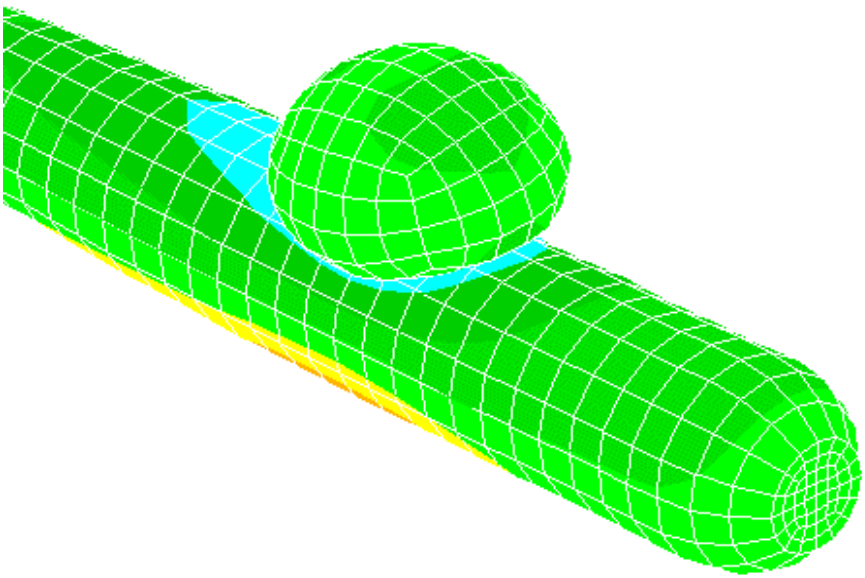

Figure 4.14 – Comparison of the barrel deformation during impact.

Starting position of bat-ball impact analysis.

Ball impacts surface of bat.

Ball reaches maximum deformation.
Bat undergoes local bending in barrel.

Ball begins to rebound off bat.

Stress impulse from ball impact traveling down length of the bat towards knob.

Ball about to leave surface of bat after 1.4 ms of contact time.

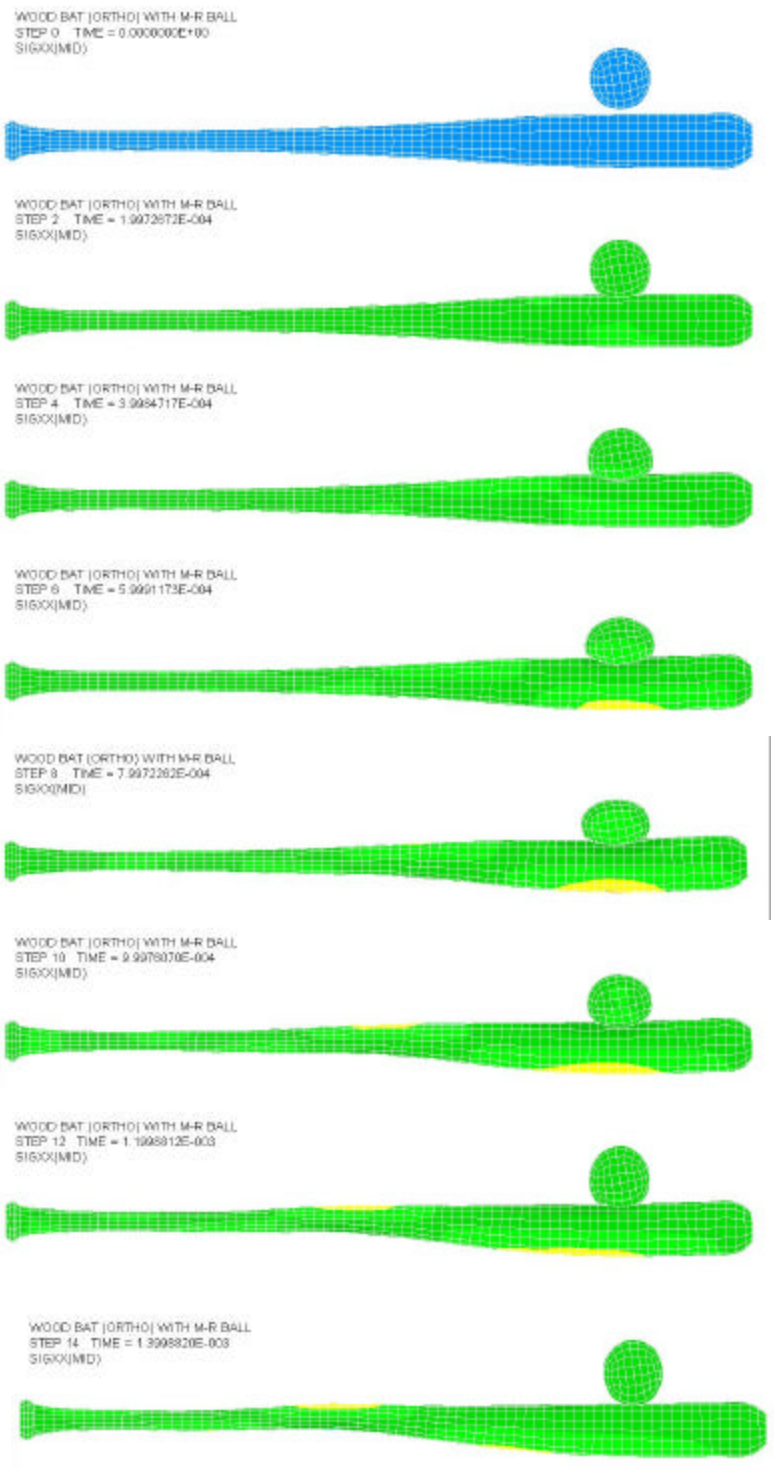

Figure 4.15 – Stress contour plots of wood bat animation.

Starting position of bat-ball impact analysis.

Ball impacts surface of bat.

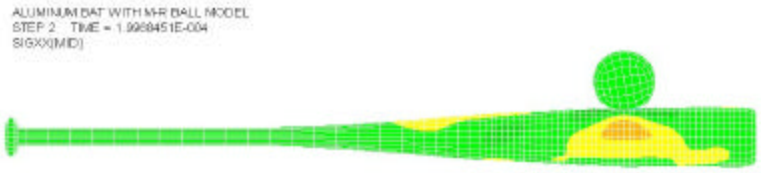

Hoop-deformation mode occurring in barrel, leading to trampoline effect.

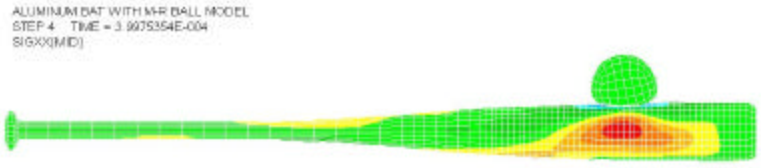

Stress impulse from ball impact traveling down length of the bat towards knob.

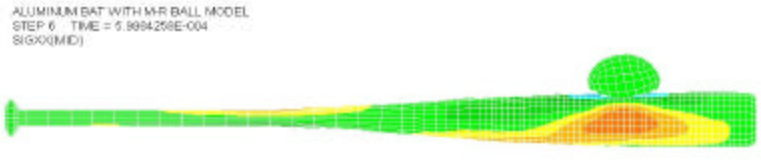

Ball reaches maximum deformation.

Ball continues to rebound off bat.

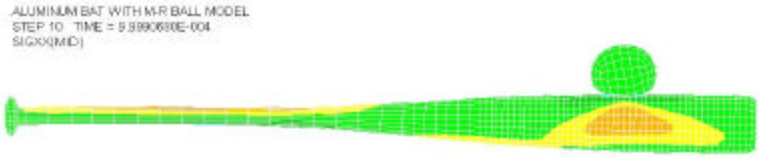

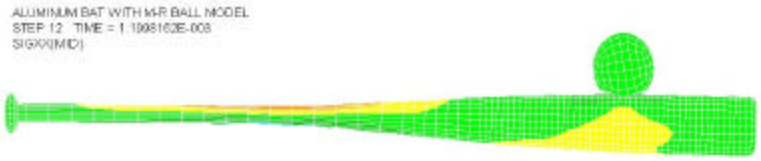

Ball about to leave surface of bat after 1.4 ms of contact time.

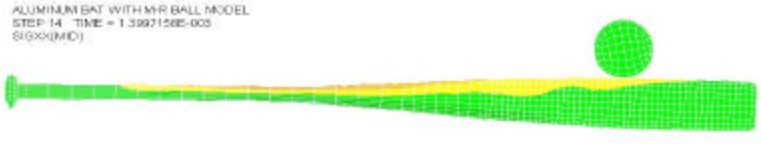

Figure 4.16 – Stress contour plots of aluminum bat animation.

5 LESSONS LEARNED

Over the course of any long-term analysis project, there are certain things that if given the chance, would be done differently. For example, improvements in finite element codes might allow the analysts to model things differently. Increasing processing power, disk-drive storage capacity and memory for personal computers allow larger finite element models with greater detail to be created and analyzed without CPU run-time penalties. Also, given the general knowledge and experience gained over the course of a project, the analyst will inevitably look back and discuss how things could have been done differently. This section provides that opportunity.

5.1 A Note on Damping

At the time that natural frequencies were experimentally determined, no effort was made to quantify the damping present in the wood and aluminum bats or the baseball. Using the *DAMPING_PART_MASS input card in LS-DYNA, where mass proportionally damping is added to a prescribed part, damping was simply used as a scaling factor to calibrate modeling results to BHM batted-ball velocity data. Further investigation during the experimental modal analysis would have quantified an appropriate value of damping to use in the modeling.

Mass proportional damping in LS-DYNA, denoted as a, is used to damp out motion including rigid body motions. Appropriate values are usually given as $2w_n$, where w_n is the fundamental natural frequency of the structure in rad/sec. Other damping options available in LS-DYNA include using the *DAMPING_PART_STIFFNESS card to add stiffness weighted damping (Rayleigh damping coefficient, b) to a prescribed part to damp high-frequency oscillatory motion. Absent of actual data, a value of 0.10 which

corresponds to approximately 10% damping of higher frequency vibrations, can be used as a starting point. The *DAMPING_GLOBAL card can be used to apply mass proportional damping globally to the model.

5.2 Appropriate Model for COR Test

Limitations on computing power and the need to get results in a reasonable amount of time (1 hour vs. 1 day) led to a modification of the ASTM 1887 procedure that was used to calibrate the baseball. Instead of measuring the inbound and the rebound velocity of the ball at essentially 18 in from the wood block surface, the velocities calculated in the finite element model were measure at 0.1 in from the wood block. Unfortunately, the effect of using large values of mass was not thoroughly examined. Looking at the original COR model to calibrate the baseball, a mass damping value of 300 was used for the ball and 650 for the wood block.

When the COR test is modeled more appropriately by placing the ball 18 in from the wood block, giving it an initial velocity of 60 mph, and then measuring the rebound velocity at the same 18-in starting location, the original COR model with the large values of damping fails the test miserably. The displacement of the baseball should travel to -18 in where it comes into contact with the block and then rebound back to it's starting point at 0 in and then beyond. The large damping value unfortunately causes the ball to come to a complete stop after traveling only 3.52 in, never even reaching the block. This is confirmed by the velocity trace of the ball as shown in Figure 5.1 shows the time-history plot of the displacement and velocity of the baseball.

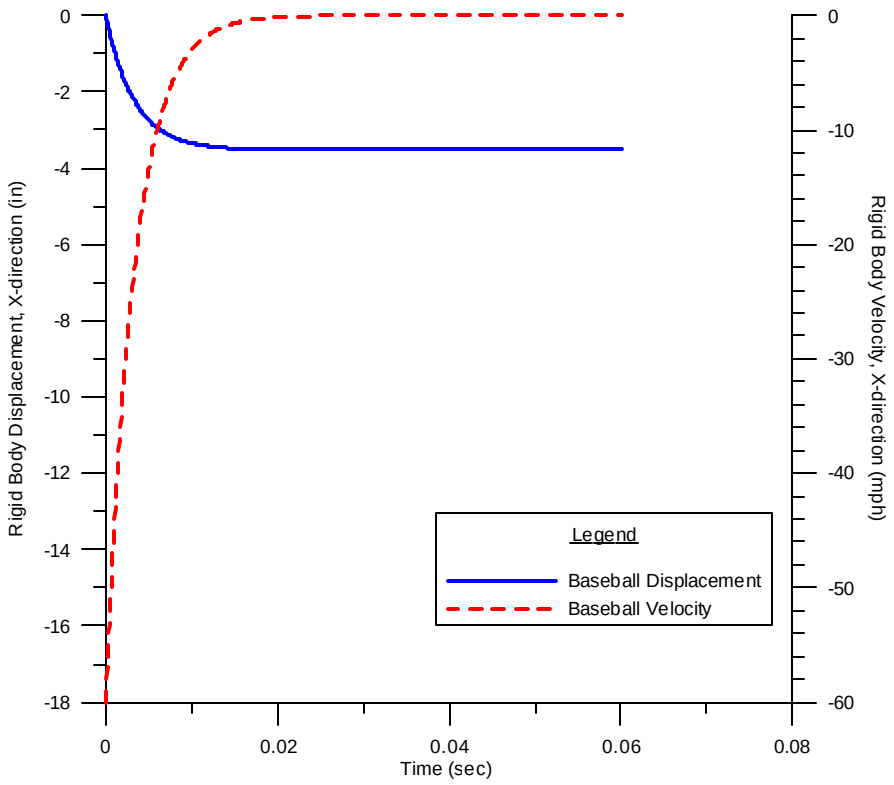

Figure 5.1 – Displacement and velocity of original baseball COR model.

Due to some of these anomalies, a new model was created. In order to apply more appropriate values of mass damping, experimental data on the natural frequency of a baseball is needed. In general, a great amount of research is devoted to quantifying the damping in a system. The work involved to quantify the damping in a baseball is too large a task and beyond the scope for this thesis. Therefore, reverting back to the iterative process to calibrate the finite element ball to have a COR of 0.555, a mass damping value of 2.0 was prescribed for the ball and a value of 3.5 was prescribed for the wood block. The resulting time-history plot for the baseball displacement and velocity is shown in Figure 5.2

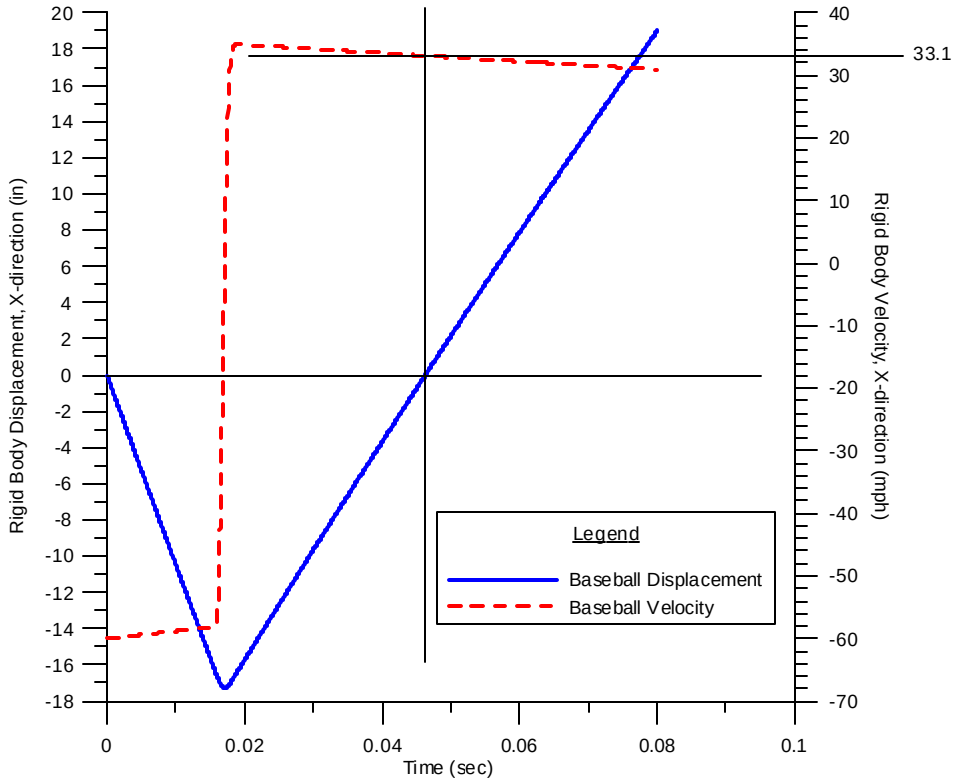

Figure 5.2 – Improved COR model results for baseball displacement and velocity.

Comparing the results of Figure 5.1 to Figure 5.2, the displacement of the baseball travels -18 in, then rebounds and travels +18 in (and beyond) as it should. The time that the rebound velocity should be measured is when it crosses the 0-in mark. Drawing a vertical guideline to intercept the velocity curve, and then a horizontal guideline from the intercept to the velocity axis, the rebound velocity can be visually determined by inspection. In this case the rebound velocity measured 33.1 mph. These inbound and rebound velocities result in a calculated COR of 0.552.

5.3 Modifying contact analysis parameters

In addition to changing the damping values used in the COR test described in the preceding section, selected parameters that govern the contact behavior were changed in

the improved COR model. Default values that have been developed by LSTC over time to produce good results for general contact problems were used for a majority of the parameters. Two specific parameter values were changed from the default values in the *CONTACT_AUTOMATIC_SURFACE_TO_SURFACE card - the master and slave stiffness and the contact damping. As shown in Figure 5.3, there was inter-penetration between the master surface (the block) and the slave surface (the ball), meaning that the nodes from each surface penetrated through each other. These penetrations are obviously not physically possible in the real world.

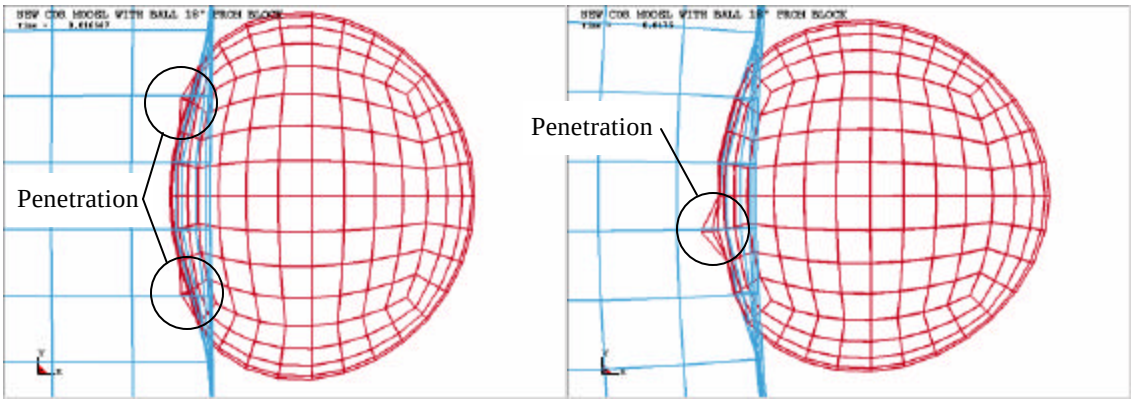

Figure 5.3 – Examples of nodal penetration of the ball into the wood block.

One method used to eliminate this penetration error is to refine the mesh in the areas that come into contact, but this refinement is not always possible. The second method is to increase the contact stiffness values used in the calculation. Artificial springs are placed between the slave nodes and the master surface by the contact algorithm and assigned some stiffness value, usually based on the material properties of the underlying element. In finding a solution, these contact forces are balanced out, usually allowing for some amount of penetration, depending on the stiffness of the spring. Increasing the

contact stiffness will cause a smaller time step to be used by the solver because it will more sensitive to small changes in displacement in trying to converge to a solution. The key trade-offs are to increase the contact stiffness value without drastically increasing the run-time of the model and to realize how much penetration can be tolerated in the solution.

Viscous damping is applied to the contact interface to eliminate unwanted oscillations due to the contact, for example high-frequency oscillations are sometimes created when modeling sheet metal forming or stamping operations. A suggested value of 20 (%) was used for the new COR model.

As a result of increasing the contact stiffness and adding viscous damping to the model, the penetration between the master and slave surfaces was significantly reduced, as shown in Figure 5.4. Although not quantified here, past experience has shown that as the penetration is reduced, more accurate contact forces and energies are modeled, leading to an overall more accurate model.

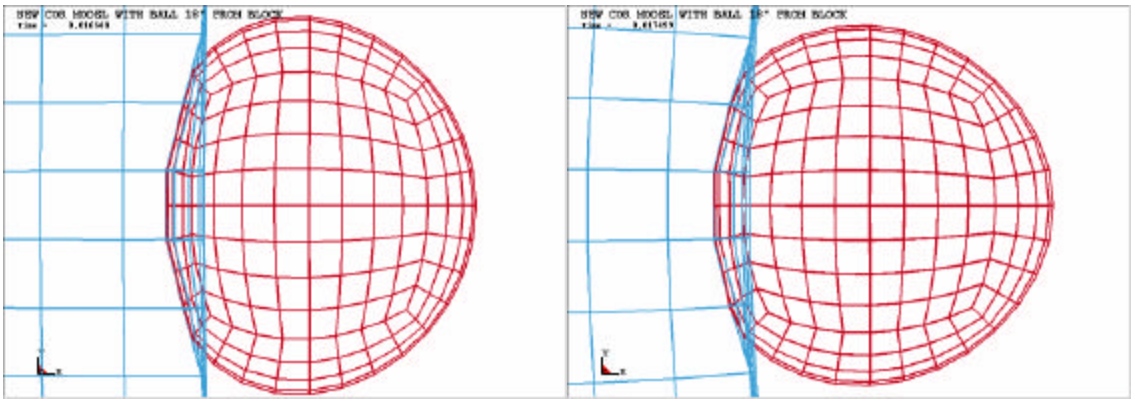

Figure 5.4 – Increasing the contact stiffness results in reducing the penetration.

5.4 Corrected Aluminum Bat Model

There were three aspects of the aluminum bat modeling that needed to be addressed in this Lessons Learned section. The first considers the calibration of the bat to experimental data. In addition to the physical attributes of length, weight, diameter profile and *cg*-location, the MOI of the bat model should have been used as another calibrating metric before the bats are subjected to a modal analysis to calibrate the bending frequencies of the bat. The MOI should not be a concern with respect to a wood bat model, because a wood bat is a solid volume of material. Nevertheless, the MOI value for the wood bat model should be calculated and compared to experimental values for completeness. Coupled with the MOI calibration is an accurate measure of the wall thickness. Due to the forming process used to make an aluminum bat, different sections of the bat will have different thicknesses. An accurate representation of the wall thickness along the length of the bat should provide a close estimate for the bat's MOI value. The final issue addresses the nodal locations for the shell elements used for the aluminum bat.

In order to address these issues, and also to bring the model up to date, a new aluminum bat model was created that subscribes to the current NCAA regulations: a length-to-weight unit difference of -3 and a $2\,^{5}/_{8}$-in barrel diameter.

5.4.1 Wall Thickness and Nodal Reference Plane for Shell Elements

A new prototype baseball bat with accurate wall-thickness measurements provided by the baseball bat manufacturer was selected for modeling. This baseball bat had a distinct advantage because it was under test for NCAA certification and therefore, was subjected to the full round of BHM testing at the UMLBRC. At the end of experimental testing,

the length, weight, cg location, MOI measurements and BHM batted-ball velocity data were all known. The only additional experimental test data needed was to find the natural frequencies of the bat.

A more accurate representation of the plastic cap was included in the model update, as shown in Figure 5.5. It was created using 2200 nodes and 1620 solid elements. Once the cap was created, it was discovered that the shell elements in the previous aluminum bat models were incorrectly used. The nodes for each shell element should have been located at the mid-plane of the modeled surface, but instead, the nodes were located at the outer diameter. The end result is that the outside diameter of the modeled bat was larger than the actual bat by half the wall thickness. Now, because the cap was created using solid elements, problems arose with how to model the shell-to-solid element interface.

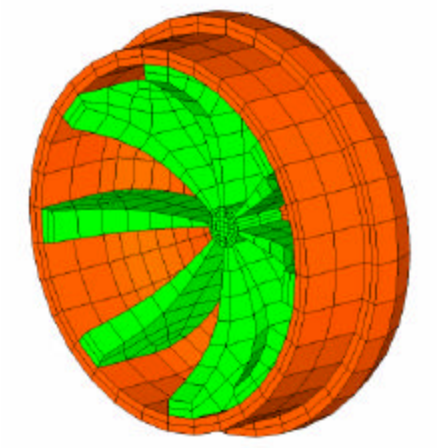

Figure 5.5 – New plastic cap model, with reinforcing ribs.

The most convenient solution was to use 8-noded solid shell elements that are available in LS-DYNA. These elements physically resemble solid brick elements, but the element formulation and behavior resembles shell elements. They are specifically designed for shell-to-solid interfaces but can be used to model thick-shelled structures.

Shell-like behavior is obtained by using multiple integration points through the thickness of the element, while a plane stress subroutine is formulated at each integration point. The baseball bat, minus the cap, was modeled with 9482 nodes and 4840 solid shell elements. The transition from the cap to the barrel of the bat was modeled by merging coincident nodes of the overlapping elements, as illustrated in Figure 5.6. The final updated -3 bat model is shown in Figure 5.7.

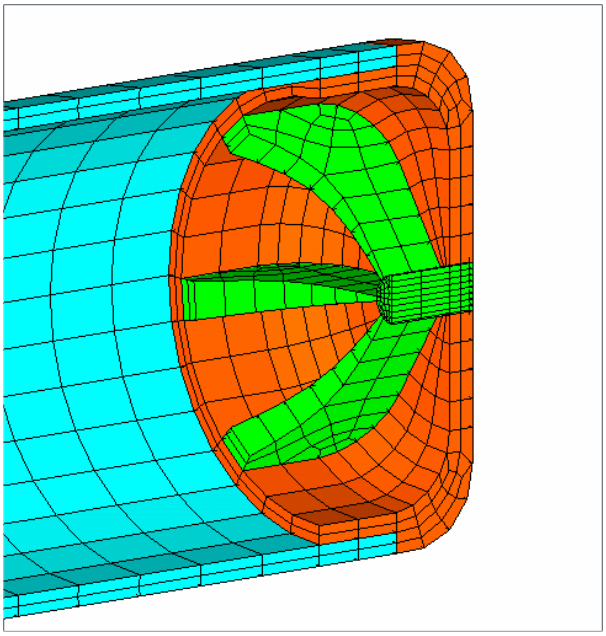

Figure 5.6 – Sectioned view showing interface with cap.

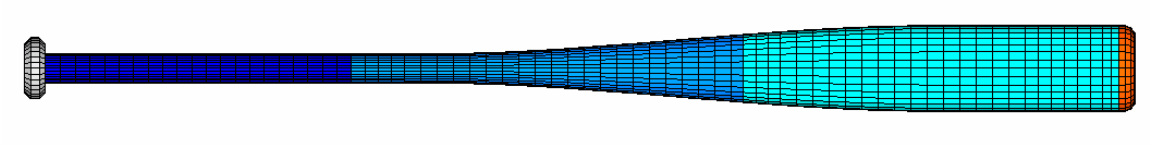

Figure 5.7 – Updated aluminum bat model.

5.4.2 MOI Calibration

The next step in completing the -3 updated bat model was to calibrate it using the procedures and methods previously described, with the addition of calibrating the MOI of the baseball bat. The calibration for the -3 aluminum bat is summarized in Table 5.1. It was possible to calibrate some properties more accurately, but at the expense of the remaining properties. For completeness, Table 5.2 summarizes the wood-bat calibration results, including MOI values.

Table 5.1 – Summary of updated aluminum bat calibration results.

Property	Experimental	Finite Element Model
Length (in)	34	34
Weight (oz)	31.39	31.17
CG Location (in, from barrel end)	12.94	13.02
MOI (oz-in^2, at cg)	3222	3165
1st Mode Natural Frequency (Hz)	176	171
2nd Mode Natural Frequency (Hz)	614	606

Table 5.2 – Summary of wood bat calibration results.

Property	Experimental	Finite Element Model
Length (in)	34	34
Weight (oz)	31.40	31.38
CG Location (in, from barrel end)	11.25	11.22
MOI (oz-in^2, at cg)	2468	2446
1st Mode Natural Frequency (Hz)	143	148
2nd Mode Natural Frequency (Hz)	481	506

5.5 Updated Model Comparison

With more appropriate model of the baseball COR test and updates to the aluminum bat model complete, comparisons against BHM data and against wood bat performance

can now be made. For both models, the baseball and baseball bats were given linear (translating) initial velocities of 70 mph towards each other. The point of impact was at the 6-inch location from the barrel end of the bat. Contact and damping parameters were duplicated from the COR model.

The results of the updated modeling were mixed. As shown in Figure 5.8, the maximum batted-ball velocity off the aluminum bat was 123.9 mph and off the wood bat was 120.4 mph. Comparing these values to BHM test data of the same bats shows a large discrepancy in the data, as summarized in Table 5.3. The average of five impacts taken at the 6-in location show that the batted-ball velocity for the -3 aluminum bat is 94.7 mph. The average of 3 impacts with the wood bat is 93.9 mph.

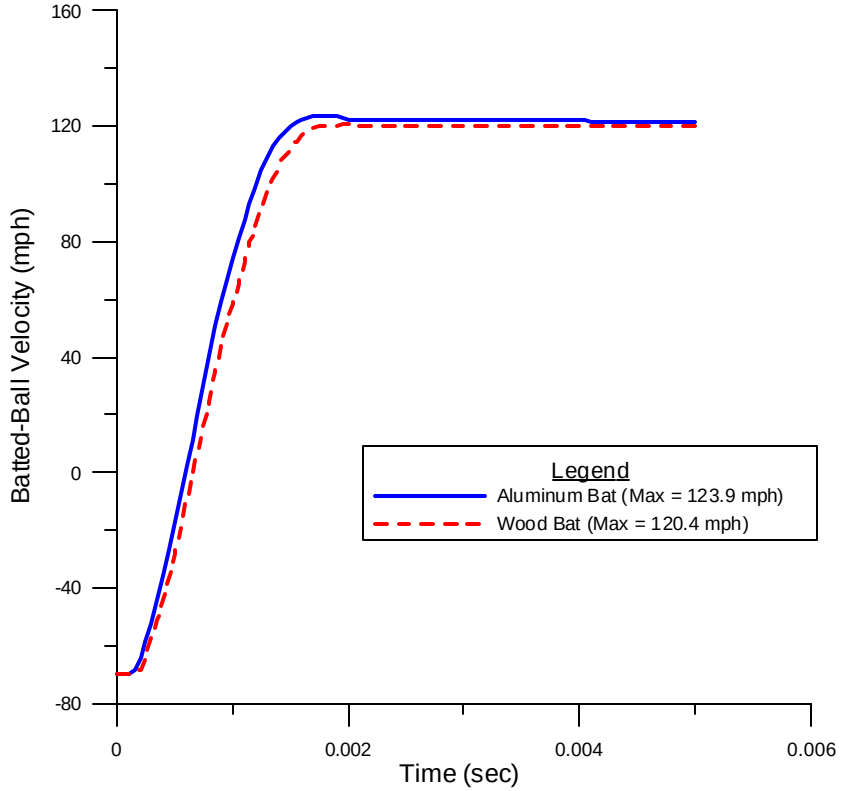

Figure 5.8 – Batted-ball velocity for updated models.

Table 5.3 – Summary of batted-ball velocity comparison.

Baseball Bat Under Test	Batted-Ball Velocity (mph)	
	Experimental	Finite Element Model
Wood Bat	93.9	120.4
-3 Aluminum Bat	94.7	123.9

The relative difference in batted-ball velocity between the wood bat and -3 aluminum bat for the BHM data is 0.9 % while the finite element model shows a 2.9 % increase in batted ball velocity for the -3 aluminum bat. It should be noted that the difference in batted-ball velocity for the two different ball lots used in this comparison is 0.083 mph, so any effects that the baseball may have in this comparison are negligible. The first station that the batted-ball velocity is measured with the BHM is located 9 in from the bat-ball impact location. From the time-history plot of Figure 5.9 showing the displacement of the ball, the ball has rebounded away from the bat approximately 8 in when the model stops after 0.005 sec. Although, the batted-ball velocities are not measured at exactly the same location, the trend in the batted-ball velocity of Figure 5.8 does not predict a sudden decrease in velocity that will correspond to BHM data.

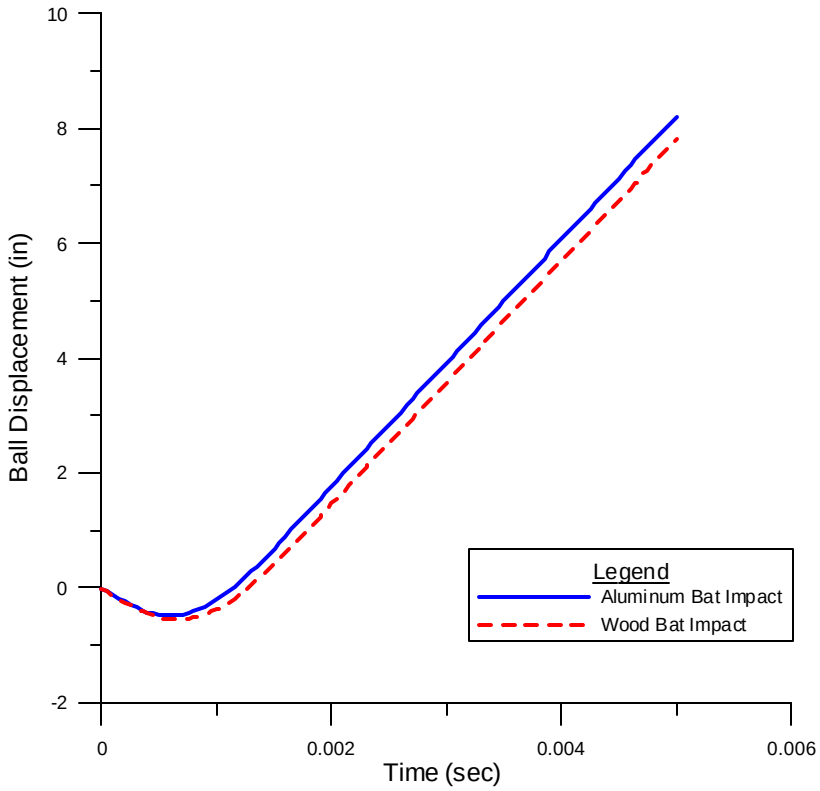

Figure 5.9 – Time-history plot of the batted-ball displacement.

Conclusions that can be drawn from these latest finite element models is that a relative batted-ball velocity difference between the wood and aluminum baseball bats can be predicted, but their magnitudes are not comparable to BHM data. Given the detailed modeling that has been conducted in order to calibrate the baseball bats to experimental data, the model's prediction of relative difference in performance is not surprising. After looking at the animation results of the impacts, it is clear that the problem lies with the baseball model.

Although it appears to be an excellent avenue to incorporate actual test data into a material model, the Mooney-Rivlin material model that is used to model rubber materials does not appear to provide a realistic simulation of the nonlinear compression of the baseball. Consider the screen captures of the deformation plots for the wood bat model,

shown in Figure 5.10. After the ball begins to impact the bat, as shown in Plot 3, it continues until it is almost flat against the barrel and has wrapped itself around the barrel of the bat in Plots 4 and 5. As the ball begins to rebound off the barrel of the bat, large oscillations begin to appear, as shown in Plots 7-12. Similar results are seen with the aluminum bat model. The deformation of the ball when it impacts the bat and the large oscillations as it rebounds away from the bat are not seen in high-speed video of bat-ball impact.

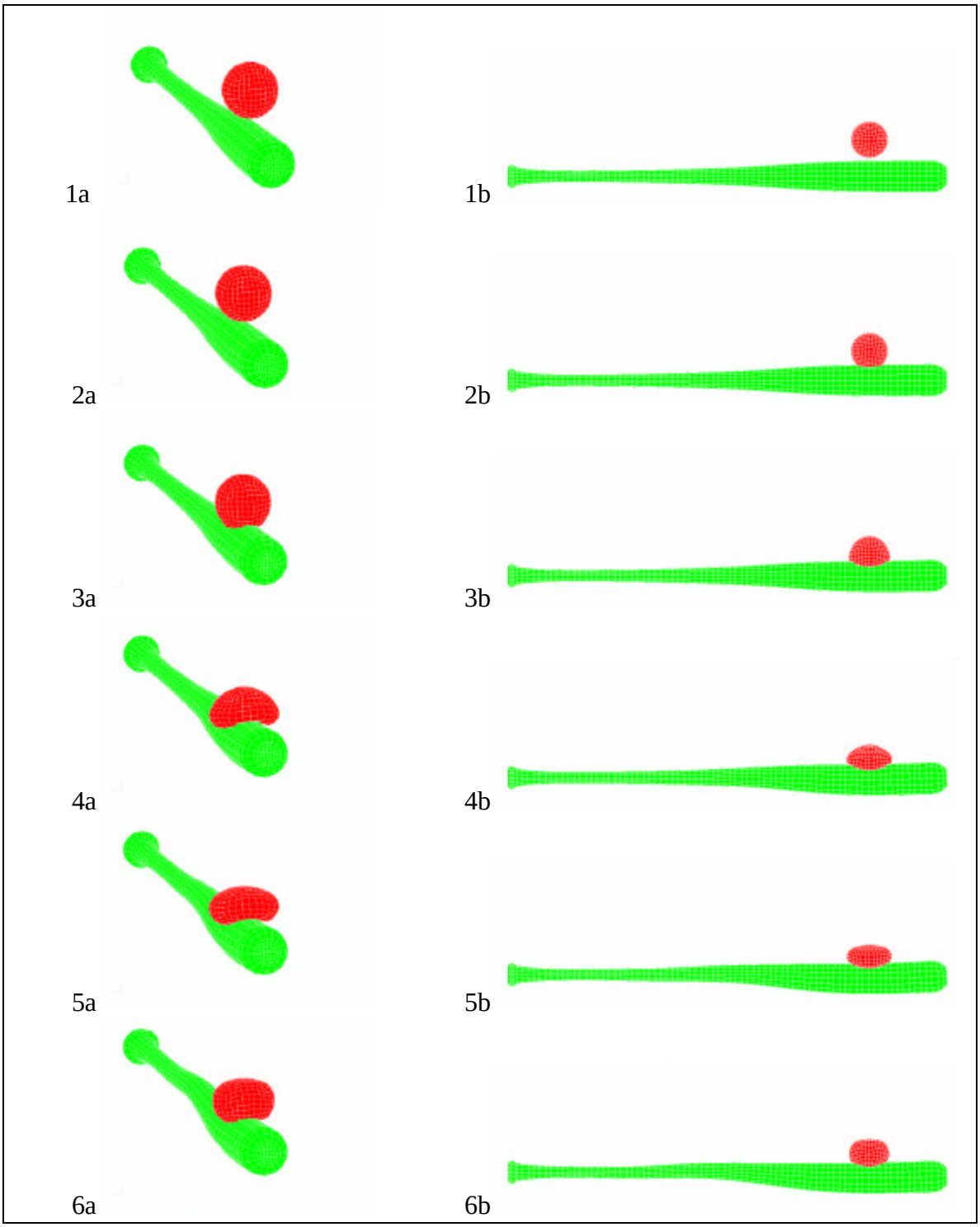
1a
1b
2a
2b
3a
3b
4a
4b
5a
5b
6a
6b

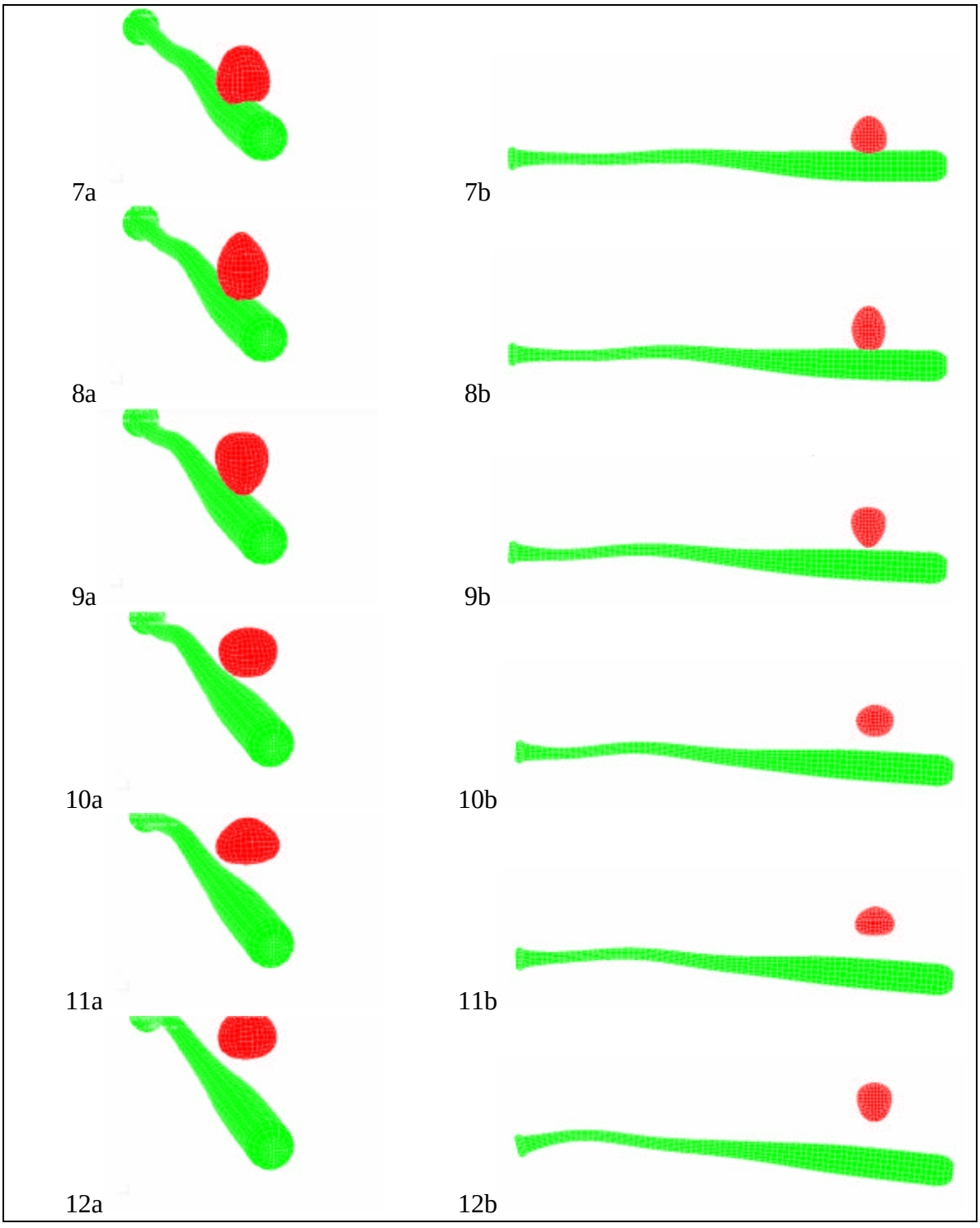

Figure 5.10 – Deformation plots of batted-ball model with the wood bat.
(Plot #1 is the starting position. Plots 2 through 12 are in 0.00005-sec increments.)

6 CONCLUSIONS AND RECOMMENDATIONS

The collision between a baseball and a baseball bat is a highly dynamic and non-linear event. All of the aspects of the impact event cannot possibly be captured in the first, second or even third generation of a finite element model. But as the modeling progresses, conclusions can be reached that provide a foundation for future modeling efforts. It is quite apparent that these finite element models can be used as a design tool for future baseball bat designs, which most certainly includes composite bats, by using the vast array of composite material models in LS-DYNA.

6.1 Conclusions

There were several conclusions reached early on with preliminary models of the BHM. As part of the validation of the BHM, there was little difference shown in the batted ball velocity if the bat was given a purely rotational versus purely translational velocity towards the ball. There was however a slight difference in batted-ball velocity, approximately 5% increase in the velocity if the bat was swing a full 290° towards the ball versus if the bat was started at 0° in the "just touching" position before impact. At the time though, there were definite computer hardware considerations to make, and that the 5% difference could not justify the extra CPU run-time needed to model the bat with a full 290° swing.

A credible methodology to validate the baseball bat and baseball models independently was created that drastically increases the accuracy of the models and provides a means to compare the finite element models to experimental data collected through baseball bat testing with the BHM. Although the end result of the updated modeling presented here showed that the Mooney-Rivlin material model is not suited for

modeling the baseball, the relative performance between the wood bat and the aluminum bats did correlate to BHM data reasonably well, but only over a time immediately before to immediately after the bat-ball collision.

Using the relative performance as a design baseline, additional studies can and have been made. For example, the contact time between the bat and ball during impact can be quantified. The models can also be used to investigate the effect on the ball exit velocity that different properties of the bat may have, such as the location of the center of gravity, weight of the bat, wall thickness and the diameter profile.

6.2 Recommendations

There are two major recommendations presented here for future modeling efforts. The first involves damping. More research is suggested in quantifying the amount of damping needed to add to the model and develop a procedure that is beyond the iterative approach taken here. The amount of proportional damping present in the baseball bats should be relatively straightforward to quantify with a more in-depth experimental modal analysis. However, the amount of damping present in the baseball must be given careful consideration. A comparison of calculated mode shapes to experimentally determined mode shapes is also suggested as part of the damping study.

The second major recommendation involves the material model selected for the baseball. The Mooney-Rivlin model, used for rubber materials, provided good results in preliminary models when looking over a time period immediately before to immediately after the bat-ball collision. But as the level of detail increased in the baseball bat and baseball models, it has become apparent that the Mooney-Rivlin model does not seem to provide an accurate measure of the baseball's load versus deflection behavior when it is

impacted with a bat. There may be other models in future releases of LS-DYNA that provide a better representation of the non-linear aspects of the baseball. Another are of development is that a user-defined material model could be implemented, after extensive experimental characterization of the baseball.

7 APPENDICES

7.1 Automatic Time Step Information

***CONTROL_TIMESTEP**

Purpose: Set structural time step size control using different options.

Card Format

	1	2	3	4	5	6	7	8
Variable	DTINIT	TSSFAC	ISDO	TSLIMT	DT2MS	LCTM	ERODE	MS1ST
Type	F	F	I	F	F	I	I	I
Default	-	0.9/0.67	0	0.0	0.0	0	0	0

Card Format (This card is optional).

Card 2	1	2	3	4	5	6	7	8
Variable	DT2MSF							
Type	F							
Default	not used							

VARIABLE	DESCRIPTION
DTINIT	Initial time step size: EQ.0.0: LS-DYNA determines initial step size.
TSSFAC	Scale factor for computed time step (old name SCFT). See Remark 1 below. (Default = .90; if high explosives are used, the default is lowered to .67).

*CONTROL

VARIABLE	DESCRIPTION
ISDO	Basis of time size calculation for 4-node shell elements. 3-node shells use the shortest altitude for options 0,1 and the shortest side for option 2. This option has no relevance to solid elements, which use a length based on the element volume divided by the largest surface area. EQ.0: characteristic length=area/(minimum of the longest side or the longest diagonal). EQ.1: characteristic length=area/(longest diagonal). EQ.2: based on bar wave speed and MAX [shortest side, area/(minimum of the longest side or the longest diagonal).]. THIS LAST OPTION CAN GIVE A MUCH LARGER TIME STEP SIZE THAT CAN LEAD TO INSTABILITIES IN SOME APPLICATIONS, ESPECIALLY WHEN TRIANGULAR ELEMENTS ARE USED. EQ.3: timestep size is based on the maximum eigenvalue. This option is okay for structural applications where the material sound speed changes slowly. The calculational cost to determine the maximum eigenvalue is significant, but the increase in the time step size often allows for significantly shorter run times without using mass scaling.
TSLIMT	Shell element minimum time step assignment, TSLIMT. When a shell controls the time step, element material properties (moduli not masses) will be modified such that the time step does not fall below the assigned step size. Applicable only to shell elements using material models *MAT_PLASTIC_KINEMATIC, *MAT_POWER_LAW_PLASTICITY, *MAT_STRAIN_RATE_DEPENDENT_PLASTICITY, *MAT_PIECE-WISE_LINEAR_PLASTICITY. The DT2MS option below applies to all materials and element classes and may be preferred.
DT2MS	Time step size for mass scaled solutions, DT2MS. Positive values are for quasi-static analyses or time history analyses where the inertial effects are insignificant. Default = 0.0. If negative, TSSFAC*|DT2MS| is the minimum time step size permitted and mass scaling is done if and only if it is necessary to meet the Courant time step size criterion. This latter option can be used in transient analyses if the mass increases remain insignificant. See *CONTROL_TERMINATION variable name "ENDMAS".
LCTM	Load curve ID that limits the maximum time step size (optional). This load curve defines the maximum time step size permitted versus time. If the solution time exceeds the final time value defined by the curve the computed step size is used. If the time step size from the load curve is exactly zero, the computed time step size is also used.
ERODE	Erosion flag for solid and solid shell elements when DTMIN (see *CONTROL_TERMINATION)is reached. If this flag is not set the calculation will terminate: EQ.0: no, EQ.1: yes.

VARIABLE	DESCRIPTION
MS1ST	Limit mass scaling to the first step and fix the mass vector according to the time steps once. The time step will not be fixed but may drop during the calculation from the specified minimum: EQ.0: no, EQ.1: yes.
DT2MSF	Reduction (or scale) factor for initial time step size to determine the minimum time step size permitted. Mass scaling is done if it is necessary to meet the Courant time step size criterion. If this option is used DT2MS=–DT2MSF multiplied by the initial time step size, Δt, before Δt is scaled by TSSFAC. This option is active if and only if DT2MS=0 above.

Remarks:

1. During the solution we loop through the elements and determine a new time step size by taking the minimum value over all elements.

$$\Delta t^{n+1} = TSSFAC \cdot \min\left\{\Delta t_1, \Delta t_2, ..., \Delta t_N\right\}$$

where N is the number of elements. The time step size roughly corresponds to the transient time of an acoustic wave through an element using the shortest characteristic distance. For stability reasons the scale factor TSSFAC is typically set to a value of .90 (default) or some smaller value. To decrease solution time we desire to use the largest possible stable time step size. Values larger than .90 will often lead to instabilities. Some comments follow:

- The sound speed in steel and aluminum is approximately 5mm per microsecond; therefore, if a steel structure is modeled with element sizes of 5mm, the computed time step size would be 1 microsecond. Elements made from materials with lower sound speeds, such as foams, will give larger time step sizes. Avoid excessively small elements and be aware of the effect of rotational inertia on the time step size in the Belytschko beam element. Sound speeds differ for each material, for example, consider:

AIR	331 m/s
WATER	1478
STEEL	5240
TITANIUM	5220
PLEXIGLAS	2598

- Model stiff components with rigid bodies, not by scaling Young's modulus which can substantially reduce the time step size.

- The altitude of the triangular element should be used to compute the time step size. Using the shortest side is okay only if the calculation is closely examined for possible instabilities. This is controlled by parameter ISDO.

19. TIME STEP CONTROL

During the solution we loop through the elements to update the stresses and the right hand side force vector. We also determine a new time step size by taking the minimum value over all elements.

$$\Delta t^{n+1} = a \cdot \min\left\{\Delta t_1, \Delta t_2, \Delta t_3, ..., \Delta t_N\right\} \tag{19.1}$$

where N is the number of elements. For stability reasons the scale factor α is typically set to a value of .90 (default) or some smaller value.

19.1 Time Step Calculations for Solid Elements

A critical time step size, Δt_e, is computed for solid elements from

$$\Delta t_e = \frac{L_e}{\left\{\left[Q + \left(Q^2 + c^2\right)^{1/2}\right]\right\}} \tag{19.2}$$

where Q is a function of the bulk viscosity coefficients C_0 and C_1:

$$Q = \begin{cases} C_1 c + C_0 L_e \left|\dot{\varepsilon}_{kk}\right| & for\ \dot{\varepsilon}_{kk} < 0 \\ 0 & for\ \dot{\varepsilon}_{kk} \geq 0 \end{cases} \tag{19.3}$$

L_e is a characteristic length:

8 node solids: $L_e = \dfrac{\upsilon_e}{A_{e_{max}}}$

4 node tetrahedras: L_e = minimum altitude

υ_e, is the element volume, $A_{e_{max}}$ is the area of the largest side, and c is the adiabatic sound speed:

$$c = \left[\frac{4G}{3\rho_0} + \frac{\partial p}{\partial \rho}\right)_s\Bigg]^{\frac{1}{2}} \tag{19.4}$$

where ρ is the specific mass density. Noting that:

$$\left.\frac{\partial p}{\partial \rho}\right)_s = \left.\frac{\partial p}{\partial \rho}\right)_E + \left.\frac{\partial p}{\partial E}\right)_\rho \left.\frac{\partial E}{\partial \rho}\right)_s \tag{19.5}$$

and that along an isentrope the incremental energy, E, in the units of pressure is the product of pressure, p, and the incremental relative volume, dV:

$$dE = -pdV \tag{19.6}$$

we obtain

$$c = \left[\left.\frac{4G}{3\rho_0} + \frac{\partial p}{\partial \rho}\right)_E + \left.\frac{pV^2}{\rho_0}\frac{\partial p}{\partial E}\right)_\rho\right]^{\frac{1}{2}} \tag{19.7}$$

For elastic materials with a constant bulk modulus the sound speed is given by:

$$c = \sqrt{\frac{E(1-\upsilon)}{(1+\upsilon)(1-2\upsilon)\rho}} \tag{19.8}$$

where E is Young's modulus, and υ is Poisson's ratio.

19.2 Time Step Calculations for Beam and Truss Elements

For the Hughes-Liu beam and truss elements, the time step size is give by:

$$\Delta t_e = \frac{L}{c} \tag{19.9}$$

where L is the length of the element and c is the wave speed:

$$c = \sqrt{\frac{E}{\rho}} \tag{19.10}$$

For the Belytschko beam the time step size given by the longitudinal sound speed is used (Equation (19.9)), unless the bending-related time step size given by [Belytschko and Tsay 1982]

$$\Delta t_e = \frac{.5L}{c\sqrt{3I\left[\frac{3}{12I + AL^2} + \frac{1}{AL^2}\right]}} \tag{19.11}$$

is smaller, where I and A are the maximum value of the moment of inertia and area of the cross section, respectively.

Comparison of critical time steps of the truss versus the elastic solid element shows that it if Poisson's ratio, υ, is nonzero the solid elements give a considerably smaller stable time step size. If we define the ratio, α, as:

$$\alpha = \frac{\Delta t_{continuum}}{\Delta t_{rod}} = \frac{C_{rod}}{C_{continuum}} = \sqrt{\frac{(1+\upsilon)(1-2\upsilon)}{1-\upsilon}}, \tag{19.12}$$

we obtain the results in Table 19.1 where we can see that as υ approaches .5 $\alpha \to 0$.

υ	0	0.2	0.3	0.4	0.45	0.49	0.50
α	1.	0.949	0.862	0.683	0.513	0.242	0.0

Table 19.1 Comparison of critical time step sizes for a truss versus a solid element.

19.3 Time Step Calculations for Shell Elements

For the shell elements, the time step size is given by:

$$\Delta t_e = \frac{L_s}{c} \tag{19.13}$$

where L_s is the characteristic length and c is the sound speed:

$$c = \sqrt{\frac{E}{\rho(1-\nu^2)}} \tag{19.14}$$

Three user options exists for choosing the characteristic length. In the default or first option the characteristic length is given by:

$$L_s = \frac{(1+\beta)A_s}{\max(L_1, L_2, L_3, (1-\beta)L_4)} \tag{19.15}$$

where $\beta = 0$ for quadrilateral and 1 for triangular shell elements, A_s is the area, and L_i, (i= 1...4) is the length of the sides defining the shell elements. In the second option a more conservative value of L_s is used:

$$L_s = \frac{(1+\beta)A_s}{\max(D_1, D_2)} \tag{19.16}$$

where D_i (i=1,2) is the length of the diagonals. The third option provides the largest time step size and is frequently used when triangular shell elements have very short altitudes. The bar wave speed, Equation (19.10), is used to compute the time step size and L_s is give by

$$L_s = \max\left[\frac{(1+\beta)A_s}{\max(L_1, L_2, L_3, (1-\beta)L_4)}, \min(L_1, L_2, L_3, L_4 + \beta 10^{20})\right] \qquad (19.17)$$

A comparison of critical time steps of truss versus shells is given in Table 19.2 with β defined as:

$$\beta = \frac{\Delta t_{2D-continuum}}{\Delta t_{rod}} = \frac{C_{rod}}{C} = \sqrt{1-\upsilon^2} \qquad (19.18)$$

υ	0	0.2	0.3	0.4	0.5
β	1.0	0.98	0.954	0.917	0.866

Table 19.2 Comparison of critical time step sizes for a truss versus a shell element.

19.4 Time Step Calculations for Solid Shell Elements

A critical time step size, Δt_e is computed for solid shell elements from

$$\Delta t_e = \frac{\upsilon_e}{cA_{e_{max}}} \qquad (19.19)$$

where υ_e is the element volume, $A_{e_{max}}$ is the area of the largest side, and c is the plane stress sound speed given in Equation (19.14).

19.5 Time Step Calculations for Discrete Elements

For spring elements such as that in Figure 19.1 there is no wave propagation speed c to calculate the critical time step size.

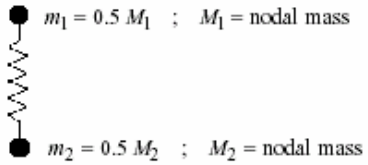

Figure 19.1 Lumped spring mass system.

The eigenvalue problem for the free vibration of spring with nodal masses m_1 and m_2, and stiffness, k, is given by:

$$\begin{bmatrix} k & -k \\ -k & k \end{bmatrix} \begin{bmatrix} u_1 \\ u_2 \end{bmatrix} - \omega^2 \begin{bmatrix} m_1 & 0 \\ 0 & m_2 \end{bmatrix} \begin{bmatrix} u_1 \\ u_2 \end{bmatrix} = \begin{bmatrix} 0 \\ 0 \end{bmatrix} \tag{19.20}$$

Since the determinant of the charactistic equation must equal zero, we can solve for the maximum eigenvalue:

$$\det \begin{bmatrix} k - \omega^2 m_1 & -k \\ -k & k - \omega^2 m_2 \end{bmatrix} = 0 \quad \rightarrow \quad \omega_{\max}^2 = \frac{k(m_1 + m_2)}{m_1 \cdot m_2} \tag{19.21}$$

Recalling the critical time step of a truss element:

$$\left.\begin{aligned} \Delta t \le \frac{\ell}{c} \\ \omega_{\max} = \frac{2c}{\ell} \end{aligned}\right\} \quad \Delta t \le \frac{2}{\omega_{\max}} \tag{19.22}$$

and approximating the spring masses by using 1/2 the actual nodal mass, we obtain:

$$\Delta t = 2\sqrt{\frac{m_1 m_2}{m_1 + m_2} \frac{1}{k}} \tag{19.23}$$

Therefore, in terms of the nodal mass we can write the critical time step size as:

$$\Delta t_e = 2\sqrt{\frac{2M_1 M_2}{k(M_1 + M_2)}} \tag{19.24}$$

The springs used in the contact interface are not checked for stability.

7.2 Damping Information

*DAMPING

The Keyword options in this section in alphabetical order are:

*DAMPING_GLOBAL

*DAMPING_PART_MASS

*DAMPING_PART_STIFFNESS

*DAMPING_RELATIVE

*DAMPING_GLOBAL

Purpose: Define mass weighted nodal damping that applies globally to the nodes of deformable bodies and to the mass center of the rigid bodies.

Card Format

	1	2	3	4	5	6	7	8
Variable	LCID	VALDMP	STX	STY	STZ	SRX	SRY	SRZ
Type	I	F	F	F	F	F	F	F
Default	0	0.0	0.0	0.0	0.0	0.0	0.0	0.0
Remarks	1		2	2	2	2	2	2

VARIABLE	DESCRIPTION
LCID	Load curve ID which specifies node system damping: EQ.0: a constant damping factor as defined by VALDMP is used, EQ.n: system damping is given by load curve n. The damping force applied to each node is f=-d(t) mv, where d(t) is defined by load curve n.
VALDMP	System damping constant, d (this option is bypassed if the load curve number defined above is non zero).
STX	Scale factor on global x translational damping forces.

*DAMPING

VARIABLE	DESCRIPTION
STY	Scale factor on global y translational damping forces.
STZ	Scale factor on global z translational damping forces.
SRX	Scale factor on global x rotational damping moments.
SRY	Scale factor on global y rotational damping moments.
SRZ	Scale factor on global z rotational damping moments.

Remarks:

1. This keyword is also used for the restart, see *RESTART.

2. If STX=STY=STZ=SRX=SRY=SRZ=0.0 in the input above, all six values are defaulted to unity.

   With mass proportional system damping the acceleration is computed as:

$$a^n = M^{-1}\left(P^n - F^n - F^n_{damp} \right)$$

   where, M is the diagonal mass matrix, P^n is the external load vector, F^n is the internal load vector, and F^n_{damp} is the force vector due to system damping. This latter vector is defined as:

$$F^n_{damp} = D_s m v$$

   The best damping constant for the system is usually based on the critical damping factor for the lowest frequency mode of interest. Therefore,

$$D_s = 2\omega_{min}$$

   is recommended where the natural frequency (given in radians per unit time) is generally taken as the fundamental frequency of the structure. Note that this damping applies to both translational and rotational degrees of freedom.

   Energy dissipated by through mass weighted damping is reported as system damping energy in the ASCII file GLSTAT. This energy is computed whenever system damping is active.

***DAMPING_PART_MASS**

Purpose: Define mass weighted damping by part ID. Parts may be either rigid or deformable. In rigid bodies the damping forces and moments act at the center of mass.

Card Format

	1	2	3	4	5	6	7	8
Variable	PID	LCID	SF	FLAG				
Type	I	I	F	I				
Default	0	0	1.0	0				

Card Format (This card is optional and is read if and only if FLAG=1. If this card is not read STX, STY, STZ, SRX, SRY, and SRZ default to unity.)

Card 2	1	2	3	4	5	6	7	8
Variable	STX	STR	STZ	SRX	SRY	SRZ		
Type	F	F	F	F	F	F		
Default	0.0	0.0	0.0	0.0	0.0	0.0		

VARIABLE	DESCRIPTION
PID	Part ID, see *PART.
LCID	Load curve ID which specifies system damping for parts.
SF	Scale factor for load curve. This allows a simple modification of the load curve values.
FLAG	Set this flag to unity if the global components of the damping forces require separate scale factors.
STX	Scale factor on global x translational damping forces.

*DAMPING

VARIABLE	DESCRIPTION
STY	Scale factor on global y translational damping forces.
STZ	Scale factor on global z translational damping forces.
SRX	Scale factor on global x rotational damping moments.
SRY	Scale factor on global y rotational damping moments.
SRZ	Scale factor on global z rotational damping moments.

Remarks:

Mass weighted damping damps all motions including rigid body motions. For high frequency oscillatory motion stiffness weighted damping may be preferred. With mass proportional system damping the acceleration is computed as:

$$a^n = M^{-1}\left(P^n - F^n - F^n_{damp} \right)$$

where, M is the diagonal mass matrix, P^n is the external load vector, F^n is the internal load vector, and F^n_{damp} is the force vector due to system damping. This latter vector is defined as:

$$F^n_{damp} = D_s m v$$

The best damping constant for the system is usually based on the critical damping factor for the lowest frequency mode of interest. Therefore,

$$D_s = 2\omega_{min}$$

is recommended where the natural frequency (given in radians per unit time) is generally taken as the fundamental frequency of the structure. The damping is applied to both translational and rotational degrees of freedom. The component scale factors can be used to limit which global components see damping forces.

Energy dissipated by through mass weighted damping is reported as system damping energy in the ASCII file GLSTAT. This energy is computed whenever system damping is active.

***DAMPING_PART_STIFFNESS**

Purpose: Assign Rayleigh stiffness damping coefficient by part ID.

Card Format

	1	2	3	4	5	6	7	8
Variable	PID	COEF						
Type	I	F						
Default								

VARIABLE	DESCRIPTION
PID	Part ID, see *PART.
COEF	Rayleigh damping coefficient for stiffness weighted damping. Values between 0.01 and 0.25 are recommended. Higher values are strongly discouraged, and values less than 0.01 may have little effect.

Remarks:

The damping matrix in Rayleigh damping is defined as:

$$C = \alpha M + \beta K$$

where C, M, and K are the damping, mass, and stiffness matrices, respectively. The constants α. and β are the mass and stiffness proportional damping constants. The mass proportional damping can be treated by system damping, see keywords: *DAMPING_GLOBAL and DAMPING_PART_ MASS. Transforming C with the ith eigenvector ϕ_i gives:

$$\phi_i^t C \phi_i = \phi_i^t (\alpha M + \beta K) \phi_i = \alpha + \beta \omega_i^2 = 2\omega_i \xi_i \delta_{ij}$$

where ω_i is the ith frequency (radians/unit time) and ξ_i is the corresponding modal damping parameter.

Generally, the stiffness proportional damping is effective for high frequencies and is orthogonal to rigid body motion. Mass proportional damping is more effective for low frequencies and will damp rigid body motion. If a large value of the stiffness based damping coefficient is used, it may be necessary to lower the time step size significantly. This must be done manually by reducing the time step scale factor on the *CONTROL_TIMESTEP control card. Since a good value of β is not easily identified, the coefficient, COEF, is defined such that a value of .10 roughly corresponds to 10% damping in the high frequency domain.

*DAMPING

Energy dissipated by Rayleigh damping is computed if and only if the flag, RYLEN, on the control card, *CONTROL_ENERGY is set to 2. This energy is acummulated as element internal energy and is included in the energy balance. In the GLSTAT file this energy will be lumped in with the internal energy.

***DAMPING_RELATIVE**

Purpose: Apply damping relative to the motion of a rigid body.

Card Format

	1	2	3	4	5	6	7	8
Variable	CDAMP	FREQ	PIDRB	PSID				
Type	F	F	F	I				
Default	0	0	0	0				

VARIABLE	DESCRIPTION
CDAMP	Fraction of critical damping.
FREQ	Frequency at which CDAMP is to apply (cycles per unit time, e.g. Hz if time unit is seconds).
PIDRB	Part ID of rigid body, see *PART. Motion relative to this rigid body will be damped.
PSID	Part set ID. The requested damping is applied only to the parts in the set.

Remarks:

1. This feature provides damping of vibrations for objects that are moving through space. The vibrations are damped, but not the rigid body motion. This is achieved by calculating the velocity of each node relative to that of a rigid body, and applying a damping force proportional to that velocity. The forces are reacted onto the rigid body such that overall momentum is conserved. It is intended that the rigid body is embedded within the moving object.

2. Vibrations at frequencies below FREQ are damped by more than CDAMP, while those at frequencies above FREQ are damped by less than CDAMP. It is recommended that FREQ be set to the frequency of the lowest mode of vibration.

7.3 Mooney-Rivlin Material Model Information

*MAT_MOONEY-RIVLIN_RUBBER *MAT

*MAT_MOONEY-RIVLIN_RUBBER

This is Material Type 27. A two-parametric material model for rubber can be defined.

Card Format

Card 1	1	2	3	4	5	6	7	8
Variable	MID	RO	PR	A	B	REF		
Type	I	F	F	F	F	F		

Card 2	1	2	3	4	5	6	7	8
Variable	SGL	SW	ST	LCID				
Type	F	F	F	F				

VARIABLE	DESCRIPTION
MID	Material identification. A unique number has to be chosen.
RO	Mass density.
PR	Poisson's ratio (> .49 is recommended, smaller values may not work).
A	Constant, see literature and equations defined below.
B	Constant, see literature and equations defined below.
REF	Use reference geometry to initialize the stress tensor. The reference geometriy is defined by the keyword:*INITIAL_FOAM_REFERENCE_GEOMETRY. This option is currently restricted to 8-noded solid elements with one point integration. EQ.0.0: off, EQ.1.0: on.

If A=B=0.0, then a least square fit is computed from tabulated uniaxial data via a load curve. The following information should be defined.

SGL	Specimen gauge length l_0, see Figure 20.10.

LS-DYNA Version 960 113 (MAT)

VARIABLE	DESCRIPTION
SW	Specimen width, see Figure 20.10.
ST	Specimen thickness, see Figure 20.10.
LCID	Load curve ID, see *DEFINE_CURVE, giving the force versus actual change ΔL in the gauge length. See also Figure 20.11 for an alternative definition.

Remarks:

The strain energy density function is defined as:

$$W = A(I-3) + B(II-3) + C(III^{-2} - 1) + D(III-1)^2$$

where

$$C = 0.5\ A + B$$

$$D = \frac{A(5\upsilon - 2) + B(11\upsilon - 5)}{2(1 - 2\upsilon)}$$

υ = Poisson's ratio

2(A+B) = shear modulus of linear elasticity

I, II, III = invariants of right Cauchy-Green Tensor C.

The load curve definition that provides the uniaxial data should give the change in gauge length, ΔL, versus the corresponding force. In compression both the force and the change in gauge length must be specified as negative values. In tension the force and change in gauge length should be input as positive values. The principal stretch ratio in the uniaxial direction, λ_1, is then given by

$$\lambda_1 = \frac{L_o + \Delta L}{L_o}$$

with L_O being the initial length and L being the actual length.

Alternatively, the stress versus strain curve can also be input by setting the gauge length, thickness, and width to unity (1.0) and defining the engineering strain in place of the change in gauge length and the nominal (engineering) stress in place of the force, see Figure 20.11.

The least square fit to the experimental data is performed during the initialization phase and is a comparison between the fit and the actual input is provided in the printed file. It is a good idea to visually check to make sure it is acceptable. The coefficients A and B are also printed in the output file. It is also advised to use the material driver (see Appendix H) for checking out the material model.

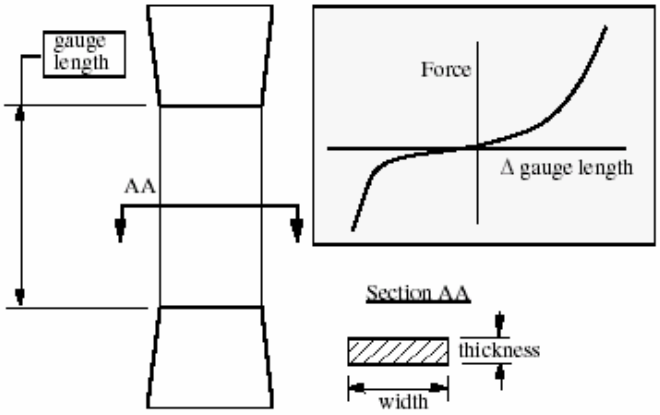

20.10 Uniaxial specimen for experimental data.

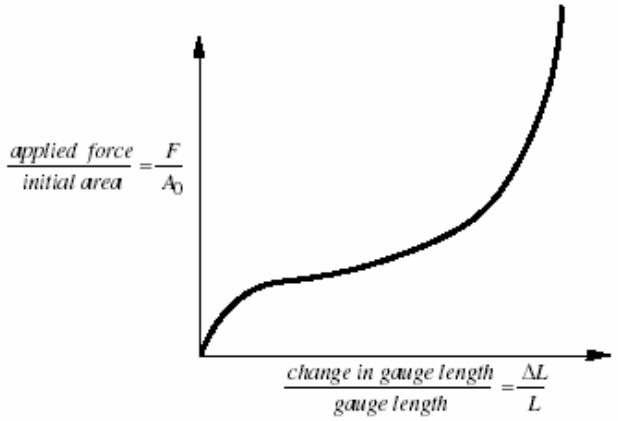

Figure 20.11 The stress versus strain curve can used instead of the force versus the change in the gauge length by setting the gauge length, thickness, and width to unity (1.0) and defining the engineering strain in place of the change in gauge length and the nominal (engineering) stress in place of the force.

Material Type 27: Incompressible Mooney-Rivlin Rubber

This material model, available for solid elements only, provides an alternative to the Blatz-Ko rubber model. The implementation is due to Maker [private communication]. The strain energy density function is defined as in terms of the input constants A, B, and υ as:

$$W(I_1,I_2,I_3) = A(I_1-3) + B(I_2-3) + C(\frac{1}{I_3^2}-1) + D(I_3-1)^2 \qquad (16.27.1)$$

where

$$C = .5 * A + B \qquad (16.27.2a)$$

$$D = \frac{A(5\upsilon-2) + B(11\upsilon-5)}{2(1-2\upsilon)} \qquad (16.27.2b)$$

υ = Poisson's ratio

G=2(A+B) = shear modulus of linear elasticity

I_1, I_2, I_3 = strain invariants in terms of the principal stretches

$$_1 = \lambda_1^2 + \lambda_2^2 + \lambda_3^2$$

$$I_2 = \lambda_1^2\lambda_2^2 + \lambda_2^2\lambda_3^2 + \lambda_3^2\lambda_1^2$$

$$I_3 = \lambda_1^2\lambda_2^2\lambda_3^2$$

Recommended values for Poisson's ratio are between .490 and .495 or higher. Lower values may lead to instabilities. In the derivation of the constants C and D incompressibility is assumed.

The derivation of the constants C and D is straigthforward [Feng, 1993] and is included here since we were unable to locate it in the literature. The principal components of Cauchy stress, σ_i, are given by [Ogden, 1984]

$$J\sigma_i = \lambda_i \frac{\partial W}{\partial \lambda_i}$$

For uniform dilation

$$\lambda_1 = \lambda_2 = \lambda_3 = \lambda$$

thus the pressure, p, is obtained (please note the sign convention),

$$p = \sigma_1 = \sigma_2 = \sigma_3 = \frac{2}{\lambda^3}\left(\lambda^2 \frac{\partial W}{\partial I_1} + 2\lambda^4 \frac{\partial W}{\partial I_2} + \lambda^6 \frac{\partial W}{\partial I_3}\right)$$

The relative volume, V, can be defined in terms of the stretches as:

$$V = \lambda^3 = \frac{\text{new volume}}{\text{old volume}}$$

For small volumetric deformations the bulk modulus, K, can be defined as the ratio of the pressure over the volumetric strain as the relative volume approaches unity:

$$K = \lim_{V \to 1}\left(\frac{p}{V-1}\right)$$

The partial derivatives of W lead to:

$$\frac{\partial W}{\partial I_1} = A$$

$$\frac{\partial W}{\partial I_2} = B$$

$$\frac{\partial W}{\partial I_3} = -2CI_3^{-3} + 2D(I_3 - 1) = -2C\lambda^{-18} + 2D(\lambda^6 - 1)$$

$$p = \frac{2}{\lambda^3}\left\{A\lambda^2 + 2\lambda^4 B + \lambda^6\left[-2C\lambda^{-18} + 2D(\lambda^6 - 1)\right]\right\}$$

$$= \frac{2}{\lambda^3}\left\{A\lambda^2 + 2\lambda^4 B - 2C\lambda^{-12} + 2D(\lambda^{12} - \lambda^6)\right\}$$

In the limit as the stretch ratio approaches unity, the pressure must approach zero:

$$\lim_{\lambda \to 1} p = 0$$

Therefore, $A + 2B - 2C = 0$ and

$$\therefore C = 0.5A + B$$

To solve for D we note that:

$$K = \lim_{V \to 1}\left(\frac{p}{V-1}\right) = \lim_{\lambda \to 1} \frac{\frac{2}{\lambda^3}\left\{A\lambda^2 + 2\lambda^4 B - 2C\lambda^{-12} + 2D(\lambda^{12} - \lambda^6)\right\}}{\lambda^3 - 1}$$

$$= 2\lim_{\lambda \to 1} \frac{A\lambda^2 + 2\lambda^4 B - 2C\lambda^{-12} + 2D\left(\lambda^{12} - \lambda^6\right)}{\lambda^6 - \lambda^3}$$

$$= 2\lim_{\lambda \to 1} \frac{2A\lambda + 8\lambda^3 B + 24C\lambda^{-13} + 2D\left(12\lambda^{11} - 6\lambda^5\right)}{6\lambda^5 - 3\lambda^2}$$

$$= \frac{2}{3}(2A + 8B + 24C + 12D) = \frac{2}{3}(14A + 32B + 12D)$$

We therefore obtain:

$$14A + 32B + 12D = \frac{3}{2}K = \frac{3}{2}\left(\frac{2G(1+\upsilon)}{3(1-2\upsilon)}\right) = \frac{2(A+B)(1+\upsilon)}{(1-2\upsilon)}$$

Solving for D we obtain the desired equation:

$$D = \frac{A(5\upsilon - 2) + B(11\upsilon - 5)}{2(1-2\upsilon)}$$

7.4 LS-DYNA COR test input deck

```
*KEYWORD
*TITLE
New COR model with ball 18" from block
$$ HM_OUTPUT_DECK created 22:30:32 04-08-2003 by HyperMesh Version 5.1
$$ Generated using HyperMesh-Ls-dyna Template Version : 5.1-3
*CONTROL_TERMINATION
$$  ENDTIM    ENDCYC     DTMIN    ENDENG    ENDMAS
      0.06         0       0.0       0.0       0.0
*CONTROL_TIMESTEP
$$  DTINIT    TSSFAC      ISDO    TSLIMT     DT2MS      LCTM     ERODE     MSIST
       0.0       0.9         0       0.0       0.0         0         0         0
*CONTROL_CONTACT
$$  SLSFAC    RWPNAL    ISLCHK    SHLTHK    PENOPT    THKCHG     ORIEN    ENMASS
       0.1                    2         0         1         1         1
$$  USRSTR    USRFRC     NSBCS    INTERM     XPENE     SSTHK      ECDT   TIEDPRJ
         0         0        10         0       4.0         0         0
*DATABASE_BINARY_D3PLOT
$$ DT/CYCL      LCDT      BEAM     NPLTC
5.0000E-05         0         0         0
*NODE
       118.15337106317520.70675272349013-0.1533504915022
       2-1.33333333333330.27272727272727-0.1818181818181
       3-1.33333333333330.272727272727270.18181818181818
$
$ Node listing...
$

*MAT_ORTHOTROPIC_ELASTIC
$HMNAME MATS       2ortho wood
         26.5350E-05 1907000.0  902000.0  178300.0     0.027     0.044     0.067
  102200.0  342300.0  138000.0       0.0

                                                                          0.0
*MAT_MOONEY-RIVLIN_RUBBER
$HMNAME MATS       1ball
         16.4700E-05      0.49       0.0       0.0
       2.4       2.4       2.4         2
*PART
$HMNAME COMPS       1thesis_ball
$HMCOLOR COMPS       1       1

         1         1         1
*DAMPING_PART_MASS
         1         1       2.0
*PART
$HMNAME COMPS       2block
$HMCOLOR COMPS       2       2

         2         2         1
*DAMPING_PART_MASS
         2         1       3.5
*SECTION_SOLID
$HMNAME PROPS       2solid_block
         2         1
$HMNAME PROPS       1solid_ball
         1         1
*ELEMENT_SOLID
       1       1     982     973     976     981     781     782     771     768
       2       1     764     982     981     752     780     781     768     779
       3       1     981     976     967     979     768     771     772     770
$
$ Element listing...
$

*CONTACT_AUTOMATIC_SURFACE_TO_SURFACE
$HMNAME GROUPS       1impact
$HMCOLOR GROUPS       1       7
         1         2         3         3         0         0         0         0
```

```
       0.0       0.0       0.0       0.0      20.0         0       0.01.0000E+20
      20.0      20.0       0.0       0.0       1.0       1.0       1.0       1.0
*BOUNDARY_SPC_NODE
$HMNAME LOADCOLS       1auto1.1
$HMCOLOR LOADCOLS       1       1
      3052         0         1         1         1         1         1         1
      3053         0         1         1         1         1         1         1
      3058         0         1         1         1         1         1         1
$
$ Boundary condition listing...
$

*INITIAL_VELOCITY_NODE
$HMNAME LOADCOLS       2auto1
$HMCOLOR LOADCOLS       2       1
         1   -1056.0       0.0       0.0
         4   -1056.0       0.0       0.0
         5   -1056.0       0.0       0.0

$
$ Initial velocity listing
$
*DEFINE_CURVE
$HMNAME CURVES       2curve1
$HMCOLOR CURVES       2       1
$HMCURVE     1    1 LoadCurve2
         2         0       1.0       1.0       0.0       0.0         0
$
$ Define load-deflection curve for ball...
$

*DEFINE_CURVE
$HMNAME CURVES       1LoadCurve5
$HMCOLOR CURVES       1       1
$HMCURVE     1    1 LoadCurve5
         1         0       1.0       1.0       0.0       0.0         0
                 0.0                 1.0
                 1.0                 1.0
   $
$ Load curve for damping...
$
*END
```

7.5 LS-DYNA -3 aluminum bat model input deck

```
$This is a -3 bat model with a detailed cap.
$The bat is meshed with thick shells (8-noded bricks)
$The bat is broken down into 4 diffrent parts - the barrel, throat, handle and
$accurate wall thickness maintained by ruled mesh with nodes instead of lines.
*KEYWORD
*TITLE
-3 XXXXXXXXX 34"
$$ HM_OUTPUT_DECK created 03:07:27 04-17-2003 by HyperMesh Version 5.1
$$ Generated using HyperMesh-Ls-dyna Template Version : 5.1-3
*CONTROL_TERMINATION
$$  ENDTIM    ENDCYC     DTMIN    ENDENG    ENDMAS
     0.005
*CONTROL_TIMESTEP
$$  DTINIT    TSSFAC      ISDO    TSLIMT     DT2MS      LCTM     ERODE     MSIST
       0.0       0.9         0       0.0       0.0         0         0         0
*CONTROL_CONTACT
$$  SLSFAC    RWPNAL    ISLCHK    SHLTHK    PENOPT    THKCHG     ORIEN    ENMASS
       0.1                 2         0         1         1         1
$$  USRSTR    USRFRC     NSBCS     INTERM     XPENE     SSTHK      ECDT   TIEDPRJ
         0         0        10         0       4.0         0         0
*DATABASE_BINARY_D3PLOT
$$ DT/CYCL      LCDT      BEAM     NPLTC
5.0000E-05         0         0         0
*NODE
       133.5000000049012-0.2238416235478-1.1253278340436
       2          32.625           1.304             0.0
       3          30.625           1.196             0.0
$
$ Node listing...
$

*MAT_ELASTIC
$HMNAME MATS       1urethane
         17.5000E-05  300000.0       0.4
*MAT_ELASTIC
$HMNAME MATS       3al_knob
         33.8820E-0410500000.0      0.33
*MAT_ORTHOTROPIC_ELASTIC
$HMNAME MATS       4ortho wood
         46.5350E-05 1907000.0  902000.0  178300.0     0.027     0.044     0.067
  102200.0  342300.0  138000.0       0.0

                                                                           0.0
*MAT_PLASTIC_KINEMATIC
$HMNAME MATS       2aluminum
         22.8986E-0410500000.0      0.33   90000.0    7500.0       0.5

*MAT_MOONEY-RIVLIN_RUBBER
$HMNAME MATS       5ball
         56.4700E-05      0.45       0.0       0.0
       1.5       1.5       1.5         1
*PART
$HMNAME COMPS       1barrel
$HMCOLOR COMPS       1       9

         1         2         2
*DAMPING_PART_MASS
         1         2       3.5
*PART
$HMNAME COMPS       2throat
$HMCOLOR COMPS       2       8

         2         2         2
*DAMPING_PART_MASS
         2         2       3.5
```

```
*PART
$HMNAME COMPS       3handle
$HMCOLOR COMPS       3       7

         3         2         2
*DAMPING_PART_MASS
         3         2       3.5
*PART
$HMNAME COMPS       4knob
$HMCOLOR COMPS       4       1

         4         2         3
*DAMPING_PART_MASS
         4         2       3.5
*PART
$HMNAME COMPS       5cap
$HMCOLOR COMPS       5      14

         5         1         1
*DAMPING_PART_MASS
         5         2       3.5
*PART
$HMNAME COMPS       6ribs
$HMCOLOR COMPS       6      10

         6         1         1
*DAMPING_PART_MASS
         6         2       3.5
*PART
$HMNAME COMPS       7thesis_ball
$HMCOLOR COMPS       7       1

         7         4         5
*DAMPING_PART_MASS
         7         2       2.0
*SECTION_SOLID
$HMNAME PROPS       1solid_cap
         1         1
$HMNAME PROPS       4solid_ball
         4         1
*SECTION_TSHELL
$HMNAME PROPS       2thick_shell
         2         1  0.833333         2       1.0       0.0         0
*ELEMENT_SOLID
    4841       5      60    7821    7866      92    3135    7657    7749    3138
    4842       5    7821    7887    7874    7866    7657    7746    7747    7749
    4843       5      92    7866    7867      61    3138    7749    7745    3141
$
$Element listing...
$

*ELEMENT_TSHELL
       1       1    3137    3134    3133    3136     134      79      59      91
       2       1    3138    3135    3134    3137      92      60      79     134
       3       1    3140    3137    3136    3139     132     134      91      63

$
$ Element listing...
$

*CONTACT_AUTOMATIC_SURFACE_TO_SURFACE
$HMNAME GROUPS       1impact
$HMCOLOR GROUPS       1       7
         1         7         3         3         0         0         0         0
       0.0       0.0       0.0       0.0      20.0         0       0.01.0000E+20
      20.0      20.0       0.0       0.0       1.0       1.0       1.0       1.0
*INITIAL_VELOCITY_NODE
$HMNAME LOADCOLS       1auto1
$HMCOLOR LOADCOLS       1       1
       144       0.0    1232.0       0.0
       143       0.0    1232.0       0.0
```

```
       142       0.0    1232.0       0.0
$
$ Initial velocity listing...
$

*DEFINE_CURVE
$HMNAME CURVES       1curve1
$HMCOLOR CURVES       1       1
$HMCURVE     1    1 LoadCurve2
         1         0       1.0       1.0       0.0       0.0         0


$
$ Define load-deflection curve for ball
$

*DEFINE_CURVE
$HMNAME CURVES       1LoadCurve5
$HMCOLOR CURVES       1       1
$HMCURVE     1    1 LoadCurve5
         2         0       1.0       1.0       0.0       0.0         0
                 0.0                 1.0
                 1.0                 1.0
$
$ Load curve for damping...
$
*END
```

7.6 LS-DYNA Implicit input deck for modal analysis

```
*KEYWORD
*TITLE
Wood bat (ortho) with M-R ball
$$ HM_OUTPUT_DECK created 23:14:12 03-11-2003 by HyperMesh Version 5.1
$$ Generated using HyperMesh-Ls-dyna Template Version : 5.1-3
*CONTROL_TERMINATION
$$  ENDTIM    ENDCYC     DTMIN    ENDENG    ENDMAS
       1.0
*CONTROL_IMPLICIT_EIGENVALUE
$$    NEIG    CENTER     LFLAG    LFTEND     RFLAG    RHTEND    EIGMTH    SHFSCL
        20
*CONTROL_IMPLICIT_GENERAL
$$  IMFLAG       DT0    IMFLAG      NSBS       IGS     CNSTN      FORM
         1       1.0
*NODE
       1            34.07.2064216570E-15          -0.688
       2            34.0 -0.263286201467 -0.635629118367

$
$ Node and element listing...
```

8 REFERENCES

[1] Thurston, Wm., Amherst College, personal communication (1997)

[2] "Bat issue goes extra innings in Divisions II and III," Hagwell, Stephen R., **The NCAA News**, February 1, 1999.

[3] NCAA Press Release, "NCAA Committee Recommends Baseball Bat Performance Standard, New Specs for 1999," August 6, 1998.

[4] Riley, William F., and Sturges, Leroy D., **Engineering Mechanics: Dynamics**, John Wiley and Sons, New York, 1993, pp. 347-348

[5] Riley and Sturges, pp. 195-199

[6] *Webster's Revised Unabridged Dictionary, 1996*

[7] Adair, Robert K., **The Physics of Baseball, 2nd Edition**, Harper Penennial, New York, 1994

[8] Watts , Robert G., and Bahill, A. Terry, Keep Your Eye on the Ball: The Science and Folklore of Baseball, W. H. Freeman and Co., New York, 1990, pp 116-123

[9] Crisco, J. J., "Final Report: NCAA Research Program on Bat and Ball Performance," November 1997.

[10] Cassidy, Paul E., and Burton, Allen W., "Response Time in Baseball: Implications for the Safety of Infielders and Pitchers," October 1997, Appendix of Crisco, 1997

[11] "Bat issue goes extra innings in Divisions II and III," Hagwell, Stephen R., **The NCAA News**, February 1, 1999.

[12] **Annual Book of ASTM Standards**, Volume 15.07

[13] **Annual Book of ASTM Standards**, Volume 15.07

[14] **Annual Book of ASTM Standards**, Volume 15.07

[15] Fallon, Lawrence P. , Sherwood, James A., Collier, Robert D., "Program to Develop Baseball Bat Performance Procedures using the Baum Hitting Machine and Provide Verification using Laboratory Test Methods, FINAL REPORT," October 1997

[16] Van Zandt, L. L., “The Dynamical Theory of the Baseball Bat,” American Journal of Physics, Vol. 60, No. 2., February 1992, pp. 172-181

[17] Fleisig, Glenn S., Zheng, Nigel, Stodden, David, Andrews, James R., "The Relationship Among Baseball Bat Weight, Moment of Inertia, and Velocity," American Sports Medicine Institute, August 1997

[18] Koenig, K.; Hannigan, T.; Davis, N.; Hillhouse, M.; Spencer, L.; "Inertial Effects on Baseball Bat Swing Speed," Mississippi State University, October 1997

[19] Watts and Bahill, pp. 83-132